

**Navy Experimental Diving Unit
321 Bullfinch Road
Panama City, FL 32407-7015**

**TA 10-12
NEDU TR 18-01
Jan 2018**

A Probabilistic Model of Altitude Decompression Sickness Based on the 3RUT-MB Model of Gas Bubble Evolution in Perfused Tissue



**Authors:
Wayne A. Gerth
Ramachandra Srini Srinivasan
F. Gregory Murphy
Keith A. Gault**

**Distribution Statement A:
Approved for public release;
distribution is unlimited.**

REPORT DOCUMENTATION PAGE

Form Approved
OMB No. 0704-0188

Public reporting burden for this collection of information is estimated to average 1 hour per response, including the time for reviewing instructions, searching existing data sources, gathering and maintaining the data needed, and completing and reviewing this collection of information. Send comments regarding this burden estimate or any other aspect of this collection of information, including suggestions for reducing this burden to Department of Defense, Washington Headquarters Services, Directorate for Information Operations and Reports (0704-0188), 1215 Jefferson Davis Highway, Suite 1204, Arlington, VA 22202-4302. Respondents should be aware that notwithstanding any other provision of law, no person shall be subject to any penalty for failing to comply with a collection of information if it does not display a currently valid OMB control number. **PLEASE DO NOT RETURN YOUR FORM TO THE ABOVE ADDRESS.**

| | | | | | |
|--|------------------------------------|---|---|---|--|
| 1. REPORT DATE (DD-MM-YYYY) 19-01-2018 | | 2. REPORT TYPE Technical Report | | 3. DATES COVERED (From - To) Oct 2004 TO Sep 2017 | |
| 4. TITLE AND SUBTITLE A Probabilistic Model of Altitude Decompression Sickness Based on the 3RUT-MB Model of Gas Bubble Evolution in Perfused Tissue | | | | 5a. CONTRACT NUMBER | |
| | | | | 5b. GRANT NUMBER | |
| | | | | 5c. PROGRAM ELEMENT NUMBER | |
| 6. AUTHOR(S) Wayne A. Gerth, Ramachandra Srin Srinivasan; F. Gregory Murphy, Keith A. Gault. | | | | 5d. PROJECT NUMBER | |
| | | | | 5e. TASK NUMBER 04-13 | |
| | | | | 5f. WORK UNIT NUMBER | |
| 7. PERFORMING ORGANIZATION NAME(S) AND ADDRESS(ES) Navy Experimental Diving Unit 321 Bullfinch Road Panama City FL 32407-7015 | | | | 8. PERFORMING ORGANIZATION REPORT NUMBER 18-01 | |
| 9. SPONSORING / MONITORING AGENCY NAME(S) AND ADDRESS(ES) Naval Sea Systems Command 1333 Isaac Hull Avenue, SE Washington Navy Yard D.C. 2037 | | | | 10. SPONSOR/MONITOR'S ACRONYM(S) NAVSEA 00C | |
| | | | | 11. SPONSOR/MONITOR'S REPORT NUMBER(S) | |
| 12. DISTRIBUTION / AVAILABILITY STATEMENT Distribution Statement A: Approved for public release; distribution is unlimited | | | | | |
| 13. SUPPLEMENTARY NOTES | | | | | |
| 14. ABSTRACT Decompression sickness (DCS) in man can occur with excessively rapid and extensive reductions of the ambient pressure in diving, aviation, and spaceflight operations. Probabilistic models of DCS occurrence are particularly well suited for managing the risks of DCS in these operations, but have been limited in ability to accommodate the influences of known factors that govern DCS outcomes as such factors may come in and out of play during arbitrarily varying periods in an exposure. We here describe a probabilistic model of DCS occurrence able to accommodate the influences of pressure, changing inspired inert gas, oxygen breathing, and exercise in profiles of arbitrary complexity. The model is a time-dependent covariate survival model in which the risks of DCS during an exposure are determined as functions of the prevailing volumes and profusions of gas bubbles in a perfusion-limited gas exchange compartment. The bubbles vary in volume by diffusion-limited exchange of gas between the bubbles and their surroundings according to an implementation of a three-region unstirred tissue model of gas bubble evolution elaborated to accommodate the influences of exercise and oxygen breathing on compartmental gas exchange and bubble nucleation. Parameters in the model were fit with maximum likelihood techniques to training data comprising detailed descriptions of actual human decompressions and their observed DCS outcomes in 2598 man-exposures to hypobaric pressures completed in a wide variety of NASA, NASA-sponsored, and U.S. Air Force chamber trials. The model underestimates the observed DCS occurrence density in the first four hours after start of the last decompression and consequently fails to fit the data. However, when model estimates of DCS occurrence are made with planned times at altitude, not actual times that are shorter than planned due to occurrence of DCS, the model fits data from 84 of the 117 groups in the training data to within a chi-square $P < 0.05$. In this form, the model is shown to perform better than other published models on a variety of data subset collections that is much more diverse than can be handled by any one of the other models. | | | | | |
| 15. SUBJECT TERMS Decompression sickness risk, hypobaric exposure, survival analysis, maximum likelihood, probabilistic models, gas and bubble dynamics | | | | | |
| 16. SECURITY CLASSIFICATION OF: | | | 17. LIMITATION OF ABSTRACT Unclassified | 18. NUMBER OF PAGES 123 | 19a. NAME OF RESPONSIBLE PERSON NEDU Librarian |
| a. REPORT Unclassified | b. ABSTRACT Unclassified | c. THIS PAGE Unclassified | | | 19b. TELEPHONE NUMBER (include area code) 850-230-3100 |

Standard Form 298 (Rev. 8-98)
Prescribed by ANSI Std. Z39.18

CONTENTS

| <u>Section</u> | <u>Page No.</u> |
|---|-----------------|
| Report Documentation Page | i |
| Contents..... | ii |
| Nomenclature..... | iv |
| 1. Introduction | 1 |
| 2. Methods..... | 3 |
| 2.1 3RUT-MB Model | 3 |
| 2.1.1 Quantification of Exercise..... | 5 |
| 2.1.2 Compartmental Oxygen Consumption, Perfusion, and O ₂ Tension..... | 5 |
| 2.1.3 Bubble Nucleation | 6 |
| 2.1.4 Venous Gas Emboli (VGE) Formation..... | 7 |
| 2.2 Definition of the Hazard Function..... | 7 |
| 2.3 Model Optimization by Likelihood Maximization..... | 8 |
| 2.4 Model Training Data..... | 9 |
| 2.4.1 Augmented NMRI Standard format | 9 |
| 2.4.2 USAF Data | 9 |
| 2.4.3 NASA Data | 10 |
| 2.4.4 Exercise Coding | 10 |
| 2.4.5 Overall Training Data Summary | 13 |
| 3. Results..... | 14 |
| 3.1 Optimized 3RUT-MBe1 Model Parameters..... | 14 |
| 3.2 Model Goodness-of-Fit | 16 |
| 3.2.1 Observed and Estimated DCS Occurrence Density Distributions | 16 |
| 3.2.2 Pearson Residuals and Global Chi-Square | 17 |
| 4. Discussion | 21 |
| 4.1 Prebreathe and Exercise Effects on Gas Elimination..... | 21 |
| 4.2 Prebreathe and Exercise Effects on Bubble Nucleation..... | 23 |
| 4.3 Comparative Model Performance | 27 |
| 4.4 Features of Model Performance..... | 32 |
| 4.5 Model Deficiencies and Remaining Issues..... | 35 |
| 5. Conclusions | 37 |
| 6. Acknowledgements..... | 38 |
| 7. References | 39 |
| 8. Appendix A. Three-Region Unstirred Tissue Multiple Bubble (3RUT-MB) Model of Tissue Gas and Bubble Dynamics | A-1 |

| | | |
|-----------|--|---------|
| 8.1 | Single Diffusible Gas..... | A-1 |
| 8.1.1 | Multiple Bubbles of Same Size | A-1 |
| 8.1.2 | Multiple Bubbles of Different Sizes..... | A-3 |
| 8.1.3 | Exercise Effects on Blood-Tissue Gas Exchange | A-4 |
| 8.2 | Multiple Diffusible Gases | A-4 |
| 8.2.1 | Tissue O ₂ Tension with O ₂ as a Diffusible Gas..... | A-6 |
| 8.2.2 | Exercise Effects on Tissue O ₂ Consumption | A-8 |
| 8.3 | Bubble Nucleation and Variable Bubble Number | A-9 |
| 8.3.1 | Single Time-Dependent Bubble Size Approximation | A-12 |
| 8.4 | Scaled 3RUT-MB Model | A-13 |
| 8.5 | Model Operation and Initial Values | A-15 |
| 9. | Appendix B. Piece-Wise Analytic Approximation of the Three-Region Unstirred Tissue Multiple Bubble (3RUT-MB) Model of Tissue Gas and Bubble Dynamics | B-1 |
| 9.1 | Single Diffusible Gas..... | B-1 |
| 9.1.1 | Multiple Bubbles of Same Size | B-1 |
| 9.1.1.1 | Changes in Bubble Radius and Bubble Gas Pressure..... | B-1 |
| 9.1.1.2 | Tissue Gas Tension with Time-Dependent Changes in Tissue Blood Flow | B-11 |
| 9.1.1.2.1 | General Model of Time-Dependent Changes in Blood Flow | B-12 |
| 9.1.1.2.2 | Multi-Exponential Model of Time-Dependent Changes in Blood Flow | B-14 |
| 9.1.1.2.3 | Coupling of Compartmental O ₂ Consumption and Blood flow..... | B-18 |
| 9.1.2 | Multiple Bubbles of Different Sizes | B-19 |
| 9.2 | Multiple Diffusible Gases | B-21 |
| 9.2.1 | Tissue O ₂ Tension with O ₂ as a Diffusible Gas..... | B-23 |
| 9.2.1.1 | Multiple Bubbles of Same Size..... | B-23 |
| 9.2.1.2 | Multiple Bubbles of Different Size | B-26 |
| 9.2.2 | Variable Bubble Number: Single Time-Dependent Bubble Size Approximation | B-27 |
| 9.3 | Semi-Analytic Solution of the Fick Equation in the 3RUT-MB Model | B-31 |
| 10. | Appendix C. Summary of Recursive Equations for Solution of 3RUT-MBe1 Model..... | C-1–C-6 |
| 11. | Appendix D. Hazard Function Formulation and Optimization | D-1–D-2 |
| 12. | Appendix E. Summary Description of A1309 Model Training Data | E-1–E-5 |
| 13. | Appendix F. Pearson χ^2 Statistics for Optimized 3RUT-MBe1 Model on its A1309 Training Data | F-1–F-3 |

NOMENCLATURE

| | |
|-----------------------------|--|
| A_b | = bubble surface area |
| α_{b_k} | = solubility of gas k in blood |
| α_{t_k} | = solubility of gas k in tissue |
| $\alpha_{b_{O_2}}$ | = O ₂ solubility in blood |
| $\alpha_{t_{O_2}}$ | = O ₂ solubility in tissue |
| α'_{O_2} | = slope of the whole blood O ₂ solubility curve in the region of the prevailing venous O ₂ tension |
| $B_{N,j}$ | = bubble number power factor |
| β | = vector of adjustable parameters in the hazard function; combination of ρ and W parameter vectors |
| $\beta_0, \beta_1, \beta_2$ | = adjustable parameters in fitted \dot{V}_{O_2} versus work rate (Watts) equation |
| β | = generalized slope factor for integral distribution of bubble nuclei sizes |
| β^0 | = slope factor for initial integral distribution of bubble nuclei sizes |
| β_{ex} | = dimensionless exercise-dependent β modifying factor |
| β_f | = prevailing slope factor for integral distribution of bubble nuclei sizes after accommodation of P_{crush} and exercise effects |
| $C_{a_{O_2}}$ | = O ₂ concentration in arterial blood entering tissue |
| $C_{\bar{v}_{O_2}}$ | = O ₂ concentration in mixed venous blood leaving tissue |
| $D_{t,k}$ | = diffusivity of gas k in tissue |
| dt | = integration time step |
| dt_{max} | = maximum allowed integration time step |
| dt_{min} | = minimum allowed integration time step |
| dt_k | = integration time step decay constant |
| Δt_n | = integration time step n |
| $\Delta_{i,j}(t)$ | = time-dependent dose in compartment j during the i th exposure |
| δ_i | = binary outcome variable, exposure i |

| | |
|-----------------------------|---|
| $\delta\hat{r}_{m,n}$ | = scaled radius change of bubble in m^{th} size group in integration step n |
| $F_{\text{I}_{\text{O}_2}}$ | = inspired oxygen fraction |
| $f(t)$ | = function in linearization of the Fick equation |
| $G_k(t)$ | = with $x_k(t)$, amount of gas k in N_b bubbles |
| $g(t)$ | = function in linearization of the Fick equation |
| g_j | = j^{th} compartment gain factor in hazard function |
| $h(t)$ | = hazard function |
| $I_q(t)$ | = indefinite integral in integrating factor for general solution of $p_i(t)$ with exercise |
| I_{ex} | = exercise intensity \equiv whole body O_2 consumption rate |
| i | = subscript for individual exposure, suppressed when reference is clear from context |
| j | = subscript for individual compartment, suppressed when reference is clear from context |
| K_m | = bubble surface permeability; may be subscripted for individual gas, hatted if scaled |
| k | = subscript for individual diffusible gas |
| $L(\beta)$ | = likelihood of a data set of N individual exposures, as function of β |
| $l_i(\beta)$ | = likelihood of individual exposure i |
| LR | = compartmental bubble loss rate via VGE formation |
| Λ | = 3RUT-MB scale factor |
| M | = modulus of elasticity; may be subscripted for bubble size group, hatted if scaled |
| m | = subscript for individual bubble size group, suppressed when reference is clear from context |
| $m_{\beta_{\text{ex}}}$ | = factor (≥ 0) governing the sensitivity of β to exercise intensity, I_{ex} |
| $m_{\dot{V}_{\text{O}_2}}$ | = rate of change of \dot{V}_{O_2} with I_{ex} |
| $m_{\dot{Q}}$ | = rate of change of \dot{Q} with \dot{V}_{O_2} |
| N | = number of exposures in training data |

| | |
|---------------------|--|
| N_b^o | = total number of bubble nuclei in a compartment |
| N_b | = total number of bubbles from recruited nuclei in a compartment |
| N_{bs} | = number of bubble size groups in a compartment |
| N_g | = total number of diffusible gases in model |
| n | = subscript for integration step |
| n_b | = number of bubbles in size group m |
| n_c | = number of gas-exchange compartments in model |
| $U_{k,n}$ | = rate of change of arterial gas k partial pressure in integration step n |
| $P(0)$ | = probability of no-DCS |
| $P(E)$ | = probability of DCS |
| P_{amb} | = ambient hydrostatic pressure |
| P'_{amb} | = ambient hydrostatic pressure less partial pressures of the infinitely diffusible gases, assumed the same in all compartments |
| P_{DCS} | $\equiv P(E)$, probability of DCS |
| $P_{A_{CO_2}}$ | = alveolar CO_2 partial pressure |
| $P_{A_{O_2}}$ | = alveolar O_2 partial pressure |
| p_{a_k} | = arterial O_2 partial pressure |
| $P_{\bar{V}_{O_2}}$ | = O_2 partial pressure in mixed venous blood |
| PB | = “prebreathe” |
| $P_{b_{T,m}}$ | = total pressure of all diffusible gases in bubbles of m^{th} size group |
| $P_{b,k}$ | = partial pressure of gas k in bubble |
| P_∞ | = total pressure of the infinitely diffusible gases in bubble |
| P_{crush} | = bubble nucleus crush pressure |
| P_{ss} | = prevailing compartmental gas supersaturation |
| $P_{t,k}$ | = partial pressure of gas k in tissue |
| $\dot{Q}(t)$ | = blood flow per unit volume of tissue |

| | |
|-------------------------|--|
| q | = coefficient proportional to blood flow; may be a function of time t |
| RQ | = respiratory quotient |
| r | = bubble radius, hatted if scaled |
| r_{\min}^o | = minimum bubble nuclear radius that can be recruited for growth at prevailing gas-supersaturation |
| ρ | = total number of adjustable parameters in model |
| $\boldsymbol{\rho}$ | = vector of adjustable parameters in $\Delta_{i,j}(t)$; $i=1, \dots, N$; $j=1, \dots, n_c$ |
| S_{x_n} | = gas loss rate into bubbles in time step n |
| σ | = gas-liquid surface tension, hatted if scaled |
| σ_c | = crumbling compression; counters surface tension, hatted if scaled |
| t_1 | = time an individual is last known to be DCS-free in an exposure |
| t_2 | = time an individual is first known to have DCS in an exposure |
| τ | = compartmental blood-tissue gas exchange time constant; may be subscripted for individual gas |
| τ_{P_c} | = P_{crush} decay time constant |
| $\tau_{\dot{V}_{O_2}}$ | = time constant associated with the exponential change in \dot{V}_{O_2} |
| V_b | = bubble volume, hatted if scaled |
| V_{r0} | = nucleonic bubble volume, hatted if scaled |
| \dot{V}_{O_2} | = compartmental O_2 consumption rate |
| $\dot{V}_{O_2,wb}$ | = whole-body O_2 consumption rate |
| $\dot{V}_{O_2,wb,rest}$ | = assumed whole body O_2 consumption rate during rest |
| $\Delta\dot{V}_{O_2ex}$ | = change in compartmental O_2 consumption rate with exercise relative to resting rate |
| W | = work rate (Watts) |
| \mathbf{W} | = vector of compartmental weights in the hazard function |
| $x_k(t)$ | = with $G_k(t)$, amount of gas k in N_b bubbles, hatted if scaled |
| χ^2 | = chi-square statistic |

1. Introduction

Decompression sickness (DCS) in man can occur with excessively rapid and extensive reductions of the ambient pressure.¹ Reductions of ambient pressure that put personnel at risk for DCS occur in diving, aviation, and spaceflight operations. Programmatic management of these risks requires: a) definition of risk envelopes for all routine and emergency decompressions that are or may be encountered by at-risk personnel; b) quantitative consideration of the inclusion or introduction of DCS risks in the design, testing, and implementation of new operational procedures and equipment, and; c) real-time monitoring of DCS risk incurred by personnel during various operations.

Probabilistic models of DCS occurrence are particularly well suited for application to these problems.² Such models are readily used to estimate the probabilities of DCS in different pressure profiles and to compute decompression schedules that keep estimated risks of DCS within any user-specified acceptable limit.^{3,4}

Risks of DCS in early probabilistic models of DCS occurrence were based on time-independent covariates, i.e., governing factors that are fixed properties of an exposure. Empirical log-logistic models of this type required additional model terms to accommodate added features of an exposure. As a result, such models were tailored to decompression profiles of particular type, limiting their ability to accommodate exposure profiles of arbitrary complexity. Models of this type were developed for no-stop air-diving⁵ and for simple single-ascent hypobaric exposures⁶⁻¹¹. Other dose-response models were applicable to more complex exposures for which a single-valued DCS dose could be computed. Gernhardt described the first model of this class in which the probability of DCS was given in terms of a computed maximum bubble volume attained in a series of parallel-perfused gas exchange compartments, a volume that could be computed for a profile of arbitrary complexity.¹² Other models of this type were described by Gerth and Vann.¹³ Such models provided a mechanistic foundation that conformed to the well-accepted idea that DCS is initiated by *in vivo* bubble formation and growth.^{1,14}

More comprehensive probabilistic models of DCS occurrence have been developed based on the formalism of survival analysis.¹⁵ Such models not only account for DCS occurrence per se, but also account for the time of DCS occurrence in an exposure. With consideration that an exposure can be completed only with an outcome of DCS or no DCS, the probability $P(t)$ of surviving DCS-free to time t in an exposure profile is given in survival models by

$$P(t) = \exp \left[- \int_0^t h(t) dt \right], \quad (1)$$

where $h(t)$ is the hazard function that gives the instantaneous rate of DCS occurrence at time t in those individuals in the exposure that have not developed DCS up to time t and

hence remain at risk for DCS at that time.^{16,17} The hazard function^a expresses the quantitative relationships between the putative governing factors of DCS onset and the DCS or no DCS outcome. The probability P(E) that DCS will occur between times t₁ and t₂ in the profile is given by Eq. (2):

$$P(E) = \left\{ \exp \left[- \int_0^{t_1} h(t) dt \right] \right\} \cdot \left\{ 1 - \exp \left[- \int_{t_1}^{t_2} h(t) dt \right] \right\}. \quad (2)$$

The challenge in the development of these models is to define the hazard function in such a fashion that it properly accommodates the known or suspected factors or covariates that govern DCS outcomes in the exposures of interest.

A variety of survival models have been developed in which the hazard is cast in terms of time-independent covariates.¹⁸⁻²³ Such accelerated failure time models incorporate time as a fixed-valued internal covariate which, when once specified, results in a hazard expression that does not vary with time in an exposure. As with other time-independent covariate models, additional model terms are required to accommodate added features of an exposure, preventing any one model from accommodating exposure profiles different from those for which the model was designed.

Survival models are also readily based on hazard functions that vary with time in an exposure. Such functions respond to a *covariate process* given by the time-dependent variation of a limited number of covariates throughout an exposure.¹⁶ The covariate process is external to the individual at risk and hence to the model. Because the path of the covariate process through time (e.g., a matrix of pressure, time, inspired gas composition, and exercise that describes the time course of how these parameters vary during an exposure) is not fixed in such models, the models do not need to increase in complexity as the complexity of the covariate process increases. Such models can consequently accommodate the influences of known factors that govern DCS outcomes as the factors come in and out of play during different periods in exposures of arbitrary complexity, but exploitation of this capability has been limited in models developed to date.

Probabilistic gas and bubble dynamics models of DCS occurrence provide the structural flexibility to accommodate the influences of pressure, inspired gas, and exercise on DCS outcomes as these factors may change in arbitrarily complex exposure profiles. Such models are time-dependent covariate models in which the body is represented by a series of hypothetical tissues or compartments that exchange gas with the environment via the lungs and blood. Risks of DCS are determined as functions of the prevailing volumes and numbers of gas bubbles in the compartments, bubbles that vary in volume by diffusion-limited exchange of gas between the bubbles and their surroundings. Tikuisis and coworkers described the first models of this type based on a model of extravascular gas bubble evolution similar to that described by Gernhardt.^{24,25} Shortly thereafter Gerth and Vann described a time-dependent covariate model of DCS

^a The terms “hazard function” and “risk function” are used synonymously in this report. The hazard is also referred to as the “instantaneous risk.”

occurrence^{26,27} based on a model of gas bubble evolution developed by Van Liew and Hlastala.²⁸ Theoretical inconsistencies in this model of bubble evolution²⁹ were corrected in a more rigorous three region unstirred tissue model able to accommodate multiple bubbles in a compartment.^{30,31} This 3RUT-MB model of gas and bubble dynamics was enhanced in present work to account for effects of exercise and oxygen breathing on *in vivo* gas exchange and bubble nucleation and optimized about laboratory data from 2598 man-exposures in widely varying types of hypobaric decompression profiles.

2. Methods

Our modeling approach followed the paradigm for the pathophysiology of DCS described by Tikuisis and Gerth.¹ Excessively rapid and extensive decompression can cause the hydrostatic pressure in one or more body tissues to fall below the sum of the dissolved gas partial pressures in the tissue, producing a thermodynamically unstable gas-supersaturated state. The latter may be relieved with return to a gas-saturated state either by physiological gas elimination or by *in situ* nucleation and growth of gas bubbles. The instantaneous risk of DCS is assumed to be a function of the numbers and volumes of gas bubbles formed in the latter event. Following the approach pioneered by Haldane and coworkers,³² the body was modeled in present work as a hypothetical series of parallel-perfused compartments. Bubble evolution producing risk of DCS was then modeled in each compartment with an enhanced version of the 3RUT-MB model.

2.1 3RUT-MB Model

Essential features of the 3RUT-MB model are schematized in Figure 1. The hypothetical series of parallel perfused compartments comprising the body is shown on the left, and a detail of one compartment is shown on the right.

As originally described, each compartment was envisioned to be perfused at a constant rate and contain a fixed number of bubbles of potentially different sizes. It was noted in principle that the model could account for the participation of multiple diffusible gases in the evolution of any given bubble, but the equations to do so were not explicitly given. Finally, oxygen was presumed to be present in tissue at a fixed partial pressure and participate in bubble evolution with water vapor and carbon dioxide as an infinitely diffusible gas. The quantitative relationships comprising the original 3RUT-MB model are outlined in Appendix A.

Provisions were added to the model in present work to accommodate hypothetical mechanisms by which risks of DCS may be influenced by performance of exercise during different parts of an exposure profile. These provisions included mechanisms for time-dependent variation of the compartmental perfusion rate and number of bubbles, and for the participation of oxygen as a diffusible gas in bubble evolution with exercise-dependent variation of the tissue oxygen partial pressure. These model enhancements are summarized below and described in more detail in Appendix A. A piece-wise

analytic approximation of the model equations was developed by exploiting the linear structure of the Fick equation, as described in Appendix B. The approximation is formulated as a set of recursive analytic relationships that advance the model state from one integration step to the next throughout an exposure profile.

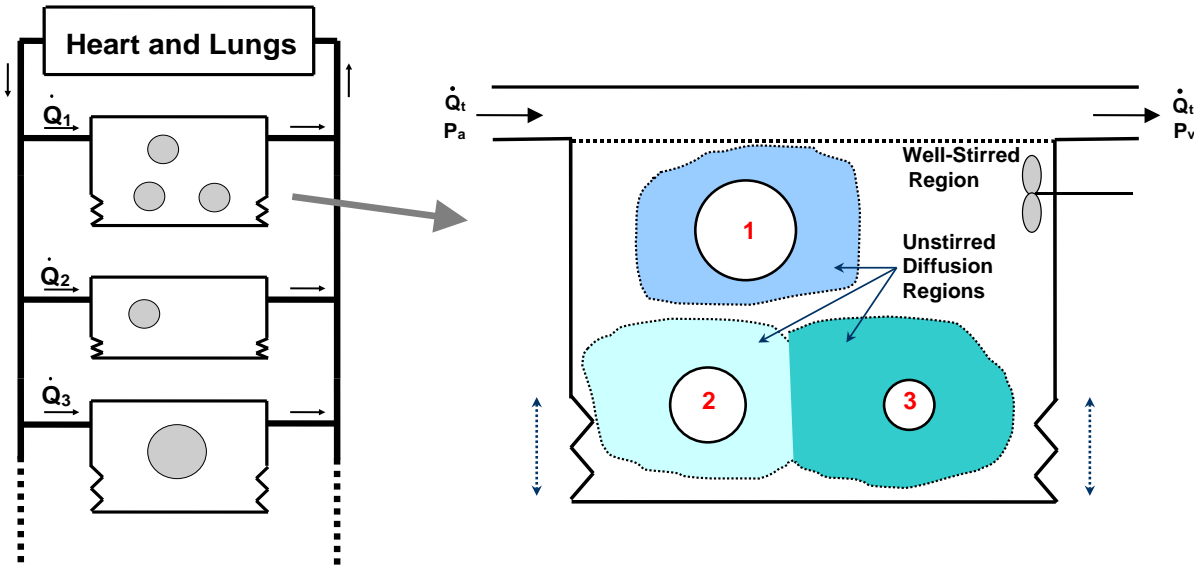


Figure 1. Schematic of the three-region unstirred tissue multiple bubble (3RUT-MB) compartmental model underlying the DCS hazard function in present work. The hypothetical series of parallel perfused compartments comprising the body is shown on the left. Each compartment is perfused with arterial blood at a characteristic volume-average rate of \dot{Q} ($\text{mL}\cdot\text{mL tissue}^{-1}\cdot\text{minute}^{-1}$), which is subscripted to indicate individual compartments. One or more bubbles can nucleate in any compartment depending on the history of ambient pressure and breathing gas. The compartment shown in detail on the right has three bubbles. The diffusion region around each bubble is unstirred and heterogeneously perfused with zero gas flux at the outer boundary indicated by the light dotted line. Bubble 1 is totally isolated while bubbles 2 and 3 have some common boundary, on either side of which gas diffuses in opposite directions. P_a denotes the vector of arterial gas tensions, which is the same for all compartments. P_v denotes the vector of compartment-specific venous gas tensions. Dotted double-headed arrows indicate that the overall compartmental volume varies with bubble volumes, while the compartmental liquid volume remains constant.

Theoretical development of the model in Appendices A and B is presented for arbitrary numbers of hypothetical tissue-blood gas exchange compartments and diffusible gases. The final enhanced 3RUT-MB model in present work, designated 3RUT-MBe1, was a one-compartment model with two diffusible gases, nitrogen and oxygen, implemented with relationships summarized in Appendix C.

2.1.1 Quantification of Exercise

Exercise is the use of energy to generate force to do work or oppose a resistance. Power is the rate of energy usage, or equivalently, the rate of doing work. It is well known that the whole-body O₂ consumption rate, $\dot{V}_{O_2,wb}$, increases linearly with the power output (W/time) for most types of exercise.^{33,34} Accordingly, the intensity of exercise performed during any given period of time in an exposure, regardless of the type of exercise, was characterized in present work by the prevailing $\dot{V}_{O_2,wb}$ during the period. Exercise effects on model parameters in the period were then considered in terms of the exercise intensity level, I_{ex} , given by

$$I_{ex} = \text{MAX}(\dot{V}_{O_2,wb} - \dot{V}_{O_2,wb,rest}, 0.0), \quad (3)$$

where $\dot{V}_{O_2,wb}$ is the rate of whole-body O₂ consumption during the period of exercise and $\dot{V}_{O_2,wb,rest}$ is an assumed rate of whole body O₂ consumption during rest.

2.1.2 Compartmental Oxygen Consumption, Perfusion, and O₂ Tension

Cardiac output and regional blood flow have been shown to be linear functions of the rate of whole body O₂ consumption ($\dot{V}_{O_2,wb}$) and the regional oxygen consumption rate (\dot{V}_{O_2}), respectively.³⁵ It was assumed on this basis that the O₂ consumption rate in a given model compartment is a linear function of the whole body O₂ consumption rate:

$$\dot{V}_{O_2} = m_{V_{O_2}} \cdot I_{ex} + \dot{V}_{O_2,rest}, \quad (4)$$

where $m_{V_{O_2}}$ is the rate of \dot{V}_{O_2} change with I_{ex} , and $\dot{V}_{O_2,rest}$ is the rate of tissue O₂ consumption at rest. The compartmental blood flow rate was then assumed to increase linearly with the compartmental O₂ consumption rate:

$$\dot{Q} = m_Q \cdot (\dot{V}_{O_2} - \dot{V}_{O_2,rest}) + \dot{Q}_{rest}, \quad (5)$$

where m_Q is the rate of change of \dot{Q} with \dot{V}_{O_2} , \dot{Q}_{rest} is the resting compartmental blood flow rate at $\dot{V}_{O_2} = \dot{V}_{O_2,rest}$, and \dot{Q} and \dot{Q}_{rest} are in units of flow per unit tissue volume. Exercise then directly affects the kinetics of blood-tissue exchange of gas k by altering the compartmental time constants for such exchange:

$$\tau_k = \frac{\alpha_{t_k}}{\dot{Q}\alpha_{b_k}} \text{ for inert gases and } \tau_{O_2} = \frac{\alpha_{t_{O_2}}}{\dot{Q}\alpha'_{O_2}} \text{ for O}_2, \quad (6)$$

where α_{t_k} and α_{b_k} are the solubilities of inert gas k in tissue and blood, respectively, and α'_{O_2} is the slope of the whole blood O_2 solubility curve in the region of the prevailing venous O_2 tension [see Eq. (B.50)]. The respective compartmental gas exchange half times are $\tau_{k,1/2} = \ln(2) \cdot \tau_k$ and $\tau_{O_2,1/2} = \ln(2) \cdot \tau_{O_2}$.

Exercise also affects tissue O_2 tension by increasing the rate of metabolic O_2 consumption:

$$C_{av,O_2} = C_{a,O_2} - C_{v,O_2} = \dot{V}_{O_2} / \dot{Q} \quad (7)$$

Because oxygen constitutes only a small fraction of the overall gas pressures during diving, most models for computing diving decompressions either neglect the presence of oxygen altogether or consider oxygen to contribute only a constant small quantity to the prevailing total gas tension in tissue.³⁶ In earlier gas and bubble dynamics models, oxygen was additionally assumed to be infinitely diffusible – and always in equilibrium – between bubble and tissue.^{13,25-27} A number of models of DCS incidence in diving exposures have been developed in which oxygen at arterial tensions above a certain threshold tension contributes to DCS risk accumulation as if it were an inert gas.^{37,38} More rigorously, the compartmental oxygen tension varies nonlinearly with lower values of the arterial oxygen tension because of the metabolic consumption of oxygen and the sigmoidal nature of the oxyhemoglobin dissociation curve.³⁹ This nonlinear behavior and its dependence on exercise was accommodated in the present model by consideration of exercise-dependent variations of compartmental oxygen consumption and numerical integration of the oxyhemoglobin dissociation curve [Appendix B].

Exercise-induced changes in compartmental gas exchange time constants were assumed to occur instantaneously with onset or cessation of exercise and were incorporated into expressions for the time-dependence of compartmental dissolved gas tensions as described in Appendix A. Methods to account for kinetics of such changes are considered in Appendix B.

2.1.3 *Bubble Nucleation*

The number of bubbles in each modeled compartment was allowed to increase with the compartmental gas supersaturation during decompression, as nuclei were recruited from a hypothetical pre-existing population in the compartment. The population of pre-existing nuclei was assumed to have a logarithmic distribution of sizes that could be affected by pressure and exercise. Increases in pressure shifted each distribution to smaller, more difficult to recruit sizes, while exercise shifted each distribution to larger, easier to recruit sizes. The nucleation model for this recruitment process was adopted from Yount^{40,41} as described in Appendix A.

Notably the Yount model considers only integer numbers of bubbles, with one sensibly being the minimum nonzero number of bubbles in a compartment. In contrast, the

present implementation of the Yount model allows fractional numbers of bubbles to avoid discontinuities in the hazard as compartmental gas supersaturations increase during decompression. The rationale for this allowance follows from the recognition that each modeled gas exchange compartment is not associated with any particular anatomic site, but is considered to represent a collection of sites distributed arbitrarily throughout the body. Quantities characterizing the compartment are averages from across the collection of distributed elements that the compartment represents. Thus, most compartmental properties, such as the blood-tissue gas exchange half-time, are intrinsic properties independent of the volumes or distribution of elements comprising the compartment, while the bubble number is an extrinsic property dependent in an indeterminate fashion on the overall volume of the compartment.

2.1.4 Venous Gas Emboli (VGE) Formation

VGE formation caused by migration of bubbles from the tissue into the vasculature was modeled as a mechanism for non-diffusive loss of gas from the tissue.⁴² VGE formation was assumed to decrease the number of bubbles remaining in a modeled compartment while the size of the remaining bubbles remains unchanged. The number of bubbles in a compartment was reduced at the end of each integration step by a proportion, LR, of the prevailing number of bubbles, so that the number remaining for the next integration step was given by

$$N_{b_{n+1}} = \text{MAX} \left[0, N_{b_n} \cdot (1 - \text{LR}) \right], \quad (8)$$

where the subscripts n and $n+1$ refer to values at the beginning and end of the n^{th} integration step. In turn, the proportionality factor was increased with bubble volume:

$$\text{LR} = (V_b - V_{r0}) \cdot \dot{N}_{\text{VGE}} \cdot \Delta t_n, \quad (9)$$

where $(V_b - V_{r0})$ is the amount by which the prevailing volume of any one of the N_b bubbles in the compartment exceeds the nucleonic volume and \dot{N}_{VGE} ($\text{mL}^{-1}\text{min}^{-1}$) is the rate of change of the proportionality constant. The number of bubbles lost to the vasculature as VGE at the end of each $[t_n, t_{n+1}]$ interval is $N_{b_n} - N_{b_{n+1}}$. Note that this bubble loss increases with exercise to the extent that exercise increases N_{b_n} .

2.2 Definition of the Hazard Function

As described in Appendix D, the instantaneous risk of DCS at time t , $h(t)$, was expressed as a function of the prevailing compartmental bubble volumes and modified bubble number at the end of each integration step:

$$h(t) = \sum_j^{n_c} g_j (V_{b,j} - V_{r0j}) \cdot (N_{b,j})^{B_{N,j}}, \quad (10)$$

where n_c is the number of modeled gas exchange compartments, g_j is a compartmental gain factor, and the prevailing number of bubbles $N_{b,j}$ in each compartment at time t is raised to a power of $B_{N,j}$. The instantaneous risk was integrated over time by numerical trapezoidal integration, while varying the time step size depending on the rate of bubble growth or resolution (Appendix A, Section 8.5). Note that the compartmental contribution to the instantaneous risk increases more sharply with increasing compartmental bubble number as the power factor $B_{N,j}$ increases.

2.3 Model Optimization by Likelihood Maximization

The implementation of Eq. (10) contains parameters, $\beta = (\beta_1, \beta_2, \dots, \beta_p)$, that govern its quantitative behavior. These parameters scale the influences of explanatory variables (e.g., pressure, time, inspired O_2 fraction, etc.) or are required “mechanistic” constants.⁴³ Values of these parameters required to yield model performance in best possible conformance with selected training data are found by maximizing a likelihood function of the parameters.^{16,17} The likelihood, $L(\beta)$, of one or more trials is defined as the probability of the observed overall outcome. Assuming statistical independence of all possible outcomes, the likelihood of an individual exposure, $l_i(\beta)$, is the product of the probabilities of the possible outcomes, each conditioned by actual experience through the influence of an outcome variable, δ_i :

$$l_i(\beta) = P_i(E)^{\delta_i} \cdot P_i(0)^{(1-\delta_i)}, \quad (11)$$

where $P_i(E)$ and $P_i(0)$ are given by Eqs. (1) and (2), respectively, $\delta_i = 0$ if DCS does not occur in the exposure, and $\delta_i = 1$ if DCS occurs. Marginal outcomes, for which $0 < \delta_i < 1$, are also allowed.^b The likelihood of a trial of N exposures is then given as the product of the likelihoods of the individual exposures:

$$L(\beta) = \prod_{i=1}^N l_i(\beta). \quad (12)$$

Parameter values were systematically adjusted to maximize Eq. (12) about the training data described in Section 2.4 using an implementation of the Marquardt algorithm.⁴⁶ For convenience, Eq. (12) was cast in terms of the natural log of the likelihood to obviate need to work with excessively small-valued numbers. The results are the “best fit” values of the parameters for use in model applications. The maximum log likelihood

^b The tendency for marginal outcomes in diving exposures to occur predominantly in only certain profile types has been shown to adversely bias model performance on other types of profiles, motivating a recommendation to code marginal events as nonevents ($\delta_i = 0$).^{45,45} The few marginal outcomes in the present altitude data were coded with outcome variable $\delta_i = 0.1$.

achieved by the model on the data serves as a quantitative index of model goodness-of-fit. A central and singularly most important feature of this approach is that a model is made to provide estimates of DCS risks and times of DCS occurrence that are in closest possible agreement with observed DCS incidences and times of occurrence in the actual experience expressed in the training data.

2.4 Model Training Data

2.4.1 *Augmented NMRI Standard format*

The description of the pressure and respired gas profile for each exposure in the model training data was coded in Augmented NMRI Standard (ANS) format, which comprised a record of exposure outcome followed by a sequence of nodes that gave the pressure and inspired gas composition at successive times in the exposure.²⁷ Each node gave the conditions prevailing at the end of a profile stage or segment that was either a travel stage (compression or decompression) or an isobaric stage, either of which may have ended with start of a breathing gas switch that completed in the ensuing stage or stages. An unbroken description of the profile was obtained by linear interpolation in the time domain between successive nodes. The model was exercised on the profile by sequentially processing these nodes, preserving the model state at the end of each stage as the initial state for the next stage. The format accommodates an arbitrary number of nodes per profile, allowing representation of profiles of arbitrary complexity.

2.4.2 *USAF Data*

Altitude exposure data from the United States Air Force Armstrong Laboratory (USAFAL) Hypobaric Decompression Sickness Database comprised a large portion of the model training data. This database existed in two different architectures as it evolved from its inception in the early 1980s to its most current form described by Webb.⁴⁷

In its first form, the database contained exposure profile information sufficient to construct a detailed node-by-node description of each profile.⁴⁸ This information faithfully described each exposure as it was actually completed: Time at altitude ended at actual time of descent start when the occurrence of DCS caused termination of the exposure before completion of the planned time at altitude. Data for 1194 man-exposures completed at USAFAL between 1983 and 1993 had been extracted from the data base in this first form for earlier work¹³ and was used in present work. DCS onset t_1 and t_2 times for application of Eq. (2) were arbitrarily defined for each exposure that culminated with a DCS incident. In such cases, t_1 and t_2 were defined to bracket the last 10 min of the isobaric stage preceding final descent to ground level. This was equivalent to assuming that the subject remained DCS-free until 10 min before reporting DCS, which then caused immediate termination of the exposure with descent to ground. These t_1 and t_2 assignments are consistent with the use of DCS onset as the experimental end-point for the exposures in the USAFAL protocols. Thus, with the

exception of DCS cases that might have occurred after final return to ground, the assumed t_1 and t_2 values did not differ substantially from the actual values.

Data for an additional 673 man-exposures completed after 1993 were extracted from the USAFAL Hypobaric Decompression Sickness Database in its second and current form.⁴⁷ In this form, the detailed node-by-node description of each profile is replaced with a summary description of the profile as it was planned: Actual time at altitude is replaced with planned time at altitude, although time of DCS onset is recorded for those exposures that terminated with DCS. DCS onset t_2 times were taken as the recorded DCS onset times and, as with the legacy USAFAL data, each corresponding t_1 time was arbitrarily defined to be 10 min before the recorded DCS onset time.

2.4.3 NASA Data

Data from eleven chamber tests conducted at NASA-JSC between 1980 and 1995 and recorded in the NASA-JSC historical database of altitude tests comprised the preponderance of the remaining data used for model calibration.^{49,50,51,52,53} Missing and erroneous entries were corrected by review of original laboratory logbooks. Deficiencies in profile descriptions were rectified and DCS onset times were determined from case summaries. The number of protocols per test varied from 1 to 6, with a total of 31 across the 11 tests. The data were from 237 subjects; 176 males and 61 females; who participated in a total number of 549 altitude exposures, 82 of which culminated in diagnosed cases of DCS and 467 of which were completed with no DCS for a 14.9% overall incidence of DCS. Data for male and female subjects within a given test series were pooled.

As in the legacy USAFAL data, time at altitude in each profile ended at the actual time of descent start when the occurrence of DCS caused termination of the exposure before completion of the planned time at altitude. No DCS onset after return to ground was recorded. Profiles were terminated at time of completion of planned time at altitude if DCS did not occur, or at time of DCS onset if DCS occurred.

Data from an additional 178 man-exposures completed at Duke University, the Canadian Defense and Civil Institute of Environmental Medicine, and the University of Texas Medical Branch in the course of Phases I through IV of a NASA prebreathe reduction protocol^{54,55,56} comprised the remainder of the model training data.

2.4.4 Exercise Coding

As described in Section 2.1.1, periods of exercise in each profile were characterized by the whole body O_2 consumption rate during the period. Work rates reported in units of percent peak whole body O_2 consumption rate ($\dot{V}_{O_2,peak}$) were converted to absolute whole-body O_2 consumption rates in $L \cdot \text{min}^{-1}$ by assuming $100\% \dot{V}_{O_2,peak} = 3.15 L \cdot \text{min}^{-1}$

^{1. c} Work rates reported in watts (W) were converted to whole-body O₂ consumption rates with the following quadratic formula parameterized by fitting to the data of Astrand, et. al.,³⁴ highlighted in Table 1:

$$\dot{V}_{O_2} \text{ (L}\cdot\text{min}^{-1}\text{)} = \beta_0 + \beta_1 W + \beta_2 W^2, \quad (13)$$

where:

$$\beta_0 = 3.0536 \times 10^{-1}$$

$$\beta_1 = 1.1369 \times 10^{-2}$$

$$\beta_2 = 5.4762 \times 10^{-6}$$

The goodness-of-fit of Eq. (13) to its calibration data is shown graphically in Figure 2. The fitted y-intercept, $\beta_0=0.305 \text{ L}\cdot\text{min}^{-1}$, is the value used for the resting whole-body \dot{V}_{O_2} assumed for all subjects.

Work rates reported in kcal·hr⁻¹ were converted to whole-body O₂ consumption rates in L·min⁻¹ by assuming 0.2 L O₂ are consumed to produce each kcal of energy (5 kcal·L O₂⁻¹).³³ Finally, work rates reported in mL O₂·kg⁻¹·min⁻¹ were converted to whole-body O₂ consumption rates in L·min⁻¹ by assuming a subject body weight of 70 kg.

Along with the calibration data for Eq. (13), Table 1 gives metabolic rates in various units during exercises typical of those performed during USAF and NASA EVA altitude exposures. The tabulated data for whole body $\dot{V}_{O_2,wb}$ versus work rate in watts are included in Figure 2.

^c A whole-body $\dot{V}_{O_2,peak}$ of 40.8 mL·kg⁻¹·min⁻¹ was assumed for development of a NASA Exercise Prebreathe Model.⁵⁷ This value corresponds to 3.15 L·min⁻¹ for a 77.3 kg subject.

Table 1. Metabolic Rates During Exercise*

| Watts | kcal·hr ⁻¹ | mL O ₂ ·kg ⁻¹ ·min ⁻¹ | L·min ⁻¹ | % $\dot{V}_{O_{2,peak}}$ |
|--------|-----------------------|--|---------------------|--------------------------|
| 0.00 | 91.6 | 4.4 | 0.305 | 9.7 |
| 6.46 | 113.8 | 4.8 ¹ | 0.379 | 12.0 |
| 8.81 | 121.8 | 5.8 ² | 0.406 | 12.9 |
| 14.90 | 142.8 | 6.8 ³ | 0.476 | 15.1 |
| 20.59 | 162.5 | 7.7 | 0.542 | 17.2 ⁴ |
| 21.59 | 166.0 ⁵ | 7.9 | 0.553 | 17.6 |
| 25.00 | 177.9 | 8.5 | 0.593 | 18.8 |
| 28.17 | 189.0 | 9.0 | 0.630 | 20.0 |
| 50.00 | 266.3 | 12.7 | 0.888 (0.9) | 28.2 |
| 100.00 | 449.1 | 21.4 | 1.497 (1.5) | 47.5 |
| 139.66 | 600.0 | 28.6 | 2.000 | 63.5 |
| 150.00 | 640.2 | 30.5 | 2.134 (2.1) | 67.7 |
| 155.45 | 661.5 | 31.5 | 2.205 | 70.0 |
| 167.44 | 708.8 | 33.8 | 2.363 | 75.0 |
| 200.00 | 839.5 | 40.0 | 2.798 (2.8) | 88.8 |
| 225.68 | 945.0 | 45.0 | 3.150 | 100.0 |
| 250.00 | 1047.0 | 49.9 | 3.490 (3.5) | 110.8 |

* Highlighted data from Table 9.5 in Astrand, et al.³⁴

1.) knee bends and overhead presses; "BSI exercises."⁵⁸

2.) light exercise, Shuttle suit donning simulation, NASA PRP.⁵⁶

3.) leg ergometer exercise, NASA PRP.⁵⁶

4.) work rate of 15-20% $\dot{V}_{O_{2,peak}}$ stated for 4-station (3 exercise, 1 rest)/16 min NASA EVA exercise simulation.⁵⁹

[The simulation consisted of arm exercise for 4 min at each of 3 stations;

a) subject standing: cycle ergometer hand-cranking at 24 rpm, 4

Newtons resistance, alternating arms after every two revolutions,

b) subject standing: apply 25 ft-lbs force with torque wrench for 5 sec to each of 5 bolt-like projections mounted on the top, bottom, left, right, and forward-facing surfaces of a wall-mounted rectangular box, alternating arms from position-to-position, and

c) subject seated: rope pull against 17 lb (8.5 kg) resistance from arm's reach at head level to waist once each 5 sec, alternating left, right, then both arms;

and a 4-min period of Doppler VGE monitoring during which subject was supine and sequentially flexed the four limbs while otherwise remaining at rest. The four-station cycle was repeated until completion of the intended EVA simulation.]⁶⁰

5.) average metabolic rate of 166 ± 17 kcal·hr⁻¹ cited for NASA EVA exercise simulation described in (3) above.⁶¹

[also ref 62: males 119.4-193.3 kcal·hr⁻¹ (147.95 ± 24.51 SD); females 91.5-114.5 kcal·hr⁻¹ (104.6 ± 8.9 SD)].

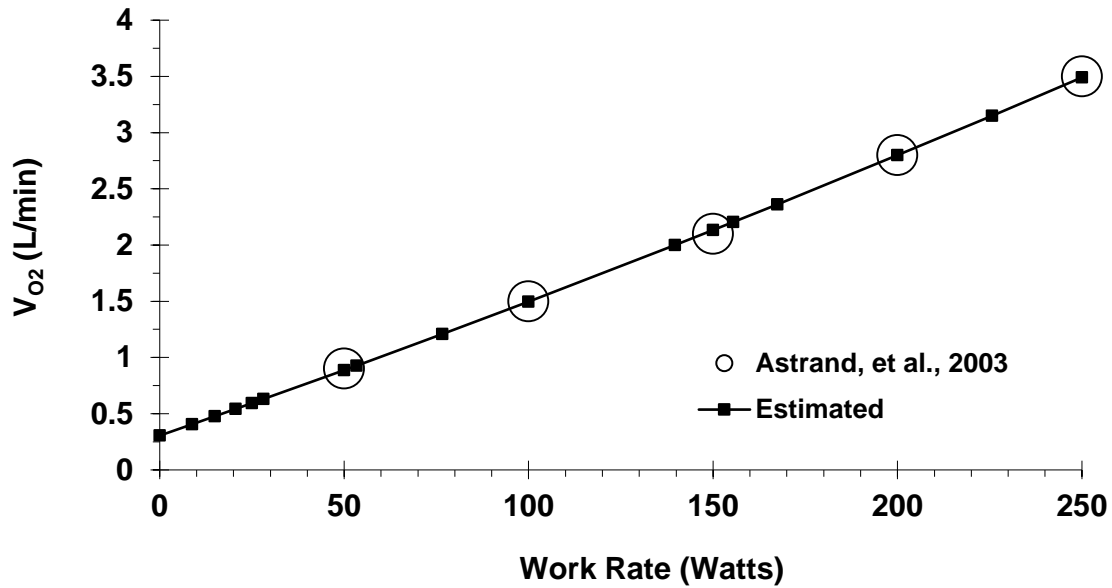


Figure 2. Whole-body O_2 consumption rate, $\dot{V}_{O_2,wb}$, versus work rate. The extrapolated value for $\dot{V}_{O_2,wb,rest}$ at zero work rate is $0.305 \text{ L}\cdot\text{min}^{-1}$.

Exercise performed during a segment was characterized by an entry in the ANS code for the segment equal to the subject $\dot{V}_{O_2,wb}$ during the segment.^{63,64} No exercise information was required for a segment if the segment was completed with the subject at rest and, conversely, subjects during segments coded without exercise information were presumed to be at rest during the segment. This convention allowed the modeling system to remain consistent with earlier profiles coded in the ANS format without exercise information, but required specification of the resting rate of whole-body O_2 consumption, $\dot{V}_{O_2,wb,rest}$, for the subject in each profile. In present work, $\dot{V}_{O_2,wb,rest} = 0.305 \text{ L}\cdot\text{min}^{-1}$ was assumed for all subjects in all profiles [Eq. (13)]. Nodes were added with appropriate time and exercise intensity information to accommodate changes in exercise intensity during segments in which no other covariate changed.

2.4.5 Overall Training Data Summary

The complete training dataset, named A1309, is summarized in Appendix E, excepting four man-exposures; man-flight numbers 88073, 91097, 93022, and 93033; of the 1194 exposures extracted from the original USAFAL Hypobaric Decompression Sickness Database. Each of these exposures had a unique profile that could not be associated with any study in the database and each culminated with occurrence of DCS. The coded NASA data included information on observed grades (0 – IV Spencer scale) and onset times of venous gas emboli detected with Doppler ultrasound instruments, but such information was not used in the present modeling work.

3. Results

3.1 Optimized 3RUT-MBe1 Model Parameters

The single compartment 3RUT-MBe1 model was fit to the combined NASA and USAF altitude data to obtain the optimized parameters given in Tables 2 and 3. Parameters assigned fixed values in the optimization process are indicated in Table 3.

Table 2. 3RUT-MBe1 Model Fit Statistics

Profiles in dataset = 2153
Total # individual trials = 2598
Total # DCS marginals = 3
Total # DCS positives = 862
Overall DCS incidence = 33.191 %

| MODEL | Log Likelihood |
|-----------|----------------|
| Fitted | -3774.066872 |
| Perfect | -0.97524892 |
| I-O Null | -1651.0873 |
| c-index = | 0.674018 |

| Tissue | Gas | Half-time (min) |
|--------|----------------|-----------------|
| 1 | O ₂ | 284.05 |
| | N ₂ | 284.05 |

Integration control parameters*:

5.000×10^{-04} : dt_{\min} ; Minimum time step (Max resolution, minutes)

1.000×10^{-02} : dt_{\max} ; Maximum time step (Min resolution, minutes)

6.931×10^{-03} : dt_k ; time step decay constant

*See Appendix A, Eq. (A.52)

The optimized model yields a log likelihood of -1771.5 and c-index^d of 0.612 on the 1194 man-exposures from the first version of the USAFAL database compared to -1742.0 and 0.560, respectively, yielded on the same data by an earlier model in which DCS was expressed in terms of the evolution of only a single bubble in the modeled compartment, exercise effects on blood tissue gas exchange were not considered, and compartmental dissolved oxygen was considered as a component of the fixed metabolic gases.¹³ Reoptimization of the present model about these data yielded a log likelihood of -1743.0 and c-index of 0.645.

^d Concordance index. Gives the fraction of all possible pairs of exposures in the data for which the model-estimated risks of DCS are in the same order as the observed incidences of DCS.⁶⁵

Table 3. Optimized 3RUT-MBe1 Model Parameters

| Parameter | Type* | Value | Std Error | Coeff. of Variation |
|--|-------|-----------|-----------|---------------------|
| P_{H_2O} ; water vapor pressure (mm-Hg) | F | 4.700E+01 | --- | --- |
| RQ; Respiratory Quotient | F | 1.000E+00 | --- | --- |
| P_{t,CO_2} ; Tissue CO_2 partial pressure (mm-Hg); all tissues. | F | 4.500E+01 | --- | --- |
| Gain, g | A | 6.188E-02 | 7.38E-03 | 1.19E-01 |
| α_{b,O_2} ; O_2 solubility in blood | F | 2.356E-02 | --- | --- |
| α_{b,N_2} ; N_2 solubility in blood | F | 1.410E-02 | --- | --- |
| N_b^0 ; Total # nuclei | A | 1.198E+00 | 8.70E-02 | 7.26E-02 |
| β^0 ; initial nuclei size distribution slope | A | 4.868E-05 | 1.11E-06 | 2.27E-02 |
| M; elastic modulus (atm·V ⁻¹) | A | 1.341E-07 | 9.09E-02 | 6.77E+05 |
| \dot{N}_{VGE} ; VGE gas loss rate (mL ⁻¹ ·min ⁻¹) | A | 4.758E+00 | 3.28E-01 | 6.89E-02 |
| σ_c factor | A | 1.964E+01 | 1.30E+00 | 6.64E-02 |
| α_{t,O_2} ; [mL(SPD,37)·mL ⁻¹ ·atm ⁻¹] | A | 4.536E-02 | 2.70E-03 | 5.95E-02 |
| $K\alpha_{N_2}$; N_2 solubility factor: $\alpha_{t,N_2} = K\alpha_{N_2} \cdot \alpha_{t,O_2}$ [mL(SPD,37)·mL ⁻¹ ·atm ⁻¹] | F | 5.985E-01 | --- | --- |
| V_t ; tissue volume (mL) | A | 5.279E-02 | 6.51E-03 | 1.23E-01 |
| \dot{Q} ; blood flow rate (mL·min ⁻¹) | A | 4.698E-03 | 2.99E-04 | 6.37E-02 |
| D_{t,O_2} ; O_2 diffusivity (cm ² ·min ⁻¹) | A | 1.414E-03 | 7.61E-05 | 5.39E-02 |
| KD_{N_2} ; N_2 diffusivity factor: $D_{t,N_2} = KD_{N_2} \cdot D_{t,O_2}$ | F | 9.091E-01 | --- | --- |
| B_N ; bubble number power factor | A | 2.172E+00 | 3.99E-02 | 1.84E-02 |
| P_{crush} decay time constant | A | 2.014E+02 | 2.33E+02 | 1.15E+00 |
| $m_{\beta_{ex}}$; ($\beta_{ex} = 1 + m_{\beta_{ex}} \cdot I_{ex}$) | A | 6.162E-01 | 4.52E-02 | 7.33E-02 |
| $\dot{V}_{O_2,rest}$; \dot{V}_{O_2} @ rest | A | 4.401E-05 | 2.12E-06 | 4.82E-02 |
| $m_{\dot{V}_{O_2}}$; slope \dot{V}_{O_2} vs I_{ex} | A | 1.677E-03 | 6.90E-04 | 4.12E-01 |
| $m_{\dot{Q}}$; slope β_f vs \dot{V}_{O_2} | A | 6.997E+00 | 3.14E+00 | 4.49E-01 |
| σ ; surface tension (dyne·cm ⁻¹) | F | 30 | --- | --- |

*A ≡ adjustable parameter

A1309-3RUT-MBe1

F ≡ fixed parameter

3.2 Model Goodness-of-Fit

3.2.1 Observed and Estimated DCS Occurrence Density Distributions

Goodness-of-fit of the optimized model is illustrated graphically in Figure 3 by comparison of the observed DCS occurrence density distribution for the training data with that estimated for the data by the model. Eleven profiles accounting for 8.3 observed cases of DCS are omitted in this analysis for lack of t_1 and t_2 data. The small numbers of observed (30.9) and estimated (41.6) cases of DCS in the hours before the last decompression occurred after earlier decompressions in repetitive altitude and staged ascent profiles. The observed incidence of DCS onset increases sharply after the last decompression and peaks in the second hour after the last decompression. The shape of the estimated occurrence density distribution faithfully follows that of the observed distribution but with a tendency for overprediction before last decompression and a consistent trend for underprediction after last decompression. (The hour-by-hour difference between observed and estimated numbers of DCS cases is illustrated in Figure 4.) As a result, the model estimates a total number of 793.9 DCS cases (the sum of the illustrated numbers of estimated cases in each hour) compared with a total number of 854.0 observed cases.

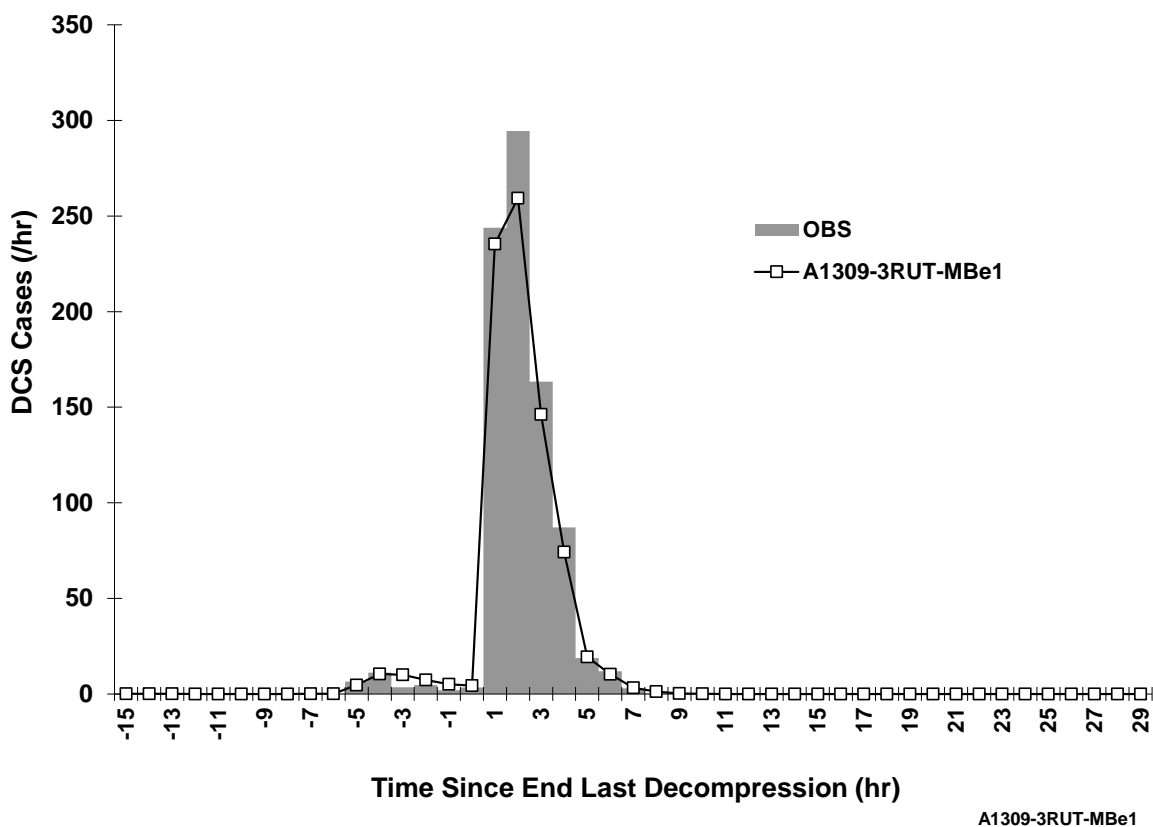


Figure 3. Observed and model-estimated occurrence density distributions for model training data computed at hourly resolution relative to the time of completion of last decompression.

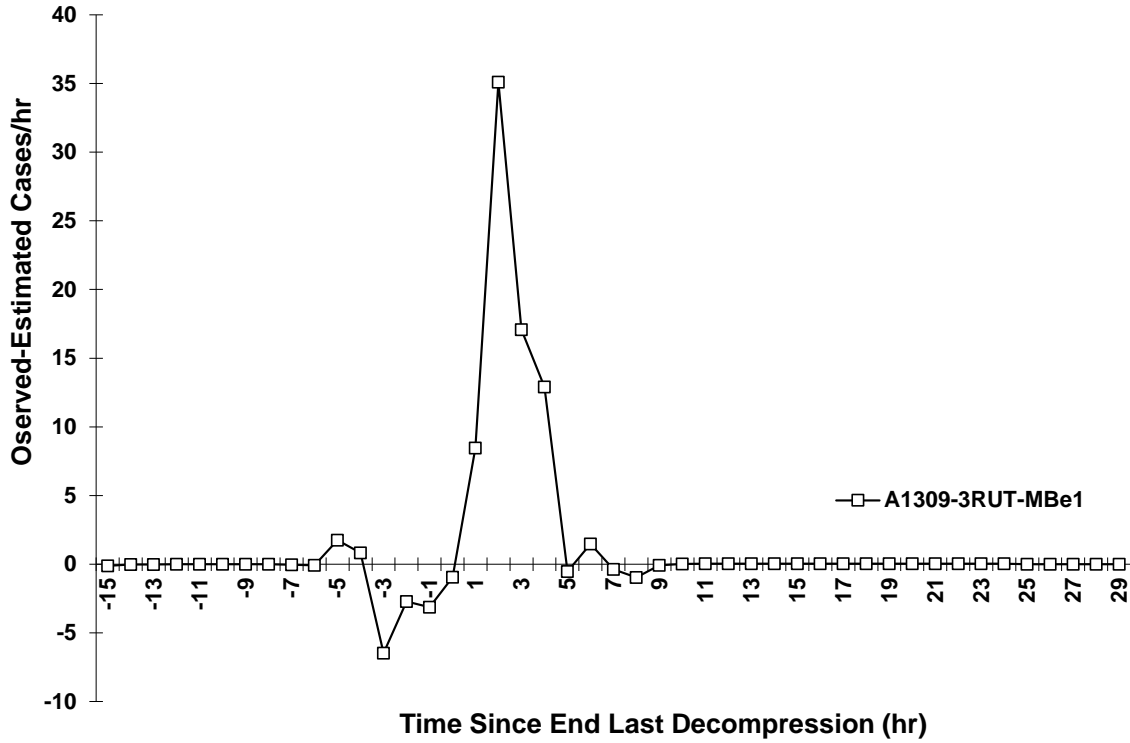


Figure 4. Differences between the observed and estimated numbers of DCS cases in hourly intervals before and after the time of completion of last decompression.

3.2.2 Pearson Residuals and Global Chi-Square

Model fit was also assessed by examining group-specific and global Pearson χ^2 statistics.¹⁷ Examination of group-specific residuals is useful to distinguish areas in a data set over which a model performs well from those over which it performs poorly. The squared Pearson residual for each group is given by

$$(\text{Pearson residual}_k)^2 = \frac{(o_k - n_k \cdot \bar{\pi}_k)^2}{n_k \cdot \bar{\pi}_k \cdot (1 - \bar{\pi}_k)}, \quad (14)$$

where o_k is the number of observed DCS cases, n_k is the number of man-exposures, and $\bar{\pi}_k$ is the average model-estimated P_{DCS} for exposures in the k^{th} group given by⁶⁶

$$\bar{\pi}_k = \sum_{j=1}^{c_k} \frac{m_j \cdot \pi_j}{n_k}. \quad (15)$$

In Equation (15), c_k is the number of profiles in the k^{th} group and m_j and π_j are the number of exposures and the model-estimated P_{DCS} for the j^{th} profile in the group, respectively.

In place of the group average model-estimated risk given by Eq. (15), all profiles in each group were assumed to have estimated DCS risk equal to that for the profile with the highest estimated risk in the group. That profile was inevitably the profile with the longest time at altitude in the group, a profile that the subject had completed DCS-free. Coded times at altitude for profiles completed without DCS in each group were nearly the same and were within minutes of the planned times at altitude. Thus, the risk estimates for profiles that were terminated early due to DCS occurrence were adjusted for the unrealized risks that would have accumulated to produce the same outcome had the profiles been continued to the planned times at altitude. These adjustments cast the present goodness-of-fit assessments in the same form as those for time-independent covariate models developed by other workers for profiles with fixed times at altitude; models based on planned times at altitude or models fit only to profiles with the same times at altitude.

Results for all of the 117 groups in the training data are shown in Appendix F with the groups in order of increasing squared Pearson residual. Also shown is the running sum of the squared Pearson residual,

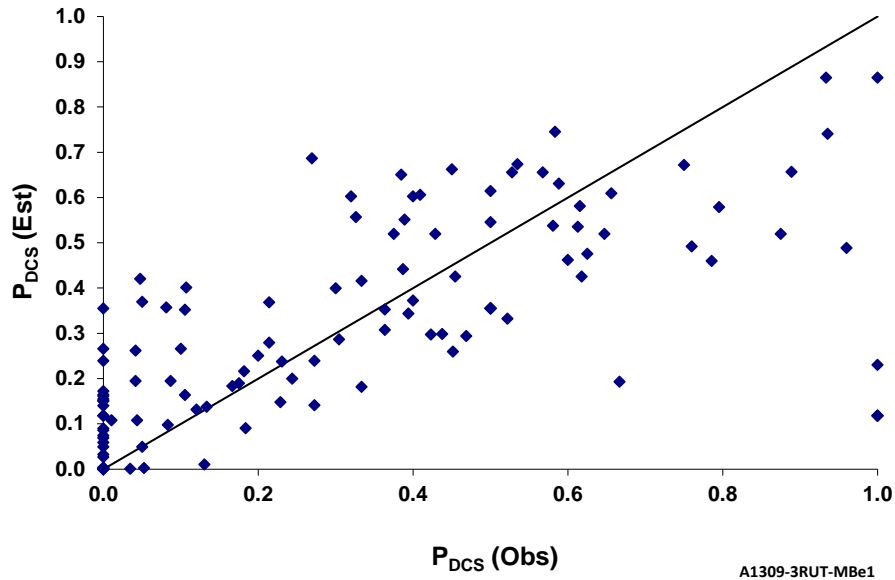
$$\chi^2 = \sum_{k=1}^g (\text{Pearson residual}_k)^2 = \sum_{k=1}^g \frac{(o_k - n_k \cdot \bar{\pi}_k)^2}{n_k \cdot \bar{\pi}_k \cdot (1 - \bar{\pi}_k)}, \quad (16)$$

each of which equals the global chi-square goodness-of-fit statistic for the g groups included in the sum. Each χ^2 follows a chi-square distribution with $g - \rho$ degrees of freedom, where ρ is the total number of adjustable parameters in the model (= 16 in 3RUT-MBe1). As the P-value of the chi-square increases, the evidence decreases that model estimated incidences are statistically different from observed incidences. Evidence is usually considered insufficient to reject a model if the $P(\chi^2)$ of its fit to the data groups exceeds 0.05. The P value corresponding to each χ^2 is shown in the rightmost column of the table in Appendix F. A double line is placed after the last group in the table with $P > 0.05$. Model fit to groups above this line cannot be rejected at $P < 0.05$ significance, while it can be concluded at $P < 0.05$ significance that the model fails to fit the data for groups below the line. Thus, model fit to data for 1621 man-exposures in 84 groups cannot be rejected, while the model fails to fit the remaining data for 973 man-exposures in 33 groups.

All profiles in the CO₂ study series, all profiles in the BSI (Bends Screening Index) study series except those in the BSI-A group, and the preponderance of the profiles completed in the EffctEX (Exercise effects) study series are among the profiles with the highest Pearson residuals. Incidences in the BSI study series were generally underestimated, while incidences in the EffctEX series were generally over-estimated. It can therefore be argued that the data from these studies is not combinable with the other data and that a more restricted training data set that excludes these studies should be used.

The estimated number of DCS cases for each group in Appendix F is plotted versus the corresponding observed number of DCS cases in Figure 5. Panel A illustrates the raw data, while the bubble plot in panel B shows regions where the data are most concentrated. Figure 6 illustrates the same information for only those groups in Appendix F for which the cumulative global chi-square P-value is greater than 0.05. Both figures show that the model overestimates – often substantially – the DCS incidences in groups with no observed cases of DCS.

A



B

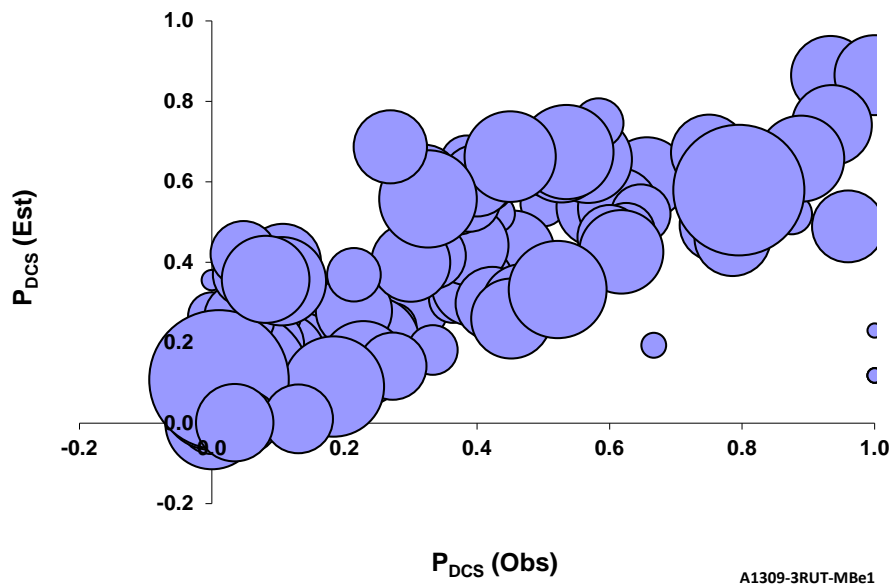
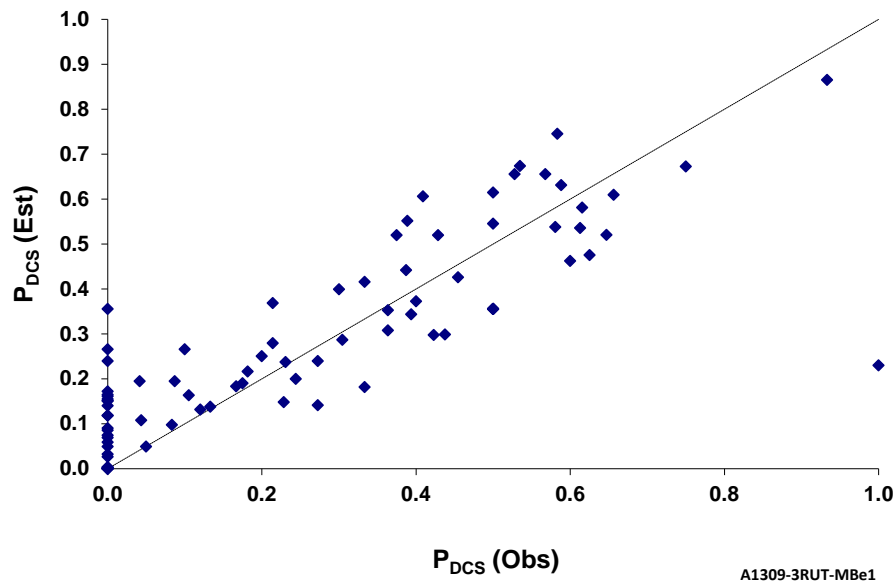


Figure 5. Plots of estimated incidences of DCS versus observed incidences for all groups in the training data. Bubble size in panel B is proportional to the number of man-exposures in each group.

A



B

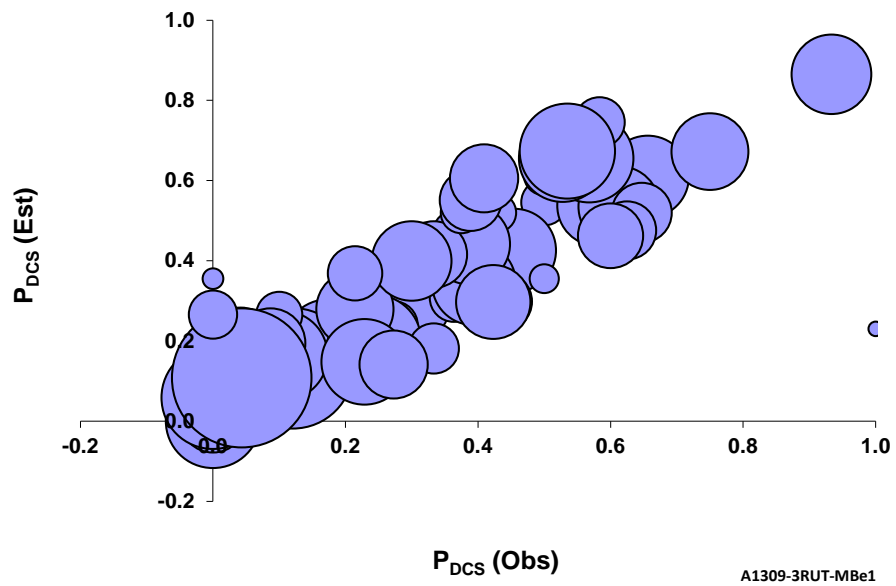


Figure 6. Plots of estimated incidences of DCS versus observed incidences for 84 groups (1621 man-exposures) in the training data fitted by the model (cumulative chi-square $P > 0.05$ for groups in order of increasing Pearson residual). Bubble size in panel B is proportional to the number of man-exposures in each group.

4. Discussion

The present model is the first applied to altitude decompression data able to accommodate how DCS risk is influenced by arbitrarily varying levels of exercise in different periods of a given exposure. This ability is facilitated by a time-dependent covariate model structure that includes explicit consideration of hypothetical exercise effects that act to enhance the efficacy of oxygen breathing before decompression (prebreathe) – reducing the risk of DCS during subsequent altitude exposure – and increase the risk of DCS when exercise is performed after decompression at altitude. The influences of exercise on DCS incidence and time of occurrence in diving exposures were also recently considered in a time-dependent covariate model able to accommodate profiles of arbitrary complexity, but were not shown to be significant.⁶⁷ This result was not unexpected, given that exercise in the diving exposures considered was typically performed only before decompression and tended only to increase risks of DCS. Exercise effects consequently added insufficient heterogeneity to the data to warrant model factors to differentiate profiles with different exercise regimens.

4.1 Prebreathe and Exercise Effects on Gas Elimination

Exercise during prebreathe reduces the risk of DCS by hastening inert gas elimination and reducing the gas supersaturation produced by subsequent ascent to altitude. The modeled exercise-induced enhancement of inert gas elimination is illustrated in Figures 7 and 8. Figure 7 shows the relationship between compartmental oxygen consumption and exercise intensity (whole-body \dot{V}_{O_2}). In turn, the compartmental oxygen consumption is the independent variable in the relationship illustrated in Figure 8 for the dependence of compartmental blood flow and the blood-tissue gas exchange half-time on exercise intensity.

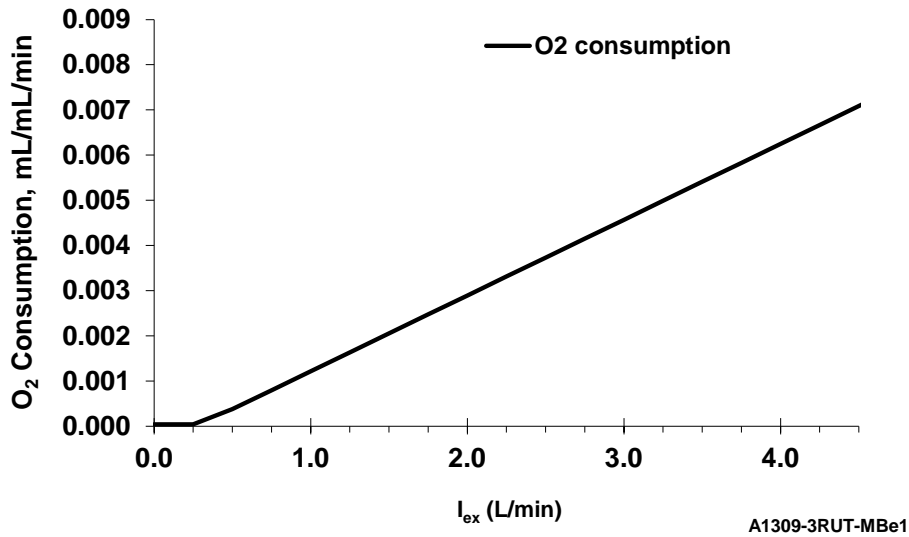


Figure 7. The relationship between compartmental oxygen consumption and whole-body \dot{V}_{O_2} (I_{ex} , L·min⁻¹) given by the parameterized Eq. (4).

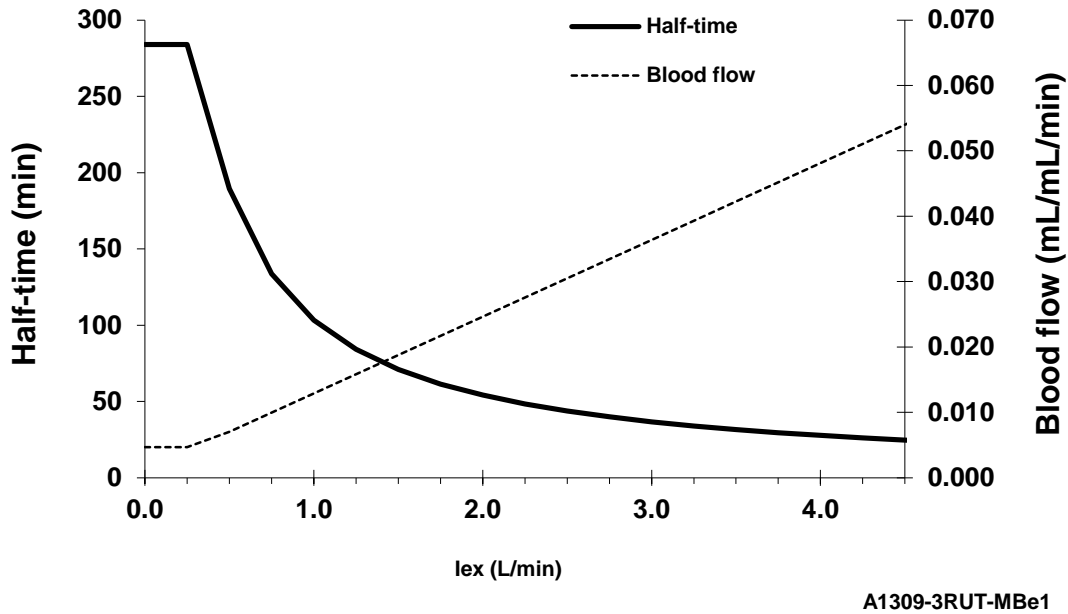


Figure 8. Compartmental blood flow (mL·mL tissue⁻¹·min⁻¹) and corresponding gas exchange half-time (minutes) as functions of whole-body \dot{V}_{O_2} (I_{ex} , L·min⁻¹).

Figure 9 illustrates how different intensities and durations of exercise manifest in the compartmental nitrogen and oxygen tensions during hypothetical 3-hr oxygen prebreathes before 30-min ascents to 0.292 atm (4.3 psia). Ten minutes of 75% $\dot{V}_{O_{2,peak}}$ exercise performed early in an otherwise resting prebreathe abruptly

decreases both nitrogen and oxygen tensions relative to their values in the resting prebreathe. The lower values persist through decompression, resulting in lower gas supersaturations during and after decompression. In comparison, while the divergence to lower nitrogen and oxygen tensions is more gradual with performance of lighter, 17.6% $\dot{V}_{O_{2,peak}}$ exercise throughout most of the prebreathe, both tensions decrease to lower values than in the resting or short, heavy exercise cases by the end of the prebreathe, resulting in the lowest gas supersaturations at altitude among the three cases.

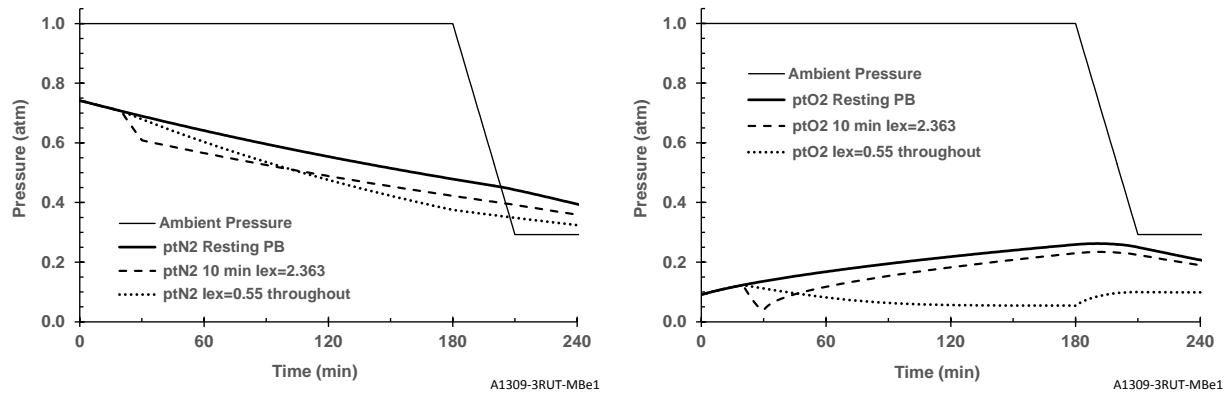


Figure 9. Modeled effects of exercise on compartmental nitrogen elimination (Left Panel) and oxygen tension (Right Panel) during ground-level oxygen prebreathes. Heavy solid lines: Resting throughout; Dashed lines: 10 min 75% $\dot{V}_{O_{2,peak}}$ ($I_{ex} = 2.363$ L·min⁻¹) exercise starting at 20 min, rest at all other times; Dotted lines: 17.6% $\dot{V}_{O_{2,peak}}$ ($I_{ex} = 0.55$ L·min⁻¹) exercise starting at 20 min and continuing until ascent start at 180 min, rest at all other times throughout.

4.2 Prebreathe and Exercise Effects on Bubble Nucleation

Both prebreathe and exercise affect the compartmental populations of pre-existing bubble nuclei from which bubbles are recruited to grow to produce risk of DCS. The numbers of nuclei recruited, along with the volumes they subsequently attain, govern the actual levels of DCS risk produced. Exercise shifts the distribution of nuclei to larger sizes, causing more nuclei to be recruited at a given supersaturation than before the exercise. Figure 10 illustrates this effect on the numbers of bubbles recruited in the presently parameterized model during 0.55 L·min⁻¹ exercise at various altitudes after no-prebreathe ascents.

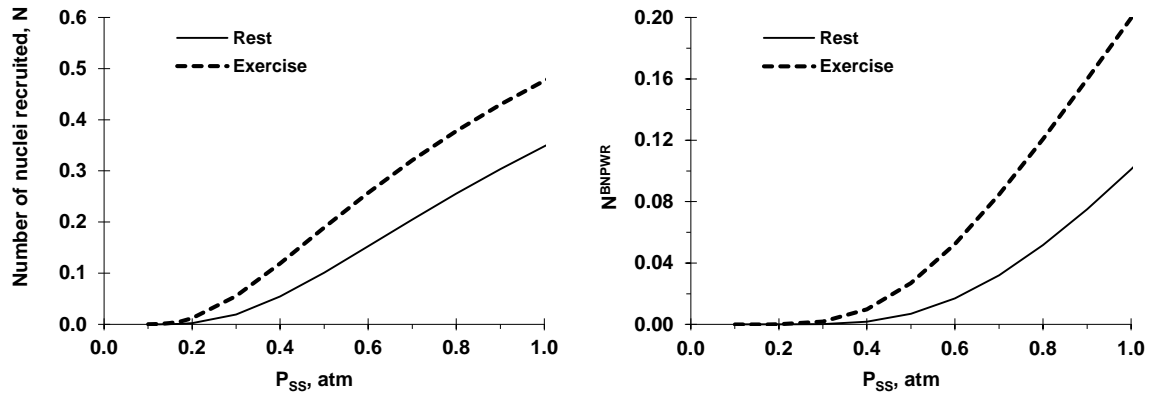


Figure 10. Modeled effects of exercise on number of bubbles nucleated at altitude with no prebreathe. Left Panel: Modeled numbers of bubbles recruited at rest and during exercise, $I_{ex} = 0.55 \text{ L}\cdot\text{min}^{-1}$, at various levels of gas-supersaturation, P_{ss} . Right Panel: $(N_b)^{B_N}$ factor in the hazard function corresponding to the recruited numbers of bubbles at the respective supersaturations in the Left Panel.

The numbers of bubbles recruited at altitude are also affected by oxygen breathing before decompression. Prebreathe shifts the distribution of nuclei to smaller sizes by imposing a P_{crush} , causing fewer nuclei to be recruited at a given supersaturation than without the prebreathe. These effects are illustrated in Figures 11 and 12 for a P_{crush} of 0.139 atm, the P_{crush} produced by a 3-hr resting ground level oxygen prebreathe.

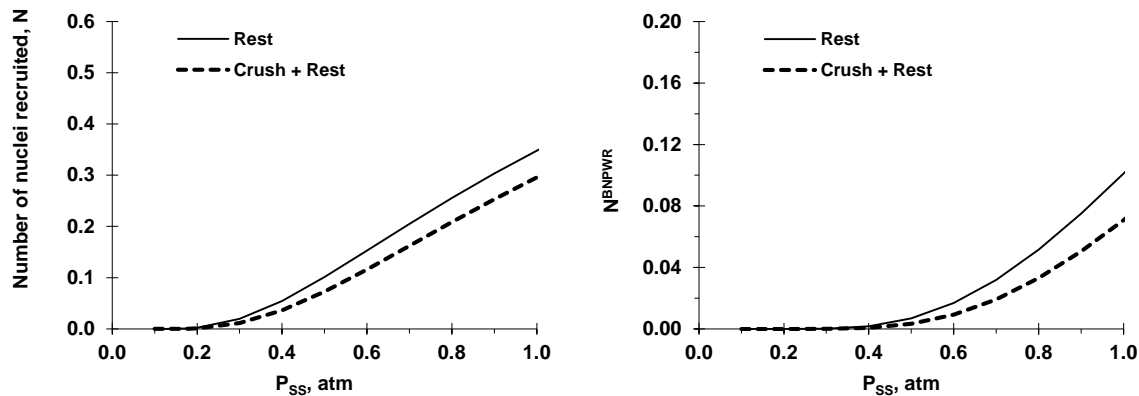


Figure 11. Modeled effects of a 3-hr resting ground-level prebreathe on numbers of bubbles recruited during resting exposures at altitude. Left Panel: Modeled numbers of bubbles recruited at rest and after a 0.139 atm crush at various levels of gas-supersaturation, P_{ss} . Right Panel: $(N_b)^{B_N}$ factor in the hazard function corresponding to the recruited numbers of bubbles at respective supersaturations in Left Panel.

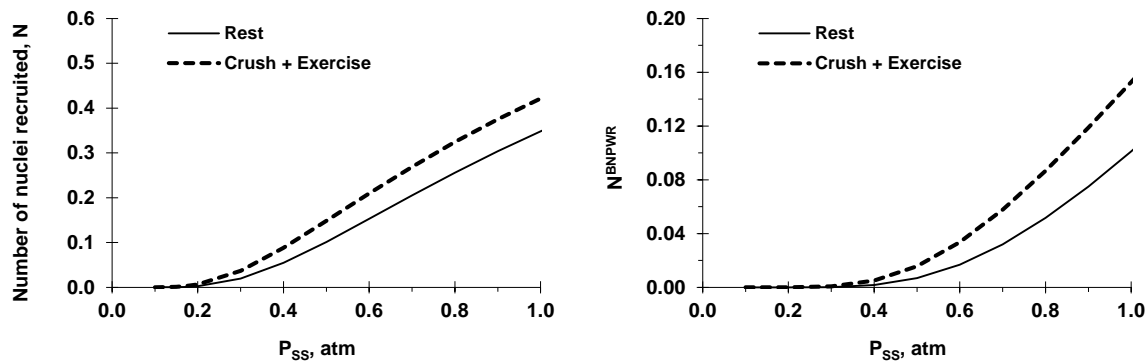
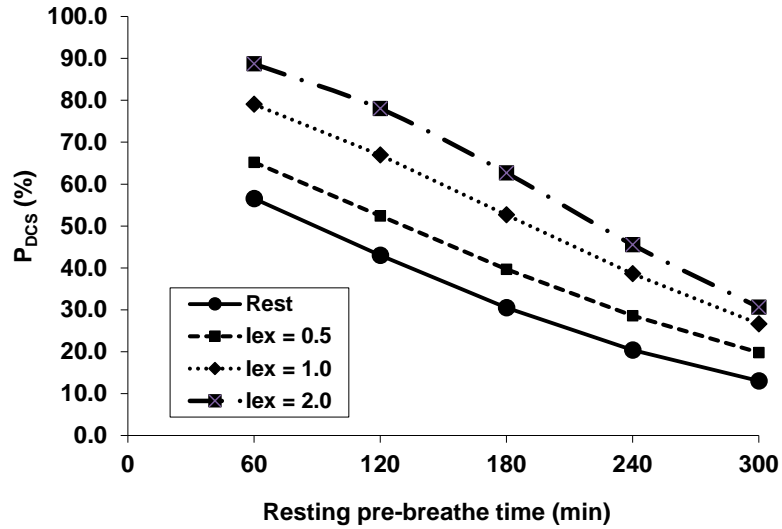


Figure 12. Modeled effects of a 3-hr resting ground-level prebreathe on numbers of bubbles recruited during exercising exposures at altitude. Left Panel: Modeled numbers of bubbles recruited at rest and during exercise, $I_{ex} = 0.55 \text{ L} \cdot \text{min}^{-1}$, after a 0.139 atm crush at various levels of gas-supersaturation, P_{SS} . Right Panel: $(N_b)^{BN}$ factor in the hazard function corresponding to the recruited numbers of bubbles at the respective supersaturations in the Left Panel.

Values of the $(N_b)^{BN}$ factor between zero and unity in the hazard function are a consequence of the fractional compartmental bubble number allowed in this model. As a result, the contribution of a given bubble volume to the hazard is potentiated by increasing numbers of bubbles, as intended, but the effect is to increasingly attenuate an overall diminution of the bubble volume contribution as the bubble number increases. One or more bubbles may attain a given volume but produce negligible risk with low numbers of bubbles. Bubble number thus acts as a potent factor that scales the contribution of bubble volume to the accumulation of DCS risk.

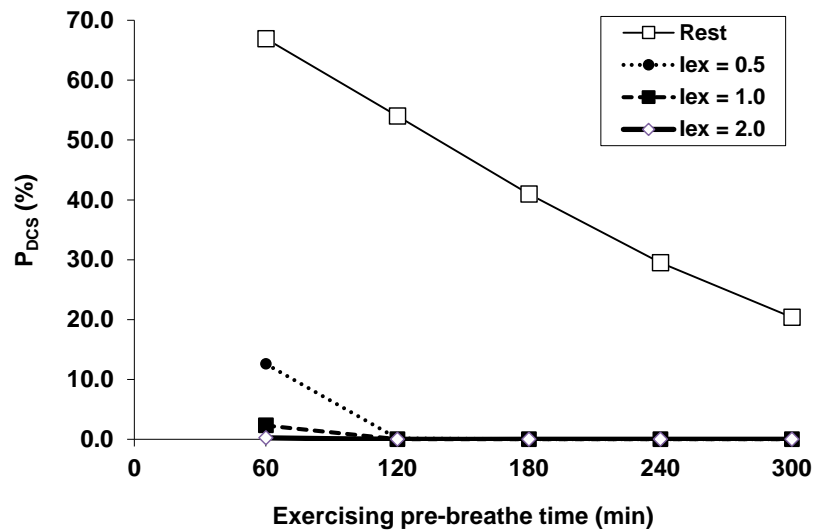
Figure 13 illustrates the modeled influence of exercise at altitude on the estimated risk of DCS during 4-hr exposures at 30,320 ft altitude (= 4.3 psia Shuttle EVA suit pressure) after resting oxygen prebreathes of various durations. At each level of exercise illustrated, the risk of DCS decreases with increasing oxygen prebreathe time. After short prebreathe times, exercise at altitude tends to increase the risk of DCS. After longer prebreathes, exercise-induced enhancement of inert gas elimination becomes increasingly important so that the risks of DCS at the higher levels of exercise tend towards the risks of DCS for resting subjects.



A1309-3RUT-MBe1

Figure 13. Estimated risks of DCS (P_{DCS}) during 4-hour exposures at 30,320 ft altitude (4.3 psia) while exercising at indicated levels (I_{ex} =whole-body \dot{V}_{O_2} , L·min⁻¹) after resting oxygen prebreathes of various duration.

Figure 14 illustrates the modeled influence of exercise on the estimated risk of DCS during 4-hr exercising exposures at 30,320 ft altitude (= 4.3 psia Shuttle EVA suit pressure) after oxygen prebreathes of various duration with exercise at indicated levels throughout. Even light exercise at a wholebody oxygen consumption rate of 0.5 L·min⁻¹ throughout the oxygen prebreathe greatly reduces the predicted risk of DCS during subsequent exposure to altitude.



A1309-3RUT-MBe1

Figure 14. Estimated risks of DCS (P_{DCS}) during 4-hour exposures at 30,320 ft altitude (4.3 psia) while exercising at $I_{ex}=0.55 \text{ L}\cdot\text{min}^{-1}$ after oxygen prebreathes of various duration with exercise at indicated levels throughout.

4.3 Comparative Model Performance

Performance of the present model can be compared with performance of other published models on selected data. An accelerated failure time model described by Conkin, et al.,⁷ is one such model from which results are readily calculated for comparison to 3RUT-MBe1 model results. Performance of the two models on NASA data subsets Test 1 through Test 7 is illustrated in Figure 15, with results of corresponding chi-square assessments of model fit given in Table 4.

The Conkin, et al., model provides estimates of DCS risk only for single exposures to altitude based on the values of computed gas tensions in a single 360-min half-time gas exchange compartment at the time of ascent start. Values for these tensions at the start of each recorded exposure were included in the raw NASA data and used to compute the illustrated risks for the Conkin, et al., model. The profiles for subsets Test 4b through Test 4f comprise data from profiles with successively increasing numbers of repetitive exposures to 4.3 psi separated by intervals at 10.2 psi. The Conkin, et al., model provides estimated conditional probabilities of DCS for the last exposure in such profiles governed only by fixed properties of the last exposure and the computed gas tensions at the start of that exposure. Because successive exposures in a given test were coded as a single profile for 3RUT-MBe1 model optimization, estimated risks of DCS tabulated for these subsets in Appendix F are the total risks accumulated over each entire multi-exposure profile. Risks of DCS for the last exposure in such profiles, conditional on the subject not having developed DCS by the start time of the last exposure, were approximated from the difference between the cumulative risk for the

profile of interest and the cumulative risk of the profile with one fewer repetitive exposure.

The chi-square for the Conkin, et al., model on all of the subsets is much lower than the chi-square for the 3RUT-MBe1 model. Corresponding P-values warrant rejection only of the 3RUT-MBe1 model. The situation reverses with omission of Test 6 data. The chi-square for the 3RUT-MBe1 model is then less than the chi-square for the Conkin, et al., model and the corresponding P-values motivate rejection of neither model. Thus, the 3RUT-MBe1 model outperforms the Conkin, et al., model on all of the subsets except Test 6. The 0.1% 3RUT-MBe1 model estimate of P_{DCS} for the Test 6 profile is considerably lower than the observed 3.4% DCS incidence for reasons that are not clear.

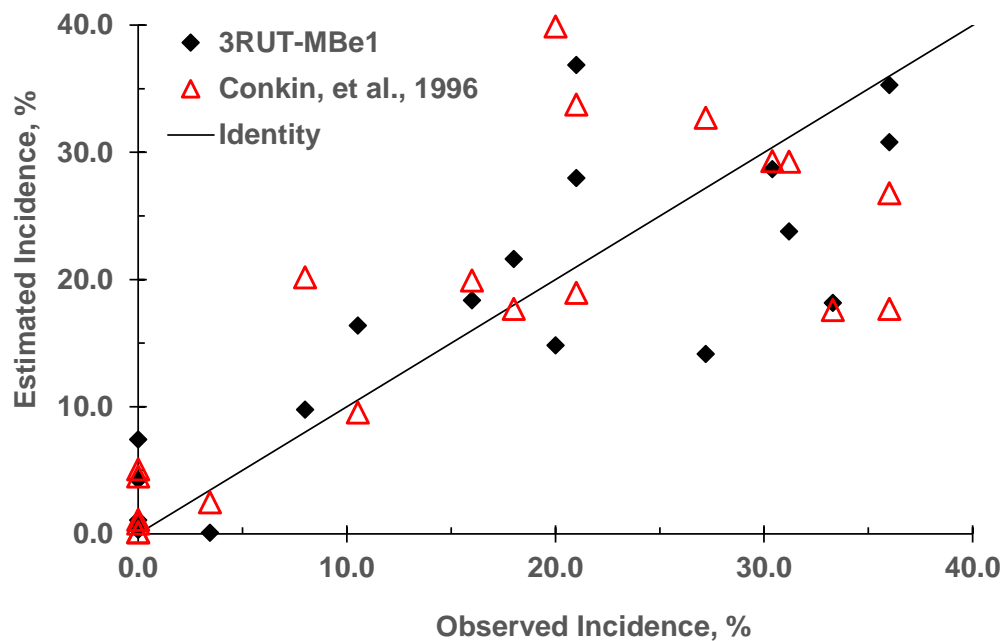


Figure 15. Model performance on data from NASA Tests 1 through 7.

Table 4. Chi-square Results for Performance of Conkin, et al., 1996 and 3RUT-MBe1 Models on Data from NASA Tests 1 through 7

| Data subset | (Pearson Residual) ² | |
|---------------------------------|---------------------------------|-----------|
| | Conkin, et al., 1996 | 3RUT-MBe1 |
| Test 1a | 0.514 | 0.006 |
| Test 1b | 0.030 | 0.003 |
| Test 1c | 2.048 | 1.854 |
| Test 2a | 0.014 | 0.035 |
| Test 2b | 0.296 | 3.127 |
| Test 3a | 1.904 | 0.595 |
| Test 3b | 5.781 | 1.791 |
| Test 3c | 0.056 | 1.434 |
| Test 3d | 0.080 | 0.023 |
| Test 4a | 1.044 | 0.028 |
| Test 4b | 0.099 | 0.536 |
| Test 4c | 0.642 | 0.130 |
| Test 4d | 0.015 | 0.046 |
| Test 4e | 0.566 | 0.078 |
| Test 4f | 0.013 | 0.038 |
| Test 5a | 0.042 | 0.951 |
| Test 5b | 0.122 | 0.883 |
| Test 6 | 0.113 | 34.358 |
| Test 7a | 2.639 | 0.160 |
| Test 7b | 0.002 | 0.077 |
| χ^2 (All) | 16.018 | 46.152 |
| P= | 0.591 | 0.000 |
| χ^2 (not including Test 6) | 15.905 | 11.794 |
| P= | 0.531 | 0.812 |

Note: Residuals in shaded cells were computed with approximated conditional probabilities of DCS for the last exposure in each profile (See text).

The USAF Altitude Decompression Sickness Risk Assessment Calculator (ADRAC) developed by Pilmanis, et al.,²³ is another accelerated failure time model from which data are available for comparison to 3RUT-MBe1 model results. ADRAC is a stratified time-independent covariate model with values of some parameters uniquely defined for different ranges of altitude. Unlike the present 3RUT-MBe1 model, ADRAC is applicable only to profiles with single ascents to a given altitude at which subjects may be either at rest or performing exercise at one of three discrete levels; mild, moderate, or heavy. The model also accommodates effects of resting ground-level oxygen prebreathes, but

exercsie during such prebreathes cannot be considered. Pilmanis and coworkers completed a series of man-exposures to validate this model. Performance of the present 3RUT-MBe1 model on the data from these exposures is compared to the corresponding performance of the ADRAC model in Figure 16. Results from corresponding chi-square assessments of model fit in Table 5 indicate that the 3RUT-MBe1 model outperforms the ADRAC model on all of these data except the data for validation profile A. The model underpredicts the observed DCS incidence for this profile that included only a moderately long resting prebreathe followed by exercising exposure to the highest altitude tested in the series.

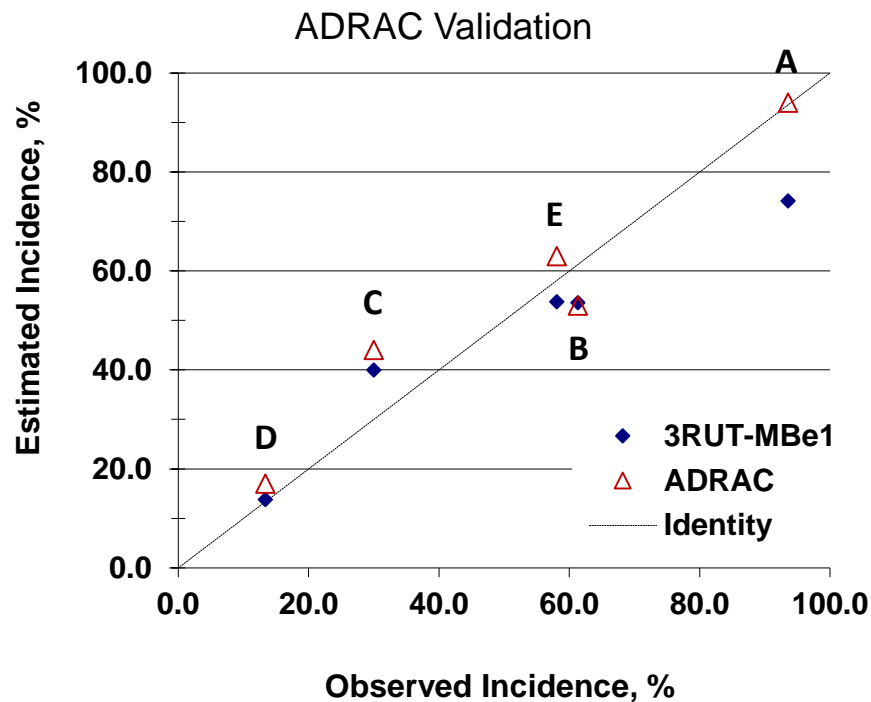


Figure 16. Model performance on USAF ADRAC validation data consisting of 153 man-exposures on five different profiles: A) 90 min prebreathe; 35K ft EVA sim (light exercise)/180 min; B) 30 min prebreathe; 25K ft, 30% $\dot{V}_{O_2,peak}$ exercise-rest cycles (heavy exercise)/240 min; C) 15 min prebreathe; 22.5K ft, 30% $\dot{V}_{O_2,peak}$ exercise-rest cycles (heavy exercise)/240 min; D) No prebreathe; 18.0K ft, 30% $\dot{V}_{O_2,peak}$ exercise-rest cycles (heavy exercise)/360 min; E) 75 min prebreathe; 30K ft rest/240 min.

Table 5. Chi-square Results for Performance of ADRAC and 3RUT-MBe1 Models on USAF ADRAC Validation Data

| Subset | (Pearson Residual) ² | |
|----------------------------|---------------------------------|-----------|
| | ADRAC | 3RUT-MBe1 |
| A | 0.011 | 6.111 |
| B | 0.855 | 0.747 |
| C | 2.386 | 1.239 |
| D | 0.286 | 0.006 |
| E | 0.324 | 0.229 |
| χ^2 (All) | 3.863 | 8.333 |
| χ^2 (not including A) | 3.851 | 2.222 |

Performance of the present 3RUT-MBe1 model on data from man-exposures completed to develop a reduced prebreathe protocol for Space Shuttle extra-vehicular activities is compared to the corresponding performance of the NASA-RM2004 model¹⁰ in Figure 17. The NASA-RM2004 model is an accelerated failure time model cast in terms of time-independent covariates applicable only to stylized profiles typical of 4-hr Shuttle extravehicular activity (EVA) exposures with astronauts at Shuttle extravehicular mobility unit (EMU) – or EVA suit – pressure of 4.3 psia (30,320 ft altitude in the U.S. Standard Atmosphere) after various types of exercising prebreathe. Results from corresponding chi-square assessments of model fit in Table 6 indicate that the 3RUT-MBe1 model outperforms the NASA-RM2004 model on all of these data except the data for PRP Phase I.

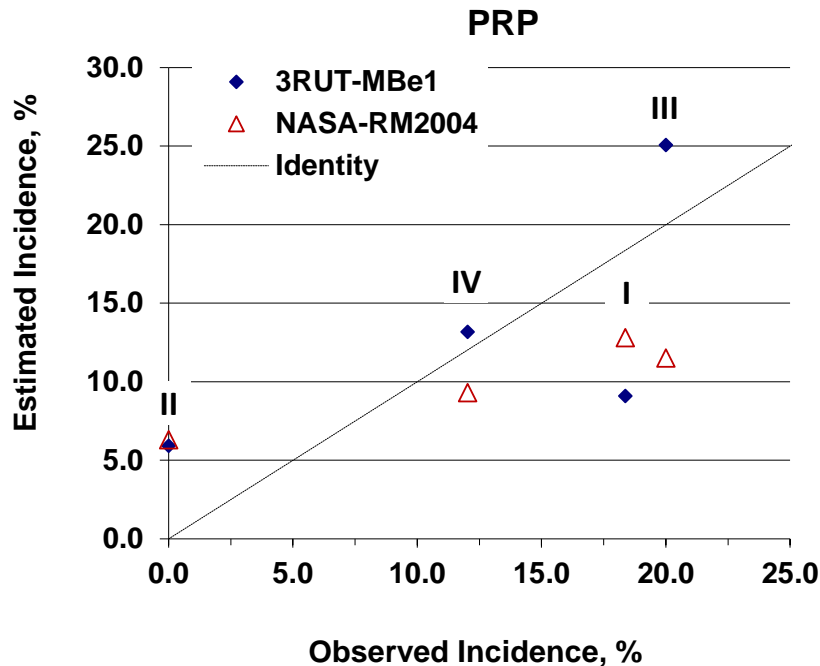


Figure 17. Model performance on NASA PRP data, Phases I through IV.

Table 6. Chi-square Results for Performance of NASA-RM2004 and 3RUT-MBe1 Models on NASA PRP Data

| Subset | (Pearson Residual) ² | |
|----------------------------|---------------------------------|-----------|
| | NASA-RM2004 | 3RUT-MBe1 |
| I | 1.361 | 5.124 |
| II | 3.362 | 3.145 |
| III | 0.710 | 0.137 |
| IV | 0.609 | 0.079 |
| χ^2 (All) | 6.042 | 8.485 |
| χ^2 (not including I) | 4.681 | 3.360 |

4.4 Features of Model Performance

Important features of the 3RUT-MBe1 model compared to those of the other log-logistic models considered above are illustrated by considering 3RUT-MBe1 model performance on the PRP Phase II profile described in Table 7. The profile is a prototype Space Shuttle extravehicular activity (EVA) profile with a 2-hr exercise-enhanced O₂ prebreathe that was ultimately transitioned into Space Shuttle operational use.⁵⁶ A requirement to breathe ambient atmosphere for a period of 15 - 90 min during the Hard Upper Torso (HUT) donning procedure in the crewlock was a significant operational constraint on prebreathe design. To mitigate the adverse impact of this air breathing break, the EVA crew complete the donning procedure for the Lower Torso Assembly (LTA) of the Shuttle EMU in the crewlock while being slowly decompressed to 9.6 psia. The crewlock is then backfilled with O₂ to bring the crewlock to a pressure of 10.2 psia with the maximum allowed FO₂ of 26.5%, after which the crew breathes ambient atmosphere to complete the HUT donning procedure.^e Oxygen breathing is resumed with recompression of the crewlock to cabin pressure and completion of a 35 min O₂ prebreathe before final decompression to EMU pressure and egress for EVA.

^e A 12-hr minimum O₂-breathing stage at 10.2 psia before decompression to Shuttle suit pressure and egress for EVA was a standard feature of Shuttle prebreathe protocols before the 2-hr prebreathe protocol was developed.

Table 7. PRP Phase II Profile Description

| | | | | | | |
|---|---|-----------------------|----------------------------|----------------|---|-----------------------|
| <ul style="list-style-type: none"> • 100 min “adynamic” air breathing period. (Ground-based micro-gravity simulation; subjects semi-recumbent and prohibited from walking from start of this period until end of the EVA simulation.) • 50 min O₂-breathing period during which exercise is performed to enhance N₂ washout. Schedule: <ul style="list-style-type: none"> 1 min rest; pulmonary residual volume washout 10 min; 75% $\dot{V}_{O_{2,peak}}$ exercise ($I_{ex} = 2.36$); dual cycle (upper and lower body) cranking on Monark cycle ergometers 39 min rest (Subject transfer to altitude chamber) <p>-----</p> <p>50 min total in segment</p> <ul style="list-style-type: none"> • 20 min decompression to 9.6 psia; lower torso assembly (LTA) donning. “Intermediate exercise” ($I_{ex} = 0.41$) programmed to simulate work of LTA donning is started 5 min into this decompression and continued throughout the ensuing 40 min. • 10 min repressurization to 10.2 psia; Backfill crewlock with O₂ to raise O₂ to 26.5%. • 30 min “air” break (26.5% O₂; balance N₂) at 10.2 psia; hard upper torso (HUT) donning, comms check, etc. ($PI_{O_2} = 0.184$ atm). End “intermediate exercise” at 15 min into “air” break. • Switch to O₂ and start 5 min repressurization to 14.7 psia cabin pressure. • 35 min O₂ breathing period at 14.7 psia; crewlock prebreathe. • 30 min crewlock decompression to 4.3 psia suit pressure. • 4 hr EVA simulation ($I_{ex} = 0.55$) at 4.3 psia. <p>-----</p> <table style="width: 100%; border-collapse: collapse;"> <tr> <td style="padding: 5px;">Total prebreathe time, including air break:</td> <td style="text-align: right; padding: 5px;">150 min (2 hr 30 min)</td> </tr> <tr> <td style="padding: 5px;">Total O₂ time:</td> <td style="text-align: right; padding: 5px;">120 min (2 hr)</td> </tr> <tr> <td style="padding: 5px;">Total Test Duration, excluding post-flight watch:</td> <td style="text-align: right; padding: 5px;">530 min (8 hr 50 min)</td> </tr> </table> | Total prebreathe time, including air break: | 150 min (2 hr 30 min) | Total O ₂ time: | 120 min (2 hr) | Total Test Duration, excluding post-flight watch: | 530 min (8 hr 50 min) |
| Total prebreathe time, including air break: | 150 min (2 hr 30 min) | | | | | |
| Total O ₂ time: | 120 min (2 hr) | | | | | |
| Total Test Duration, excluding post-flight watch: | 530 min (8 hr 50 min) | | | | | |

Various aspects of model performance on this profile are shown in Figures 18 and 19. Exercise-induced acceleration of N₂ elimination during the initial 75% $\dot{V}_{O_{2,peak}}$ exercise period is readily apparent in the compartmental N₂ tension profile shown in panel A of Figure 18. It is also apparent that as a result of the prebreathe-induced reduction of compartmental N₂, the gas supersaturation prevailing on arrival at the Shuttle suit pressure of 4.3 psia (0.293 atm) is considerably reduced from what would have prevailed had no prebreathe been performed. The bubble number and volume profiles in panel B are the modeled responses to this supersaturation. Bubbles are nucleated in increasing number as the supersaturation develops during decompression, reaching a maximum number on arrival at suit pressure. The bubble volume profile shows that each of the bubbles continues to grow throughout the ensuing 4-hr period at suit pressure. This growth drives the migration of some bubbles from the tissue to the vasculature perfusing the tissue, which in turn causes the number of bubbles to decrease. The corresponding instantaneous risk of DCS, which is a function of both bubble volume and bubble number, is shown in panel C of Figure 18. Because of the loss of bubbles to the circulation, the instantaneous risk passes through a maximum and decreases somewhat before completion of the 4-hr period at 4.3 psia.

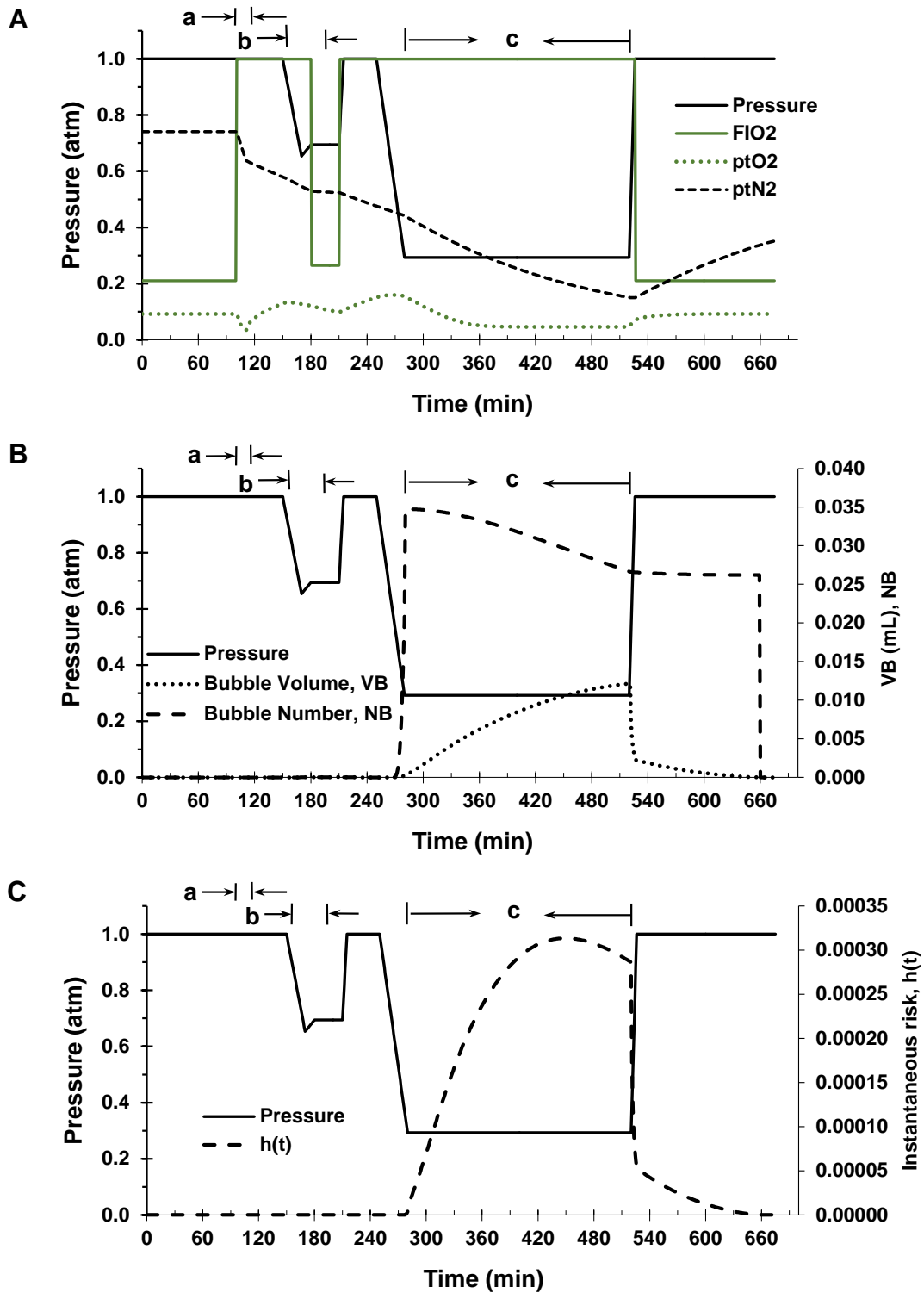


Figure 18. Model performance on a NASA PRP Phase II profile. Pressure, inspired O₂ fraction, and compartmental O₂ and N₂ tension profiles are shown in panel A. Corresponding compartmental bubble number, bubble volume, and instantaneous DCS risk profiles are shown in panels B and C. All panels: 75% $\dot{V}_{O_{2,peak}}$ exercise ($I_{ex} = 2.36$) [a arrows]; intermediate exercise ($I_{ex} = 0.41$) [b arrows]; EVA exercise ($I_{ex} = 0.55$) [c arrows].

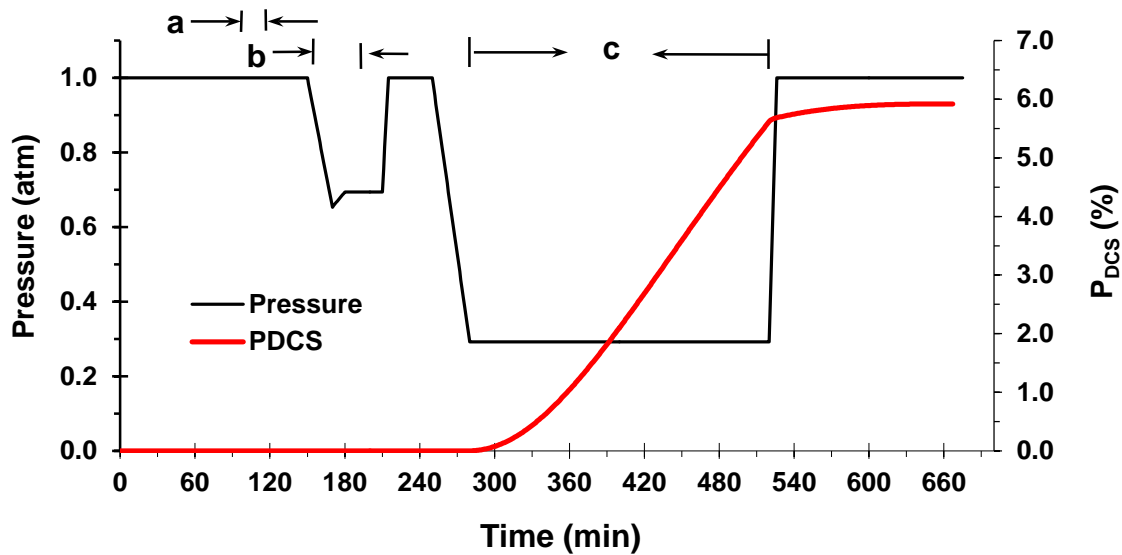


Figure 19. Pressure and model-estimated cumulative risk of DCS during the NASA PRP Phase II profile described in Table 7 and illustrated in Figure 18. Exercise periods are labeled as described in Figure 18.

All illustrated model features for this PRP Phase II profile, including the instantaneous and cumulative risks of DCS, are computed as they evolve in response to changes in the covariates of pressure, inspired O_2 fraction, and exercise intensity *within* the profile. As a result, the instantaneous risk of DCS varies with time as illustrated in panel C of Figure 18. This model behavior contrasts sharply with that of models with time-invariant covariates and constant hazards in any given profile, such as the ADRAC,²³ and Conkin, et al.,^{7,10} models considered above. Such models are based on planned times at altitude or are fit only to profiles with the same times at altitude, and reduce to simple occurrence-only binary quantal response assays, which are insensitive to the shape of the actual hazard function within any given profile.¹⁷ Such models can be used to illustrate how the probability of DCS changes with time in a given profile only by compiling model solutions for *different* profiles with successively increased times at altitude. However, because these models are not fit to actual failure times but to factitious failure times presumed equal to the planned times at altitude or to the fixed time at attitude of the data, the time-dependences of DCS risk accumulation obtained in this fashion are extrapolations strictly beyond the scope of the models.

4.5 Model Deficiencies and Remaining Issues

The favorable chi-square comparisons above depend on the adjustment of model-estimated DCS incidences for risk that would have accumulated in profiles that were terminated early due to occurrence of DCS. However, the overall results indicate that the model does not perform as favorably on other profiles in the calibration data. Referring to data in Appendix F, the sum of the adjusted estimated incidences of DCS exceeds the sum of the actual incidences by 38 (896.5 vs. 858.3) in the full set of calibration data, and by 43 (501.2 vs. 458.3) in the 84 subsets of the calibration data

considered to be fit by the model according to chi-square tests of subsets ordered by Pearson Residual. In contrast, comparison of the observed and model-estimated occurrence density functions, where such adjustments are inapplicable, indicates that the model tends to incorrectly delay DCS risk accumulation and underestimate incidences by 3 – 15 % in the first four hours after last decompression. Thus, the model overestimates risk in the latter parts of long exposures at altitude, and provides only poor representations of the actual time courses of DCS risk accumulation in many types of profile.

Model failure to capture essential features of the time courses of DCS risk accumulation may reflect that some subsets in the calibration data are not combinable due to oversimplification of exercise effects. The types of exercise performed in the profiles of the various data subsets varied widely, ranging from various isometric and isotonic arm and leg weight lifting exercises, constant torque arm pull exercises, fixed resistance rope pull arm exercises, knee bends, stair stepping, leg cycle ergometry, arm cycle ergometry, and dual cycle ergometry. The intensity of the exercises, regardless of type, was considered only in terms of the whole-body oxygen consumption rate associated with the exercise. This oxygen consumption rate was not normalized with respect to any subject-specific index such as maximum oxygen consumption rate or body weight. Other workers have argued convincingly that such normalization is essential for whole-body oxygen consumption to accurately represent the intensity of work performed by different subjects in a given type of exercise.^{10,58} Moreover, exercise at altitude in most profiles was intermittent, with periods of exercise alternated with periods of rest. Exercise intensity during profile segments in which such intermittent exercise was performed was defined in the present calibration data as the whole-body oxygen consumption rate averaged over all periods of exercise and rest in the segment. All possible characterizations of different types of exercise were collapsed into a single independent variable, the average whole-body oxygen consumption rate, because of lack of data to support more detailed descriptions and to limit the number of covariates in the model, a compromise that almost certainly limited the attainable scope of model success.

Consideration of exercise effects on compartmental bubble nucleation to be manifest instantaneously with the onset of exercise was an additional simplifying assumption in the present model. With exercise at altitude coded to commence upon arrival at altitude, the exercise-induced shifts in the compartmental populations of pre-existing nuclei occurred at the points in the profiles with the highest compartmental gas supersaturations, where conditions prevailed to recruit the largest number of bubbles and promote the highest rates of DCS risk accumulation. It is therefore unlikely that treatments of the kinetics of exercise effects on compartmental bubble nucleation different from that implemented in the present model could cause higher risks of DCS earlier in an altitude exposure. On the other hand, exercise effects on blood-tissue gas exchange were also considered to be fully manifest immediately upon commencement of exercise and fully absent immediately upon cessation of exercise. Consideration of on-effect kinetics for such effects would cause the higher gas supersaturations prevailing upon initial arrival at altitude to persist and promote early bubble growth and higher rates of DCS risk accumulation than with the instant-on exercise-induced acceleration of gas elimination presently assumed. Incorporation of on- and off-effect

kinetics for the influences of exercise on blood-tissue gas exchange – as described, for example, in Appendix B – has yet to be explored.

Finally, the Λ parameter in the 3RUT-MBe1 model was assumed constant in present work to allow use of the piece-wise analytic solution of the model equations described in Appendix B. In principle, however, the Λ parameter accommodates the influences on bubble evolution of heterogeneity in the diffusion field around each modeled bubble.³¹ Because such influences include bubble-bubble interactions when more than one bubble is present in a compartment, Λ must vary with time as a function of bubble number and volume. Such time dependent variation of Λ warrants examination as a model feature that may allow more accurate modeling of the time courses of DCS risk accumulation at altitude.

5. Conclusions

A probabilistic model of DCS incidence and time of occurrence has been developed that is able to accommodate the influences of pressure, changing inspired inert gas, oxygen breathing, and exercise in profiles of arbitrary complexity. The model is a time-dependent covariate survival model in which the risks of DCS are determined as functions of the prevailing volumes and profusions of gas bubbles in a perfusion-limited gas exchange compartment. The bubbles vary in volume by diffusion-limited exchange of gas between the bubbles and their surroundings according to an implementation of the three-region unstirred tissue model of gas bubble evolution elaborated to accommodate the influences of exercise and oxygen breathing on compartmental gas exchange and bubble nucleation. The model has been shown to provide performance superior to that of other published models on a variety of data subset collections that is much more diverse than can be handled by any one of the other models.

Model successes are tempered by model failure to accurately represent the time courses of DCS risk accumulation at altitude and consequent failure to fit all subsets of the calibration data. The subsets on which the model fails may be incombinable with the subsets on which the model succeeds, in large part due to the wide variety of exercise types performed in the different subsets and the oversimplification of the independent variable for exercise in the model. Model tendency to skew DCS risk accumulation to later periods at altitude and underestimate risk early in the exposures may be rectified with implementation of model features that were not exercised in the present model.

Numerical issues with model implementation remain to be solved before the model will be applicable to diving data.

6. Acknowledgements

Portions of this work were supported by National Aeronautics and Space Administration (NASA) Biomedical Research and Countermeasures Program grant, "Optimization of Astronaut Decompression Sickness Prevention Protocols Using Probabilistic Gas and Bubble Dynamics Models," MIPR Number NNJ04HF521, and NAVSEA Task Assignment 10-12, "Decompression Algorithm Development and Implementation." The authors are grateful to Dr. Johnny Conkin, who provided validated copies of data from NASA Tests 1 through 11 for inclusion in the present model calibration data. The authors also thank Dr. David Doolette for his critical review of this manuscript and many helpful suggestions for revision.

7. References

1. Tikuisis P, Gerth WA. Decompression theory. In: Brubakk AO, Neuman TS, editors. Bennett and Elliott's physiology and medicine of diving. 5th ed. Edinburg: W.B. Saunders Co.; 2003. p. 419-454.
2. Weathersby PK, Homer LD, Flynn ET. On the likelihood of decompression sickness, *Journal of Applied Physiology: Respiration, Environmental and Exercise Physiology* 1984; 57(3):815-25.
3. Weathersby PK, Survanshi SS, Homer LD, Hart BL, Flynn ET, Bradley ME. Statistically based decompression tables II: Equal risk air diving decompression schedules. Bethesda, MD: Naval Medical Research Institute, 1985; NMRI Technical Report 85-17.
4. Survanshi SS, Weathersby PK, Thalmann ED. Statistically based decompression tables X: Real-time decompression algorithm using a probabilistic model. Bethesda, MD: Naval Medical Research Institute, 1996; NMRI Technical Report 96-06.
5. Southerland DG. Logistic regression and decompression sickness. M.S. Thesis, Duke University, 1992.
6. Conkin, J., B.F. Edwards, J.M. Waligora, and D.J. Horrigan, Jr. Empirical models for use in designing decompression procedures for space operations. NASA Technical Memorandum 100456, Johnson Space Center, Houston, TX, June 1987.
7. Conkin J, Kumar K, Powell MR, Foster PP, Waligora JM. A probabilistic model of hypobaric decompression sickness based on 66 chamber tests. *Aviation, Space, and Environmental Medicine* 1996; 67:176-183.
8. Loftin KC, Conkin J, Powell MR. Modeling the effects of exercise during 100% oxygen prebreathe on the risk of hypobaric decompression sickness. *Aviation Space and Environmental Medicine* 1997; 68:199-204.
9. Kannan N, Raychaudhuri A, Pilmanis AA. A loglogistic model for altitude decompression sickness. *Aviation, Space, and Environmental Medicine* 1998; 69:965-70.
10. Conkin J, Gernhardt ML, Powell MR, Pollock N. A probability model of decompression sickness at 4.3 psia after exercise prebreathe. NASA/TP-2004-213158, Johnson Space Center, Houston, TX, December 2004.
11. Conkin J, Gernhardt ML, Abercromby AF, Feiveson AH. Probability of hypobaric decompression sickness including extreme exposures. *Aviation, Space, and Environmental Medicine* 2013; 84(7): 661-668.
12. Gernhardt ML. Development and evaluation of a decompression stress index based on tissue bubble dynamics [Dissertation]. Philadelphia, PA: University of Pennsylvania; 1991.

13. Gerth WA, Vann RD. Statistical bubble dynamics algorithms for assessment of altitude decompression sickness incidence. Armstrong Laboratory Technical Report AL/CF-TR-1995-0037. Brooks Air Force Base, San Antonio, TX, 1995.
14. Vann RD, Thalmann ED, Decompression physiology and practice. Bennett PB, Elliot DH, editors. The physiology and medicine of diving. 4th ed. London: W.B. Saunders, 1993: 376-432.
15. Weathersby PK, Survanshi SS, Homer LD, Parker E, Thalmann ED. Predicting the time of occurrence of decompression sickness. *Journal of Applied Physiology* 1992; 72(4):1541-8.
16. Kalbfleisch JD, Prentice RL. The statistical analysis of failure time data. New York: Wiley, 1980.
17. Gerth WA. Overview of survival functions and methodology. In: Weathersby PK and Gerth WA, editors. Survival analysis and maximum likelihood techniques as applied to physiological modeling. Fifty-first Workshop, Undersea and Hyperbaric Medical Society Inc., Bethesda, MD; 2002, p. 1-48.
18. Van Liew HD, Conkin J, Burkhard ME. Probabilistic model of altitude decompression sickness based on mechanistic principles. *Journal of Applied Physiology* 1994; 76(6):2726-34.
19. Van Liew HD, Burkhard ME, Conkin J. Testing of hypotheses about altitude decompression sickness by statistical analyses. *Undersea and Hyperbaric Medicine* 1996; 23(4):225-33.
20. Kannan N, Raychaudhuri A. Survival models for predicting altitude decompression sickness. Brooks Air Force Base, TX, 1997; AL/CF-TR-1997-0030.
21. Conkin J. Evidence-based approach to the analysis of serious decompression sickness with application to EVA astronauts. NASA/TP-2001-210196. NASA Center for Aerospace Information, Hanover MD. Jan 2001.
22. Kannan N. Survival models for altitude decompression sickness. In: Weathersby PK and Gerth WA, editors. Survival analysis and maximum likelihood techniques as applied to physiological modeling. Fifty-first Workshop, Undersea and Hyperbaric Medical Society Inc., 2002, p. 101-109.
23. Pilmanis AA, Petropoulos LJ, Kannan N, Webb JT. Decompression sickness risk model: Development and validation by 150 prospective hypobaric exposures. *Aviation, Space, and Environmental Medicine* 2004; 75:749-59.
24. Tikuisis P, Gault KA, Nishi RY. Prediction of decompression illness using bubble models. *Undersea and Hyperbaric Medicine* 1994; 21(2): 129-143.
25. Tikuisis, Nishi RY. Role of oxygen in a bubble model for predicting decompression illness. Defence and Civil Institute of Environmental Medicine, Ontario, Canada, DCIEM No. 94-04, 1994.

26. Gerth WA, Vann RD. Development of iso-DCS risk air and nitrox decompression tables using statistical bubble dynamics models. Bethesda, MD: National Oceanic and Atmospheric Administration, Office of Undersea Research, 1996; Final Report, Contract # NA46RU0505.
27. Gerth WA, Vann RD. Probabilistic gas and bubble dynamics models of DCS occurrence in air and N₂O₂ diving. *Undersea and Hyperbaric Medicine* 1997; 24(4):275-92.
28. Van Liew HD, Hlastala MP. Influence of bubble size and blood perfusion on absorption of gas bubbles in tissues. *Resp Physiol* 1969; 7:111-121.
29. Srinivasan RS, Gerth WA, Powell MR. Mathematical models of diffusion-limited gas bubble dynamics in tissue. *Journal of Applied Physiology* 1999; 86(2):732-41.
30. Srinivasan RS, Gerth WA, Powell MR. Mathematical model of diffusion-limited evolution of multiple gas bubbles in tissue. *Annals of Biomedical Engineering* 2003; 31:471-81.
31. Srinivasan RS, Gerth WA, Mathematical models of diffusion-limited gas bubble evolution in perfused tissue. NEDU TR 13-05, Navy Experimental Diving Unit, Panama City, FL, Aug 2013.
32. Boycott AE, Damant GCC, Haldane JB. The prevention compressed air illness. *Journal of Hygiene, London* 1908; 8:342-443.
33. McArdle WD, Katch FI, Katch VL. *Exercise physiology. Energy, nutrition and human performance*. 4th ed. Baltimore: Williams and Wilkins, 1996. p. 147.
34. Astrand P-O, Rodahl K, Dahl HA, Stromme SS. *Textbook of Work Physiology: Physiological Bases of Exercise*. 4th ed. Human Kinetics, Champaign, IL, 2003.
35. Kalliokoski KK et al. Relationship between muscle blood flow and oxygen uptake during exercise in endurance-trained and untrained men. *Journal of Applied Physiology* 2005; 98:380-3.
36. Thalmann ED, Parker EC, Survanshi SS, Weathersby PK. Improved probabilistic decompression model predictions using linear-exponential kinetics. *Undersea and Hyperbaric Medicine* 1997; 24(4):255-74.
37. Parker EC, Survanshi SS, Massell PB, Weathersby PK. Probabilistic models of the role of oxygen in human decompression sickness. *Journal of Applied Physiology* 1998; 84:1096-102.
38. Gerth WA, Johnson TM. Development and Validation of 1.3 ATA PO₂-in-He Decompression Tables for the MK 16 MOD 1 UBA. NEDU TR 02-10. Panama City, FL, Navy Experimental Diving Unit, 2002.
39. Severinghaus JW. Simple accurate equations for human blood O₂ dissociation computations. *J. Appl. Physiol: Respir Environ Exercise Physiol* 1979; 46: 599-602.

40. Yount DE. Skins of varying permeability: A stabilization mechanism for gas cavitation nuclei. *Journal of the Acoustical Society of America* 1979; 65:1429-39.
41. Yount DE. On the evolution, generation, and regeneration of gas cavitation nuclei. *Journal of the Acoustical Society of America* 1982; 71(6): 1473-1481.
42. Kindwall EP, Baz A, Lightfoot EN, Lanphier EH, Seireg S. Nitrogen elimination in man during decompression. *Undersea Biomedical Research* 1974; 2(4): 285-297.
43. Gerth WA. Probabilistic models of decompression sickness during flying after diving: motivation for mechanism. In: Weathersby PK and Gerth WA, editors. *Survival analysis and maximum likelihood techniques as applied to physiological modeling. Fifty-first Workshop, Undersea and Hyperbaric Medical Society Inc.*, 2002, p. 118-136.
44. Howle LE, Weber PW, Vann RD, Campbell MC. Marginal DCS events: their relation to decompression and use in DCS models. *Journal of Applied Physiology* 2009; 107: 1539-1547.
45. Murphy FG, Swingler AJ, Gerth WA, Howle LE. Iso-risk air no decompression limits after scoring marginal decompression sickness cases as non-events. *Computers in Biology and Medicine* 2018; 92(1):110-117.
46. Marquart DW. An algorithm for least-squares estimation of nonlinear parameters. *J Soc Indust Appl. Math* 1963; 11:431-441.
47. Webb JT, Documentation for the USAF School of Aerospace Medicine altitude decompression sickness research database, AFRL-SA-BR-SR-2009-0007, USAF School of Aerospace Medicine, Brooks City Base, TX, May 2010.
48. Gerth WA, Besich W, DeCelles T, Eshaghian B. The USAFSAM computerized hypobaric decompression sickness data base. Brooks Air Force Base, TX: USAF School of Aerospace Medicine; 1984. Lineprinter output of text and tables in 1 bound volume. Located at: Navy Experimental Diving Unit, Panama City, FL.
49. Conkin J. email, Transfer of all Bends 1 data. 10-Sep-2004.
50. Conkin J. email, Transfer of all Bends 2 data. 16-Sep-2004.
51. Conkin J. email, Bends 3 test series. 23-Sep-2004.
52. Conkin J. email, Bends 4, 5, 6, and 7 data. 30-Sep-2004.
53. Conkin J. email, Bends 8, 9, 10, and 11 data. 7-Oct-2004.
54. Gernhardt ML, Conkin J, Foster PP, Pilmanis AA, Butler BD, Fife CE, Vann RD, Gerth WA, Loftin KC, Dervay JP, Waligora JM and Powell MR. Design of a 2-hour prebreathe protocol for space walks from the International Space Station. 2000 Annual Scientific Meeting of the Aerospace Medical Association, Houston, TX May

14-18, 2000.

55. Gernhardt ML, Conkin J, Foster PP, Pilmanis AA, Butler BD, Beltran E, Fife CE, Vann RD, Gerth WA, Loftin KC, Acock K, Dervay JP, Waligora JM, Powell MR, Feiveson AH, Nishi RY, Sullivan PA, Schneider SM. Design and testing of a 2-hour oxygen prebreathe protocol for space walks from the International Space Station. *Undersea and Hyperbaric Medicine* 2000; 27(S): 12.
56. Gernhardt ML. Prebreathe reduction program – Phase V. Summary of research. In: Bennett PB, Michaelson R, Butler F, Moon R, editors. *Best practice guidelines for prevention and effective treatment of decompression illness proceedings: Part I*. Undersea and Hyperbaric Medical Society, Durham, NC, 2010. pp. 132-174.
57. Gernhardt ML. Modified oxygen prebreathe to include a slightly longer oxygen-breathing period with a heavy exercise period followed by a light exercise period. In: Bennett PB, Michaelson R, Butler F, Moon R, editors. *Best practice guidelines for prevention and effective treatment of decompression illness proceedings: Part 2*. Undersea and Hyperbaric Medical Society, Durham, NC, 2010. pp. 117-147.
58. Webb JT, Krock LP, Gernhardt ML. Oxygen consumption during exposure as a risk factor for altitude decompression sickness. *Aviat Sp Environ Med* 2010; 81:987-992.
59. Webb JT, Pilmanis AA, Balldin UI. "Altitude decompression sickness at 7620 m following prebreathe enhanced with exercise periods." *Aviat Space Environ Med* 2004; 75:859-864.
60. Webb JT, Fischer MD, Heaps CL, Pilmanis AA. Exercise-enhanced preoxygenation increases protection from decompression sickness. *Aviation, Space and Environmental Medicine* 1996; 67:628-4.
61. Conkin J, Waligora JM, Horrigan DJ Jr, Hadley AT. The effect of exercise on venous gas emboli and decompression sickness in human subjects at 4.3 psia. NASA Technical Memorandum 58278, Lyndon B. Johnson Space Center, Houston, TX, March 1987.
62. Inderbitzen RS and DeCarlis JJ. Energy expenditure during simulated EVA workloads. San Diego, CA: SAE Technical Paper *860921, 16th ICES, 1986:4pp.
63. Doolette DJ, Gerth WA, Gault KA. Addition of work rate and temperature information to the augmented NMRI standard (ANS) data files in the "NMRI98" subset of the USN N₂-O₂ primary data set. NEDU TR 11-02, Navy Experimental Diving Unit, Jan 2011.
64. Doolette DJ. Addition of work rate and temperature information to the augmented NMRI standard (ANS) data files in the "he8n25" subset of the U.S.N. primary data set. NEDU TR 17-10, Navy Experimental Diving Unit, 2017.

65. Harrell FE Jr. Regression modeling strategies, with applications to linear models, logistic regression, and survival analysis, 2nd ed. New York: Springer, 2015.
66. Hosmer DW, Lemeshow S. Applied logistic regression. New York: John Wiley & Sons, 1989.
67. Doolette DJ, Gerth WA, Gault KA. Decompression models with work-induced changes in compartment gas kinetic time constants. Undersea and Hyperbaric Medicine 2010; 37:294.
68. West, J. B. Respiratory physiology. Baltimore: Williams and Wilkins, 1985.
69. Lobdell DD. An invertible simple equation for computation of blood O₂ dissociation relations. Journal of Applied Physiology 1981; 50(5):971-3.
70. Van Liew HD. Simulation of the dynamics of decompression sickness bubbles and the generation of new bubbles. Undersea Biomedical Research 1991; 18:333-345.
71. Howle LE. Analytic gain in probabilistic decompression sickness models. Computers in Biology and Medicine, 2013; 43(11): 1739-1747.

8. Appendix A. Three-Region Unstirred Tissue Multiple Bubble (3RUT-MB) Model of Tissue Gas and Bubble Dynamics

In the original 3RUT-MB model,^{30,31} the total gas bubble volume $V_g(t)$ in a given hypothetical tissue compartment at time t is the sum of the volumes of N_b bubbles of equal radius $r(t)$ and volume $V_b(t) = \frac{4\pi}{3}r^3(t)$ in the compartment:

$$V_g(t) = N_b V_b(t) = N_b \frac{4\pi}{3} r^3(t). \quad (\text{A.1})$$

Several versions of the 3RUT-MB model equations for computing $V_g(t)$ have been developed as described below to handle increasingly general and more complex scenarios for bubble evolution in tissue, including cases in which the bubbles are not of equal volume, evolve under the influences of multiple diffusible gases, and are present in numbers that change with time.

8.1 Single Diffusible Gas

In single diffusible gas systems, the diffusible gas is inert and the metabolic gases water vapor, carbon dioxide (CO_2), and oxygen (O_2) are assumed to be infinitely diffusible – and hence always in equilibrium – between bubble, tissue, and blood.

8.1.1 Multiple Bubbles of Same Size

The bubble radius r and inert gas pressure P_b in each of the N_b bubbles in a single diffusible gas system satisfy the equation for the rate of change of bubble radius given by

$$\frac{dr}{dt} = \frac{\left\{ K(p_t - P_b) \left[\Lambda + \frac{1}{r} \right] \right\} - \frac{r}{3} \frac{dP_{\text{amb}}}{dt}}{P_{\text{amb}} - P_{\infty} + \frac{4\sigma}{3r} + \frac{8\pi}{3} Mr^3}, \quad (\text{A.2})$$

where the bracketed term in the numerator on the right is the inert gas flux per unit area across the bubble-tissue surface (positive for inward flux), K is the permeability (= solubility \times diffusivity) of the diffusible gas in tissue, p_t is the spatial average tissue inert gas tension, P_b is the diffusible gas partial pressure in the bubble, P_{amb} is the ambient hydrostatic pressure, σ is surface tension, M is tissue modulus of elasticity, and Λ is a

parameter with dimension $1/r$ that accommodates all effects of perfusion heterogeneity^f and bubble-bubble interactions on bubble evolution. P_∞ is the total pressure of the infinitely diffusible gases in the bubble, i.e., $P_\infty = P_{H_2O} + P_{CO_2} + P_{O_2}$, equal to p_∞ in the tissue. P_∞ and its components are assumed constant and the same in all tissue compartments. The diffusible gas partial pressure in each bubble is given by the LaPlace equation with an added term to account for the pressure exerted by tissue elasticity:

$$P_b(t) = P_{amb} - P_\infty + \frac{2\sigma}{r(t)} + \frac{4\pi}{3} M r^3(t), \quad (A.3)$$

The spatial average tissue inert gas tension p_t in Eq. (A.2) has been shown to be given by

$$\frac{dp_t}{dt} + qp_t = qp_a - G \frac{dx(t)}{dt}. \quad (A.4)$$

where $q = \frac{1}{\tau}$, with the blood-tissue gas exchange time constant $\tau = \frac{\alpha_t}{\alpha_b \dot{Q}_t}$,

$$G = \left(\frac{4\pi}{3} \right) \frac{N_b}{\alpha_t V_t}, \text{ and } x(t) = P_b(t) r^3(t).$$

Inspired gas is assumed to contain no CO_2 and equilibrium is assumed between alveolar gas and arterial blood, so p_a equals the alveolar inert gas partial pressure P_A as given by combining Dalton's law for alveolar gas and the alveolar gas equation;⁶⁸

$$P_{A_{O_2}} = P_{amb} - P_{H_2O} - P_{A_{CO_2}} - P_A = F_{I_{O_2}} (P_{amb} - P_{H_2O}) - P_{A_{CO_2}} \left[F_{I_{O_2}} + \left(1 - \frac{F_{I_{O_2}}}{RQ} \right) \right]; \quad (A.5)$$

and solving for P_A :

$$P_A = p_a = \left(1 - F_{I_{O_2}} \right) \left[(P_{amb} - P_{H_2O}) - P_{A_{CO_2}} \left(1 - \frac{1}{RQ} \right) \right], \quad (A.6)$$

where $F_{I_{O_2}}$ is the fraction of oxygen in dry inspired gas, $P_{A_{CO_2}}$ is the alveolar CO_2 partial pressure (assumed equal to 35 mm-Hg in present work), and RQ is the respiratory quotient (ratio of the rate of whole body CO_2 production to the rate of whole body O_2 consumption = $\dot{V}_{CO_2,wb} / \dot{V}_{O_2,wb}$).

^f Spatial variations in perfusion are assumed to sum to zero over the tissue volume.

The equations for dr/dt and dp_t/dt are coupled nonlinear equations that require numerical solution.

8.1.2 Multiple Bubbles of Different Sizes

The relationships in Eqs. (A.2) through (A.4) are readily elaborated to accommodate the solution for the radii and gas pressures of multiple bubbles present in an arbitrary distribution of N_{bs} different sizes. Such elaboration entails repeating the dr/dt and P_b solutions in Eqs. (A.2) and (A.3) for the bubbles of each size in the distribution. Thus, for bubbles of m^{th} size, Eq. (A.2) becomes

$$\frac{dr_m}{dt} = \frac{K_m \left[\Lambda + \frac{1}{r_m} \right] (p_t - P_{b_m}) - \frac{r_m}{3} \frac{dP_{amb}}{dt}}{P_{amb} - P_\infty + \frac{4\sigma_m}{3r_m} + \frac{8\pi}{3} M_m r_m^3}, \quad (\text{A.9})$$

and Eq. (A.3) becomes

$$P_{b_m}(t) = P_{amb} - P_\infty + \frac{2\sigma_m}{r_m(t)} + \frac{4\pi}{3} M_m r_m^3(t). \quad (\text{A.10})$$

Although not necessary, the bubble surface permeability, K_m , surface tension, σ_m , and modulus of elasticity, M_m , are considered to be different for each bubble size group.

Eq. (A.4) for the tissue gas tension, p_t , also requires modification to account for the net gas exchange between all bubbles and the tissue, as such exchange differs for bubbles of different sizes. The right-most term in Eq. (A.4) is replaced by the sum of the amounts of gas exchanged between tissue and all bubbles of N_{bs} different sizes to yield:

$$\frac{dp_t}{dt} + qp_t = qp_a - \sum_m^{N_{bs}} G_m \frac{dx_m(t)}{dt}, \quad (\text{A.11})$$

where

$$G_m = \left(\frac{4\pi}{3} \right) \frac{n_{b_m}}{\alpha_t V_t},$$

$$x_m(t) = P_{b_m}(t) r_m^3(t),$$

and n_{b_m} is the number of bubbles in the m^{th} size group; i.e., the number of identically sized bubbles of radius r_m .

Finally, the total volume of bubbles in the tissue is given by appropriate elaboration of Eq. (A.1):

$$V_g(t) = \sum_m^{N_{bs}} n_{b_m} \frac{4\pi}{3} r_m^3(t) = \sum_m^{N_{bs}} n_{b_m} V_{b_m}(t). \quad (\text{A.12})$$

Determination of r_m and P_{b_m} for bubble size groups $m=1, 2, \dots, N_{bs}$, and p_t at any time t requires computation time in excess of that required for the $N_{bs} = 1$ case (multiple bubbles of the same size) roughly in proportion to the number of bubble sizes considered.

8.1.3 Exercise Effects on Blood-Tissue Gas Exchange

Blood flow \dot{Q} changes with activity level and consequently varies with time, which causes the time constant τ to be a function of time. Accordingly, Eq. (A.11) is modified to explicitly indicate the time-dependence of the coefficients:

$$\frac{dp_t}{dt} + q(t)p_t = q(t)p_a - \sum_m^{N_{bs}} G_m \frac{dx_m(t)}{dt}, \quad (\text{A.13})$$

where $q(t) = \frac{1}{\tau(t)} = \frac{\alpha_b \dot{Q}(t)}{\alpha_t}$ is proportional to blood flow.

Eq. (A.13) is a linear differential equation in p_t with a variable coefficient $q(t)$. Solutions of Eq. (A.13) with general and specific models of $q(t)$ are described in Appendix B. The specific $q(t)$ model includes dependence of compartmental \dot{Q} on compartmental O_2 consumption, which is in turn dependent on exercise intensity.

8.2 Multiple Diffusible Gases

The bubble evolution Eq. (A.9) is elaborated as follows to accommodate more than one diffusible gas:

$$\frac{dr_m}{dt} = \frac{\left\{ \sum_{k=1}^{N_g} K_{k,m} (p_{t_k} - P_{b_{k,m}}) \right\} \left[\Lambda + \frac{1}{r_m} \right] - \frac{r_m}{3} \frac{dP_{amb}}{dt}}{P_{amb} - P_{\infty} + \frac{4\sigma_m}{3r_m} + \frac{8\pi}{3} M_m r_m^3}; \quad m = 1, 2, \dots, N_{bs}, \quad (A.14)$$

where N_g is the total number of gases with finite diffusivity and the subscript k denotes the k^{th} gas with spatial average tissue tension p_{t_k} , bubble gas partial pressure $P_{b_{k,m}}$, and bubble surface permeability $K_{k,m}$ associated with bubbles of the m^{th} size. Note that Λ is assumed to be the same for all bubble sizes and diffusible gases but that each diffusible gas beyond the first (gases for which $k > 1$) introduces an additional permeability coefficient.

The total pressure $P_{b_{T,m}}$ of all diffusible gases in bubbles of m^{th} size is computed using Eq. (A.10) as with a single gas:

$$P_{b_{T,m}}(t) = P_{amb} - P_{\infty} + \frac{2\sigma_m}{r_m(t)} + \frac{4\pi}{3} M_m r_m^3(t). \quad (A.15)$$

However, the partial pressure of each diffusible gas k in the m^{th} size bubble, $P_{b_{k,m}}$, must be determined by integrating the flux \times area product for gas k in conjunction with the dr/dt integration.

The average tissue tension is computed separately for each diffusible gas using Eq. (A.13);

$$\frac{dp_{t_k}}{dt} + q_k(t)p_{t_k} = q_k(t)p_{a_k} - \sum_m^{N_{bs}} G_{k,m} \frac{dx_{k,m}(t)}{dt}; \quad k = 1, 2, \dots, N_g; \quad (A.16)$$

where p_{t_k} and p_{a_k} are the average tissue and arterial tensions of the k^{th} diffusible

gas, respectively, $q_k(t) = \frac{1}{\tau_k(t)} = \frac{\alpha_{b_k} \dot{Q}(t)}{\alpha_{t_k}}$,

$$G_{k,m} = \left(\frac{4\pi}{3} \right) \frac{n_{b_m}}{\alpha_{t_k} V_t},$$

and

$$x_{k,m}(t) = P_{b_{k,m}}(t)r_m^3(t).$$

$\tau_k(t)$ – and hence $q_k(t)$ – is different for each gas because of differences in solubility ratio, $\alpha_{b_k}/\alpha_{t_k}$. The arterial tension of the k^{th} diffusible gas, p_{a_k} , is obtained

under the assumptions applied in the single diffusible gas case with appropriate elaboration of Eq.(A.6):

$$\sum^{N_g} P_{A_k} = \sum^{N_g} p_{a_k} = \sum^{N_g} F_{I_k} \left[(P_{amb} - P_{H_2O}) - P_{A_{CO_2}} \left(1 - \frac{1}{RQ} \right) \right], \quad (A.17)$$

$$P_{A_k} = p_{a_k} = F_{I_k} \left[(P_{amb} - P_{H_2O}) - P_{A_{CO_2}} \left(1 - \frac{1}{RQ} \right) \right], \quad k=1, \dots, N_g. \quad (A.18)$$

Note that the gas fraction sum, $\sum^{N_g} F_{I_k}$, in Eq. (A.17) must equal $(1 - F_{I_{O_2}})$.

Eqs. (A.14), (A.15), and (A.16) are the requisite equations for computing the evolution of bubbles of N_{bs} different sizes, and the corresponding bubble pressures and total volumes, when more than one diffusible gas is present in the tissue. Eq. (A.14) for the rate of change of bubble radius is more complex than Eq. (A.9) for the $N_g = 1$ case, but there is no increase in the number of equations, N_{bs} . Eq. (A.16) for the average tissue gas tension is the same as before, but there are now as many of these equations as the number of diffusible gases, N_g . Thus, the overall model comprises a total of $(N_{bs} + N_g)$ equations for each tissue compartment along with Eq. (A.12) for calculating the gas volume $V_g(t)$.

8.2.1 Tissue O_2 Tension with O_2 as a Diffusible Gas

When equilibrium of O_2 tensions between bubble and tissue is not assumed, bubble evolution is influenced by O_2 pressure gradients across the bubble-tissue interface. Under such conditions, O_2 must be treated as a gas with finite diffusivity along with the inert gases present in the tissue. Because O_2 mass balance between bubble, tissue, and blood must include accounting for the metabolic consumption of O_2 in the tissue and the nonlinear relationship between blood O_2 content and O_2 partial pressure due to O_2 binding to hemoglobin in blood, the expression for tissue O_2 tension as it is affected by bubble-tissue and tissue-blood gas exchange is more complex than the corresponding expression for the inert gases.

As for the inert gases, the expression for tissue O_2 tension, $p_{t_{O_2}}$, is obtained from the expression for mass balance of O_2 in tissue, which differs from that for the inert gases and is given by

$$\frac{d}{dt} (\alpha_{t_{O_2}} p_{t_{O_2}}) = \dot{Q}(t) [C_{a_{O_2}} - C_{\bar{v}_{O_2}}] - \frac{1}{V_t} \sum_{m=1}^{N_{bs}} n_{b_m} \frac{d}{dt} [P_{b_{O_2,m}}(t) \cdot V_{b_m}(t)] - \dot{V}_{O_2}(t), \quad (A.19)$$

where $\dot{Q}(t)$ = blood flow per unit volume of tissue

$\dot{V}_{O_2}(t)$ = tissue O_2 consumption rate

$$\begin{aligned}
C_{a_{O_2}} &= \text{O}_2 \text{ concentration in arterial blood entering tissue,} \\
C_{\bar{v}_{O_2}} &= \text{O}_2 \text{ concentration in mixed venous blood leaving tissue,} \\
p_{a_{O_2}} &= \text{arterial O}_2 \text{ partial pressure,} \\
p_{\bar{v}_{O_2}} &= \text{O}_2 \text{ partial pressure in mixed venous blood,} \\
\alpha_{t_{O_2}} &= \text{O}_2 \text{ solubility in tissue, and} \\
\alpha_{b_{O_2}} &= \text{O}_2 \text{ solubility in blood.}
\end{aligned}$$

Note that $\dot{V}_{O_2}(t)$, along with $\dot{Q}(t)$, are explicit functions of time as exercise-induced changes in compartmental \dot{Q} are presumed to be driven by changes in \dot{V}_{O_2} (Section 8.2.2).

Under steady-state conditions, the derivative terms in Eq. (A.19) are absent, and O_2 consumption is the product of blood flow and the arterial-venous O_2 content difference. Note that Eq. (A.19) reduces to Eq. (A.16) for the inert gases with substitution of the subscript k for subscript O_2 , $\dot{V}_k = 0$ (gas k inert), $C_{a_k} = \alpha_{b_k} p_{a_k}$, and $C_{\bar{v}_k} = \alpha_{b_k} p_{\bar{v}_k} = \alpha_{b_k} p_{t_k}$, with equilibrium assumed between end-capillary venous blood and tissue, in accord with the 3RUT-MB model assumption that blood-tissue gas exchange is perfusion limited.

The arterial and venous O_2 contents, $C_{a_{O_2}}$ and $C_{\bar{v}_{O_2}}$, in Eq. (A.19) are readily computed at any time from the prevailing arterial and mixed venous O_2 partial pressures; $p_{a_{O_2}}$ and $p_{\bar{v}_{O_2}} = p_{t_{O_2}}$, respectively; and a suitable approximation of the oxyhemoglobin dissociation curve. As for the inert gases, equilibrium between alveolar gas and arterial blood is assumed so that $p_{a_{O_2}}$ equals the alveolar O_2 partial pressure $P_{A_{O_2}}$ given by:

$$p_{a_{O_2}} = P_{A_{O_2}} = P_{amb} - P_{H_2O} - P_{A_{CO_2}} - \sum P_{A_k}, \quad (A.20)$$

where $\sum P_{A_k}$ is given by Eq. (A.17).

A variety of empirical equations have been described that relate O_2 content and O_2 partial pressure in blood. We use a simple expression developed by Lobdell for S_{O_2} , the fraction of hemoglobin saturated with O_2 at partial pressure P_{O_2} :⁶⁹

$$S_{O_2} = \frac{a_1 p + a_2 p^2}{1.0 + b_1 p + b_2 p^2}, \quad (\text{A.21})$$

where $a_1 = 0.34332$,

$a_2 = 0.64073$,

$b_1 = 0.34128$,

$b_2 = a_2 = 0.64073$,

$$p = \left(\frac{p_{O_2}}{p_{\text{half}}} \right)^\eta \text{ with}$$

$\eta = 1.58678$, and

$p_{\text{half}} =$ half-saturation p_{O_2} of hemoglobin
(with p_{O_2} in units of mm-Hg, $p_{\text{half}} = 25.0$ mm-Hg.)

The O_2 content of blood c_{O_2} in mL O_2 / mL blood at O_2 tension p_{O_2} is then given by

$$C_{O_2} = \alpha_{b_{O_2}} p_{O_2} + Hb_c S_{O_2}, \quad (\text{A.22})$$

where Hb_c is the O_2 carrying capacity of hemoglobin in whole blood (= 0.20 mL/mL) and $\alpha_{b_{O_2}}$ is the solubility of O_2 in plasma in mL O_2 / mL plasma mm-Hg, and s_{O_2} is obtained from Eq. (A.21).

There is no analytic solution of the nonlinear differential Eq. (A.19) for $p_{t_{O_2}}$, which must therefore be solved numerically. Recursive relations for the numerical solution of Eq. (A.19) are given in Appendix B.

8.2.2 Exercise Effects on Tissue O_2 Consumption

Exercise-induced changes in compartmental $\dot{V}_{O_2}(t)$ are readily modeled as a single exponential function of time:

$$\dot{V}_{O_2}(t) = \dot{V}_{O_2_{\text{rest}}} + \Delta \dot{V}_{O_2_{\text{ex}}} \left\{ 1 - \exp\left(-\frac{t}{\tau_{\dot{V}_{O_2}}} \right) \right\}, \quad (\text{A.25})$$

where $\dot{V}_{O_2_{\text{rest}}}$ is the resting O_2 consumption, $\tau_{\dot{V}_{O_2}}$ is the time constant associated with the exponential change in \dot{V}_{O_2} , and $\Delta \dot{V}_{O_2_{\text{ex}}}$ is the increase in O_2 consumption from its

resting value after reaching a steady state ($t = \infty$) with exercise at intensity I_{ex} .

$\Delta \dot{V}_{O2_{ex}}$ is given by

$$\Delta \dot{V}_{O2_{ex}} = m_{\dot{V}_{O2}} I_{ex}, \quad (A.26)$$

where $m_{\dot{V}_{O2}}$ is a factor governing the sensitivity of \dot{V}_{O2} to exercise. The time required to reach a given fraction f of the total \dot{V}_{O2} response to a change in exercise intensity is

given by solving $f = 1 - \exp\left(-\frac{t}{\tau_{\dot{V}_{O2}}}\right)$ for t : $t = \tau_{\dot{V}_{O2}} \ln\left[\frac{1}{(1-f)}\right]$. Thus, with a time

constant $\tau_{\dot{V}_{O2}}$ of 0.75 minute, 98% of the change to a new level of O_2 consumption is reached in approximately 3 minutes after a change in exercise intensity.

8.3 Bubble Nucleation and Variable Bubble Number

Bubbles are recruited from a pre-existing population of bubble nuclei in each compartment as the gas supersaturation increases during decompression. This recruitment process causes the number of bubble size groups to increase as decompression proceeds, so that N_{bs} becomes a function of time. In present models, the pre-existing nuclei are assumed to be stabilized against extinction by skins of adsorbed amphiphilic molecules, and have an integral distribution of sizes given by⁴⁰

$$N_b = N_b^0 \exp\left(-\frac{r_{min}}{\beta}\right), \quad (A.27)$$

where N_b is the number of nuclei present in the compartment with radius $\geq r_{min}$, N_b^0 is the constant total number of nuclei in the compartment, and β is a compartment-specific distribution slope factor.

The distribution of nuclear sizes is assumed to be affected by pressure, under the constraints that: (i) no nuclei are extinguished by any overpressures, and (ii) the original ordering of nuclear sizes is always preserved. Under these constraints, the number of nuclei with radii greater than or equal to r_{min} after exposure to an overpressure given by

$$P_{crush} = P_{amb} - \left(\sum_{k=1}^{N_g} p_{t_k} + P_{\infty} \right) \quad (A.28)$$

must equal the number of nuclei with radii greater than or equal to r_{min}^0 in the distribution before the exposure. Using Eq. (A.27), we therefore have

$$N_b = N_b^o \exp\left(-\frac{r_{\min}}{\beta}\right) = N_b^o \exp\left(-\frac{r_{\min}^o}{\beta^o}\right), \quad (\text{A.29})$$

where β^o is the slope factor for the initial nuclear size distribution.

If the adsorbed skins on the nuclei are assumed to remain always permeable to dissolved gases, the post-crush gas supersaturation P_{ss} required to nucleate the N_b bubbles in Eq. (A.29) depends on the initial r_{\min}^o and P_{crush} as given by [6]:

$$P_{ss} = \frac{2\sigma}{r_{\min}} \quad (\text{A.30})$$

$$= \frac{2\sigma(\sigma_c - \sigma)}{\sigma_c r_{\min}^o} + P_{crush} \left(\frac{\sigma}{\sigma_c}\right) = \left(\frac{\sigma}{\sigma_c}\right) \frac{2(\sigma_c - \sigma) + P_{crush} r_{\min}^o}{r_{\min}^o}, \quad (\text{A.31})$$

where Eq. (A.30) is the Laplace equation with tissue elasticity neglected and $\sigma_c (> \sigma)$ in Eq. (A.31) is the ‘‘crumpling compression’’ that counters the tendency for surface tension to extinguish nuclei of r_{\min}^o radius. The crumpling compression is constant for given r_{\min}^o and N_b , but decreases linearly with decreasing r_{\min}^o and increasing N_b .

The slope factor, β , for the distribution at a given pressure is obtained using Eqs. (A.29), (A.30), and (A.31):

$$\begin{aligned} \beta &= \left(\frac{\beta^o}{r_{\min}^o}\right) r_{\min} = \left(\frac{\beta^o}{r_{\min}^o}\right) \left(\frac{2\sigma}{P_{ss}}\right) = \left(\frac{\beta^o}{r_{\min}^o}\right) (2\sigma) \left(\frac{\sigma_c}{\sigma}\right) \left[\frac{r_{\min}^o}{2(\sigma_c - \sigma) + P_{crush} r_{\min}^o}\right] \\ &= \frac{\beta^o 2\sigma_c}{2(\sigma_c - \sigma) + P_{crush} r_{\min}^o}. \end{aligned} \quad (\text{A.32})$$

The r_{\min}^o and r_{\min} in Eq. (A.29) correspond to the respective pre- and post-crush P_{ss} values required to nucleate a given number of bubbles N_b . These radii and their corresponding β^o and β factors were initially defined in terms of the supersaturations required to form the same number of bubbles in two samples from a given gelatin preparation before and after a P_{crush} exposure.⁴⁰ In the present context, we wish to determine the supersaturation at which bubbles initially begin to form after a P_{crush} exposure. If the number of bubbles in any specific anatomical compartment must

increase in integer increments, this supersaturation is that at which the first bubble forms. Thus, for given β^o and N_b^o , Eq. (A.29) with $N_b = 1$ is rearranged to give r_{\min}^o :

$$r_{\min}^o = \beta^o \ln(N_b^o). \quad (\text{A.33a})$$

In present work, however, each hypothetical compartment represents an average of an indeterminate number of distributed anatomical sites. The number of bubbles in each of these composite compartments was consequently considered to increase continuously with allowance of fractional bubble numbers so that Eq. (A.33a) became:

$$r_{\min}^o = \beta^o \left[\ln(N_b^o) - \ln(N_b^{\min}) \right], \quad (\text{A.33b})$$

where N_b^{\min} is an arbitrary minimum number of bubbles, $0 < N_b^{\min} \ll 1$, allowed in a compartment.

Note from Eq. (A.32) that $\beta = \beta^o$ when $P_{\text{crush}} = 2\sigma/r_{\min}^o$, which consequently defines the minimum crushing pressure required to affect the initial distribution.

Substituting Eq. (A.30) into Eq. (A.27) gives the cumulative number of nucleated (or

recruited) bubbles at an arbitrary $P_{\text{SS}} = \left[\sum_{k=1}^{N_g} p_{t_k} + P_{\infty} \right] - P_{\text{amb}}$:

$$N_b = N_b^o \exp\left(-\frac{2\sigma}{\beta_f P_{\text{SS}}}\right). \quad (\text{A.34})$$

Exercise is modeled to affect the nuclei size distribution and bubble nucleation by modifying the distribution slope factor as follows:

$$\beta_f = \beta_{\text{ex}} \beta = \beta_{\text{ex}} \left[\frac{2\sigma_c \beta^o}{2(\sigma_c - \sigma) + P_{\text{crush}} r_{\min}^o} \right], \quad (\text{A.35})$$

where β_{ex} is a compartment-specific, dimensionless factor given by

$$\beta_{\text{ex}} = 1 + m_{\beta_{\text{ex}}} I_{\text{ex}}. \quad (\text{A.36})$$

I_{ex} is a measure of exercise intensity (= 0 at rest) and $m_{\beta_{\text{ex}}}$ is a factor (≥ 0) governing the sensitivity of the distribution slope factor to increasing exercise intensities.

Increasing values of P_{crush} decrease β_f and shift the population of nuclei towards smaller sizes, while increasing values of β_{ex} increase β_f and shift the population of nuclei

towards larger sizes. The bubble of largest size in the distribution governs the inception of bubble formation. The radius of this bubble is given by:

$$r_{\min} = \beta_f \left[\ln(N_b^o) - \ln(N_b^{\min}) \right]. \quad (\text{A.37})$$

The corresponding nucleonic volume, V_{\min} , is

$$V_{\min} = \frac{4}{3} \pi r_{\min}^3. \quad (\text{A.38})$$

Supersaturations of magnitude smaller than required to recruit a nucleus of r_{\min} radius are sustained metastably; i.e., without bubble formation. Larger supersaturations are accompanied by bubble nucleation and growth from increasing numbers of nuclei recruited as given by Equation (A.34). Increasing P_{crush} consequently increases the threshold supersaturation for bubble inception and reduces the number of nuclei recruited to become macroscopic bubbles at given supersaturations larger than this threshold. Increasing β_{ex} , on the other hand, decreases the threshold supersaturation for bubble inception and increases the number of nuclei recruited to macroscopic bubbles at supersaturations above this threshold. In the present model implementations, compartmental β_f is updated for effects of P_{crush} throughout a given profile only when no nucleated bubbles are present in the compartment. Compartmental β_f is updated for the effects of exercise at the outset of every stage in which exercise is performed.

Note that Eq. (A.28) indicates that P_{crush} increases with increases in P_{amb} or decreases in the total dissolved gas tension. Thus exercise-induced decreases in tissue N_2 and O_2 tensions during oxygen prebreathes increase P_{crush} and shift the distribution of nuclei to smaller sizes that require higher supersaturations to recruit.

The population of pre-existing nuclei is presumed to be dynamic, maintained by ever-active mechanisms for nuclei generation. The effects of a given crush must consequently decay over time as the population of nuclei is restored to the pre-crush state – even at pressure. Thus, the prevailing P_{crush} is considered to instantaneously achieve the computed crush pressure when the computed P_{crush} is increasing. When the computed P_{crush} is constant or decreasing, the prevailing P_{crush} is modeled to decay to its initial value P_{crush}^o according to:

$$P_{\text{crush}} = P_{\text{crush}}^o + (P_{\text{crush}} - P_{\text{crush}}^o) \exp(-t/\tau_{\text{PC}}), \quad (\text{A.39})$$

where τ_{PC} is the P_{crush} decay time constant.

8.3.1 Single Time-Dependent Bubble Size Approximation

In order to obviate need to track the evolution of multiple bubbles of different sizes in any given compartment, each newly nucleated bubble is assumed to instantaneously

attain the size of prevailing already-nucleated bubbles. Because all bubbles are consequently the same size, r_m , P_{b_m} , and p_t must be tracked for only a single bubble size group ($N_{bs} = 1$) in which only n_b changes:

$$N_b(t) = \left(\sum_m^{N_{bs}(t)} n_{b_m} \right) \equiv n_b(t), \quad N_{bs} = 1. \quad (\text{A.40})$$

Eq. (A.16) is thus simplified:

$$\frac{dp_{t_k}}{dt} + q_k(t)p_{t_k} = q_k(t)p_{a_k} - G_k(t) \frac{dx_k(t)}{dt}, \quad (\text{A.41})$$

where n_b – and hence G_k – are now explicit functions of time:

$$G_k(t) = \left(\frac{4\pi}{3} \right) \frac{N_b(t)}{\alpha_{t_k} V_t}$$

and

$$x_k(t) = P_{b_k}(t)r^3(t).$$

Maintenance of mass balance in this approach requires a change in bubble gas content and a resultant adjustment in tissue gas tension corresponding to the difference between the nucleonic volume and the prevailing bubble volume whenever a nucleus is ‘recruited’ during decompression. Regardless of the functional representation of the $G_k(t)$ factor, it may be approximated by a constant in each integration interval.

Implementation of this approach in the numerical solution of Eq. (A.41) for p_{t_k} is described in Appendix B.

8.4 Scaled 3RUT-MB Model

If the Λ parameter is constant and independent of the other parameters in the 3RUT-MB model, the dependent variable r_m can be scaled by defining $\hat{r}_m = \Lambda r_m$, where the overstrike ‘hat’ denotes a scaled quantity. Substituting for r_m in terms of \hat{r}_m in Eq. (A.14) yields

$$\frac{d\hat{r}_m}{dt} = \Lambda \frac{dr_m}{dt} = \frac{\left\{ \sum_{k=1}^{N_g} \hat{K}_{k,m} \frac{p_{t_k} - P_{b_{k,m}}}{3} \right\} \left[1 + \frac{1}{\hat{r}_m} \right] - \frac{\hat{r}_m}{3} \frac{dP_{amb}}{dt}}{P_{amb} - P_{\infty} + \frac{4\hat{\sigma}_m}{3\hat{r}_m} + 2\hat{M}_m(\hat{r}_m)^3}; \quad m = 1, 2, \dots, N_{bs}, \quad (\text{A.42})$$

where $\hat{K}_{k,m} = 3\Lambda^2 K_{k,m}$, $\hat{\sigma}_m = \Lambda\sigma_m$, and $\hat{M}_m = \left(\frac{4\pi}{3}\right)\frac{M_m}{\Lambda^3}$ are the scaled permeability,

surface tension, and tissue modulus of elasticity, respectively, for a bubble in the m^{th} bubble size group. Note that \hat{r}_m is dimensionless with Λ having dimension of 1/radius, $\hat{K}_{k,m}$ having dimension of 1/time, and $\hat{\sigma}_m$ and \hat{M}_m having dimension of pressure. The permeability coefficient for each diffusible gas beyond the first in the tissue (gases for which $k>1$) can be specified relative to the first on the basis of the unscaled coefficients:

$$\hat{K}_{k,m} = \hat{K}_{1,m} \left[\frac{\hat{K}_{k,m}}{\hat{K}_{1,m}} \right] = \hat{K}_{1,m} \left[\frac{K_{k,m}}{K_{1,m}} \right].$$

Similarly, substituting for r_m in terms of \hat{r}_m , σ_m in terms of $\hat{\sigma}_m$, and M_m in terms of \hat{M}_m in Eq. (A.15) yields the following for the total diffusible gas pressure in bubbles of the m^{th} bubble size group:

$$P_{b_{T,m}}(t) = P_{\text{amb}} - P_{\infty} + \frac{2\hat{\sigma}_m}{\hat{r}_m(t)} + \hat{M}_m \hat{r}_m^3(t). \quad (\text{A.43})$$

The components of $P_{b_{T,m}}(t)$; i.e., the individual partial pressures of the diffusible gases in the bubble, $P_{b_{k,m}}$, $k = 1, 2, \dots, N_g$; are determined as part of the numerical integration of Eq. (A.42) described in Appendix B [see Eq. (B.41)].

Finally, from Eq. (A.16) the average tissue tension of the k^{th} diffusible gas is given by

$$\frac{dp_{t_k}}{dt} + q_k(t)p_{t_k} = q_k(t)p_{a_k} - \sum_m^{N_{bs}} \hat{G}_{k,m} \frac{d\hat{x}_{k,m}(t)}{dt}; \quad k = 1, 2, \dots, N_g, \quad (\text{A.44})$$

where $\hat{G}_{k,m} = \left(\frac{4\pi}{3}\right)\frac{n_{b_m}}{\alpha_{t_k} \hat{V}_t}$ with $\hat{V}_t = V_t \Lambda^3$, and

$$\hat{x}_{k,m}(t) = P_{b_{k,m}} \hat{r}_m^3(t).$$

Neither Eq. (A.42), (A.43), or (A.44), which comprise the bubble dynamics equations for the scaled system, contain the scale factor Λ . The scale factor can therefore be chosen arbitrarily. A single solution of the equations with a given value of Λ is analytically related to all other solutions of the equations obtained with any other value of Λ . Scaling non-dimensionalizes the bubble volume for application in the hazard function of survival models.

In terms of the dimensionless scaled bubble volumes in the m^{th} size group,

$$\hat{V}_{b_m} = \frac{4\pi}{3} \hat{r}_m^3 = \frac{4\pi}{3} (\Lambda r_m)^3 = \Lambda^3 V_{b_m}.$$

Eq. (A.12) for total bubble volume is then expressed in scaled form as

$$\hat{V}_g(t) = \sum_m^{N_{bs}} \Lambda^3 V_{b_m}(t) n_{b_m} = \sum_m^{N_{bs}} \hat{V}_{b_m}(t) n_{b_m}. \quad (\text{A.45})$$

With the single time-dependent bubble size approximation in Eq. (A.40), $m=1$, and r_{\min} , r_{\min}^0 , σ_c , β^0 , and β_f in Eqs. (A.27) through (A.37) of the bubble nucleation model then scale with the compartmental Λ ; $\hat{r}_{\min} = \Lambda r_{\min}$, $\hat{r}_{\min}^0 = \Lambda r_{\min}^0$, $\hat{\sigma}_c = \Lambda \sigma_c$, $\hat{\beta}^0 = \Lambda \beta^0$, and $\hat{\beta}_f = \Lambda \beta_f$. Eq. (A.45) then becomes

$$\hat{V}_g(t) = \hat{V}_b(t) n_b(t). \quad (\text{A.46})$$

Eqs. (A.42), (A.41), (A.44), and (A.45) or (A.46) describe the scaled 3RUT-MB model in its final form.

8.5 Model Operation and Initial Values

The tissue tensions of the inert gases at profile start were assumed equal to the corresponding arterial tensions in the saturation steady state at ground level pressure breathing air.

Unlike the tissue tensions of the inert gases, the tissue O_2 tension ($p_{t_{O_2}}$) is not equal to the arterial O_2 tension in the saturation steady state because of the metabolic consumption of O_2 in the tissue ($\dot{V}_{O_2} > 0$). The tissue O_2 tension ($p_{t_{O_2}}$) for initiating the calculations at profile start was calculated assuming $p_{t_{O_2}} = p_{\bar{v}_{O_2}}$ and using the steady state O_2 mass balance relationship between blood flow and O_2 consumption given by the Fick principle:

$$\dot{Q} (C_{av_{O_2}}) = \dot{Q} (C_{a_{O_2}} - C_{\bar{v}_{O_2}}) = \dot{V}_{O_2}. \quad (\text{A.47})$$

Solving Eq. (A.47) for $C_{\bar{v}_{O_2}}$ yields

$$C_{\bar{v}_{O_2}} = C_{a_{O_2}} - \frac{\dot{V}_{O_2}}{\dot{Q}}. \quad (\text{A.48})$$

The partial pressure $p_{\bar{v}_{O_2}}$ corresponding to $C_{\bar{v}_{O_2_0}}$ was then determined using the secant method to numerically invert the blood O_2 content versus partial pressure curve, Eq. (A.22), at $C_{\bar{v}_{O_2_0}}$.

Exercise-induced changes in compartmental $\dot{V}_{O_2}(t)$ and consequent changes in compartmental blood flow, \dot{Q} , were assumed to manifest instantaneously.

Present models incorporated the simplification described in Sections 11.3.1 and 12.2.2, wherein multiple bubbles in a given tissue compartment are considered to evolve in parallel at the same size, requiring consideration of only a single bubble size group. The initial nucleus size of the bubble was specified by Eq. (A.37), which includes an accounting for the effects of O_2 prebreathe and exercise on bubble nucleation.

The initial pressure of the k^{th} diffusible gas in the bubble ($P_{b_{k,0}}$) was computed assuming that the ratio of the gas pressure to the total bubble pressure is the same as the ratio of the tissue tension of the gas to the total tissue tension at the moment of recruitment; i.e.,

$$\frac{P_{b_{k,0}}}{\sum_k P_{b_{k,0}}} = \frac{P_{t_{k,0}}}{\sum_k P_{t_{k,0}}} = c_{r_k} \quad \text{when } V_b = V_{r0}, \quad (\text{A.49})$$

where
$$\sum_{k=1}^{N_g} P_{b_{k,0}} = P'_{\text{amb}_0} + \frac{2\hat{\sigma}}{r_0} + \hat{M}r_0^3,$$

and P'_{amb_0} is the ambient hydrostatic pressure when the first bubble is nucleated, less pressures exerted by the infinitely diffusible gases (CO_2 and water vapor; O_2 pressure is not subtracted when treated as a finitely diffusible gas). Nominal values for tissue CO_2 pressure and water vapor pressure at body temperature are 45 and 47 mm-Hg, respectively. The total correction for CO_2 and water vapor was thus $45 + 47 = 92$ mm-Hg.

From Eq. (A.49), the initial bubble pressure of the k^{th} diffusible gas is

$$P_{b_{k,0}} = c_{r_k} \sum_k P_{b_{k,0}} \quad (\text{A.50})$$

and the scaled bubble gas content is

$$\hat{x}_{k,0} = P_{b_{k,0}} \hat{r}_0^3. \quad (\text{A.51})$$

Before bubble nucleation (and after complete bubble resolution), when compartmental $p_{t_{k,n}} \leq P_{b_{k,n}}$ for all diffusible gases, the bubble was assumed to remain stable at its nucleus size with $\delta r_n = 0$.

The coupled bubble radius and bubble pressure equations were solved with the piecewise analytic solution derived in Appendix B. The integration step size, dt , for each time step was reduced or increased as a function of the rate of bubble radius change, $d\hat{r}/dt$, in the previous step according to:

$$dt = (dt_{\max} - dt_{\min}) \exp[-dt_k (d\hat{r}/dt)] + dt_{\min}, \quad (\text{A.52})$$

where dt_{\max} and dt_{\min} are the largest and smallest allowed time step sizes, respectively, and dt_k is a decay constant.

Numerical instabilities in the solution were avoided by comparing the sum of the bubble diffusible gas partial pressures to the sum of the tissue diffusible gas tensions in each iteration of the recursive solution process. If the bubble pressure sum exceeded the tissue tension sum with positive dr/dt at any point in an isobaric stage, the stage was restarted with the integration step size reduced by a factor of ten.

9. Appendix B. Piece-Wise Analytic Approximation of the Three-Region Unstirred Tissue Multiple Bubble (3RUT-MB) Model of Tissue Gas and Bubble Dynamics

The three-region, unstirred-tissue, multiple-bubble (3RUT-MB) model of gas and bubble dynamics [36] comprises two sets of coupled nonlinear differential equations; one for the rates of change of volumes and pressures of gas bubbles in a hypothetical tissue compartment, and a second for the rates of change of dissolved gas tensions in the compartment. These equations must be solved simultaneously by numerical methods. A numerical piece-wise analytic approximation of the coupled equations was developed for efficient and stable solution of the equations.

To simplify the notation in the development, we begin by considering the evolution of one or more bubbles of the same size under the influence of a single diffusible gas. We then advance to consider the evolution of multiple bubbles of different sizes under the influence of a single diffusible gas and conclude by considering the evolution of multiple bubbles of different sizes under the influence of multiple diffusible gases.

9.1 Single Diffusible Gas

9.1.1 Multiple Bubbles of Same Size

9.1.1.1 Changes in Bubble Radius and Bubble Gas Pressure

The changes in bubble radius, r , as well as the bubble pressures exerted by the diffusible gases that participate in the evolution of a bubble are determined from the Fick equation, which is expressed for a single diffusible gas in the 3RUT-MB model as

$$\frac{d}{dt} (P_b V_b) = K A_b (\Lambda + 1/r)(p_t - P_b), \quad (\text{B.1})$$

where $(\Lambda + 1/r)(p_t - P_b)$ is the pressure gradient of the diffusible gas at the bubble surface, A_b is the bubble surface area ($= 4\pi r^2$), and K , p_t , P_b , and Λ are defined as before. With the dimensionless scaled bubble radius $\hat{r} = \Lambda r$, $v_b = \frac{4\pi \hat{r}^3}{3\Lambda^3}$ and $A_b = \frac{4\pi \hat{r}^2}{\Lambda^2}$.

Substituting for r , V_b , and A_b in terms of \hat{r} in Eq. (B.1), we obtain

$$\frac{4\pi}{3} \frac{1}{\Lambda^3} \frac{d}{dt} (P_b \hat{r}^3) = K (4\pi) \frac{\hat{r}^2}{\Lambda^2} \left(\Lambda + \frac{\Lambda}{\hat{r}} \right) (p_t - P_b),$$

$$\begin{aligned}
\frac{d}{dt}(P_b \hat{r}^3) &= 3 \Lambda^2 K (\hat{r}^2 + \hat{r}) (p_t - P_b) , \\
\frac{d}{dt}(P_b \hat{r}^3) + 3 \Lambda^2 K (\hat{r}^2 + \hat{r}) P_b &= 3 \Lambda^2 K (\hat{r}^2 + \hat{r}) p_t , \\
\frac{d}{dt}(P_b \hat{r}^3) + \hat{K} \left(\frac{1}{\hat{r}} + \frac{1}{\hat{r}^2} \right) (P_b \hat{r}^3) &= \hat{K} (\hat{r}^2 + \hat{r}) p_t , \tag{B.2}
\end{aligned}$$

where $\hat{K} = 3\Lambda^2 K$ is the scaled permeability, which has a dimension 1/time.

With $\hat{x} = P_b \hat{r}^3$, $f(t) = \hat{K} \left(\frac{1}{\hat{r}} + \frac{1}{\hat{r}^2} \right)$, $g(t) = \hat{K} (\hat{r}^2 + \hat{r}) p_t$, and bubble radius \hat{r} and tissue gas tension p_t treated as explicit functions of time, Eq. (B.2) becomes

$$\frac{d\hat{x}}{dt} + f(t)\hat{x} = g(t) , \tag{B.3}$$

which is a linear differential equation in \hat{x} with variable coefficients. Eq. (B.3) is solved using the integrating factor method to obtain the following recursive relationship (See Section 9.3):

$$\begin{aligned}
\hat{x}_{n+1} = \hat{x}_n + [(g_n + g_{n+1}) - (f_n + f_{n+1})\hat{x}_n] \frac{\Delta t_n}{2} + [(f_n + f_{n+1})^2 \hat{x}_n] \frac{\Delta t_n^2}{8} \\
- [3(g_n f_n + g_{n+1} f_{n+1}) + (g_n f_{n+1} - g_{n+1} f_n)] \frac{\Delta t_n^2}{12}, \quad n = 0, 1, 2, 3, \dots \tag{B.4}
\end{aligned}$$

where \hat{x}_n , f_n , and g_n are respectively the values of $\hat{x}(t)$, $f(t)$, and $g(t)$ at time t_n , and \hat{x}_{n+1} , f_{n+1} , and g_{n+1} are the corresponding values at time t_{n+1} . The step size, $\Delta t_n = t_{n+1} - t_n$, is subscripted to indicate that it may be assigned a different value for each integration step.

The coefficients on the right side of Eq. (B.4) are now evaluated using the definitions of $f(t)$ and $g(t)$ and denoting $\hat{r}(t)$ at times t_n and t_{n+1} by \hat{r}_n and \hat{r}_{n+1} , respectively, and the change $(\hat{r}_{n+1} - \hat{r}_n)$ by $\Delta \hat{r}_n$. Defining the tissue tension p_{t_n} as the value of p_t at time t_n and assuming that p_{t_n} stays steady in the interval $[t_n, t_{n+1}]$, consistent with the quasi-static approximation on which the 3RUT-MB model is based, we have the following for the coefficient $(g_n + g_{n+1})$:

$$\begin{aligned}
\frac{g_n + g_{n+1}}{\widehat{K}p_{t_n}} &= \hat{r}_n^2 + \hat{r}_n + \hat{r}_{n+1}^2 + \hat{r}_{n+1} \\
&= \hat{r}_n^2 + \hat{r}_n + (\hat{r}_n + \Delta\hat{r}_n)^2 + (\hat{r}_n + \Delta\hat{r}_n) \\
&= \hat{r}_n^2 + \hat{r}_n + (\hat{r}_n^2 + 2\hat{r}_n \Delta\hat{r}_n + \Delta\hat{r}_n^2) + (\hat{r}_n + \Delta\hat{r}_n) \\
&= 2(\hat{r}_n^2 + \hat{r}_n) + (2\hat{r}_n + 1)\Delta\hat{r}_n + \Delta\hat{r}_n^2
\end{aligned}$$

Considering $\Delta\hat{r}_n$ to be sufficiently small so that terms containing powers of $\Delta\hat{r}_n$ may be ignored, we have

$$\frac{g_n + g_{n+1}}{\widehat{K}p_{t_n}} = 2\hat{r}_n(\hat{r}_n + 1) + \hat{r}_n(2\hat{r}_n + 1)\delta\hat{r}_n, \quad (\text{B.5a})$$

where $\delta\hat{r}_n = \frac{\Delta\hat{r}_n}{\hat{r}_n}$ is the fractional change in bubble radius in the n^{th} integration step.

Now, for the coefficient $(f_n + f_{n+1})$, we have

$$\begin{aligned}
\frac{f_n + f_{n+1}}{\widehat{K}} &= \frac{1}{\hat{r}_n^2} + \frac{1}{\hat{r}_n} + \frac{1}{\hat{r}_{n+1}^2} + \frac{1}{\hat{r}_{n+1}} \\
&= \frac{1}{\hat{r}_n^2} + \frac{1}{\hat{r}_n} + \frac{1}{(\hat{r}_n + \Delta\hat{r}_n)^2} + \frac{1}{(\hat{r}_n + \Delta\hat{r}_n)} \\
&= \frac{1}{\hat{r}_n^2} + \frac{1}{\hat{r}_n} + \frac{1}{\hat{r}_n^2} (1 + \delta\hat{r}_n)^{-2} + \frac{1}{\hat{r}_n} (1 + \delta\hat{r}_n)^{-1}
\end{aligned}$$

The $(1 + \delta\hat{r}_n)^{-2}$ and $(1 + \delta\hat{r}_n)^{-1}$ terms in the above equation are of general form, $(1 + x)^n$, which is expanded about $x = 0$ and approximated to first order by $(1 + x)^n \cong (1 + nx)$.

Substituting the first order approximations for the $(1 + \delta\hat{r}_n)^{-2}$ and $(1 + \delta\hat{r}_n)^{-1}$ terms yields

$$\begin{aligned}
\frac{f_n + f_{n+1}}{\widehat{K}} &\cong \frac{1}{\hat{r}_n^2} + \frac{1}{\hat{r}_n} + \frac{1}{\hat{r}_n^2} (1 - 2\delta\hat{r}_n) + \frac{1}{\hat{r}_n} (1 - \delta\hat{r}_n) \\
&= \frac{2}{\hat{r}_n^2} + \frac{2}{\hat{r}_n} - \left[\frac{2}{\hat{r}_n^2} + \frac{1}{\hat{r}_n} \right] \delta\hat{r}_n \\
&= \frac{2(\hat{r}_n + 1)}{\hat{r}_n^2} - \left[\frac{\hat{r}_n + 2}{\hat{r}_n^2} \right] \delta\hat{r}_n \\
&= \frac{1}{\hat{r}_n^2} [2(\hat{r}_n + 1) - (\hat{r}_n + 2)\delta\hat{r}_n]. \tag{B.5b}
\end{aligned}$$

The following expression for the coefficient associated with $\Delta t_n/2$ on the right side of Eq. (B.4) is then obtained from Eqs. (B.5a) and (B.5b) and the definition of \hat{x}_n :

$$\begin{aligned}
&(g_n + g_{n+1}) - (f_n + f_{n+1})\hat{x}_n \\
&= [2\hat{r}_n(\hat{r}_n + 1) + \hat{r}_n(2\hat{r}_n + 1)\delta\hat{r}_n] \widehat{K} p_{t_n} - \left[\frac{1}{\hat{r}_n^2} \{2(\hat{r}_n + 1) - (\hat{r}_n + 2)\delta\hat{r}_n\} \widehat{K} \right] P_{b_n} \hat{r}_n^3 \\
&= [2\hat{r}_n(\hat{r}_n + 1) + \hat{r}_n(2\hat{r}_n + 1)\delta\hat{r}_n] \widehat{K} p_{t_n} - \hat{r}_n [2(\hat{r}_n + 1) - (\hat{r}_n + 2)\delta\hat{r}_n] \widehat{K} P_{b_n} \\
&= 2\hat{r}_n(\hat{r}_n + 1) \widehat{K} (p_{t_n} - P_{b_n}) + [\hat{r}_n(2\hat{r}_n + 1) \widehat{K} p_{t_n} + \hat{r}_n(\hat{r}_n + 2) \widehat{K} P_{b_n}] \delta\hat{r}_n. \tag{B.6}
\end{aligned}$$

The coefficient associated with $\Delta t_n^2/8$ on the right side of Eq. (B.4) is

$$\begin{aligned}
(f_n + f_{n+1})^2 \hat{x}_n &= \left[\frac{1}{\hat{r}_n^2} \{2(\hat{r}_n + 1) - (\hat{r}_n + 2)\delta\hat{r}_n\} \widehat{K} \right]^2 P_{b_n} \hat{r}_n^3 \\
&\cong \frac{1}{\hat{r}_n^4} [4(\hat{r}_n + 1)^2 - 4(\hat{r}_n + 1)(\hat{r}_n + 2)\delta\hat{r}_n] \widehat{K}^2 P_{b_n} \\
&= \left[\frac{4(\hat{r}_n + 1)^2}{\hat{r}_n} - \frac{4(\hat{r}_n + 1)(\hat{r}_n + 2)}{\hat{r}_n} \delta\hat{r}_n \right] \widehat{K}^2 P_{b_n}. \tag{B.7}
\end{aligned}$$

Now, for the coefficients associated with the last term on the right side of Eq. (B.4), we have

$$\begin{aligned}
\mathbf{g}_n \mathbf{f}_n + \mathbf{g}_{n+1} \mathbf{f}_{n+1} &= \left[\left(\hat{r}_n^2 + \hat{r}_n \right) \left(\frac{1}{\hat{r}_n^2} + \frac{1}{\hat{r}_n} \right) + \left(\hat{r}_{n+1}^2 + \hat{r}_{n+1} \right) \left(\frac{1}{\hat{r}_{n+1}^2} + \frac{1}{\hat{r}_{n+1}} \right) \right] \widehat{\mathbf{K}}^2 \mathbf{p}_{t_n} \\
&= \left[1 + \hat{r}_n + \frac{1}{\hat{r}_n} + 1 + 1 + \bar{r}_{n+1} + \frac{1}{\hat{r}_{n+1}} + 1 \right] \widehat{\mathbf{K}}^2 \mathbf{p}_{t_n} \\
&= \left[4 + \hat{r}_n + \frac{1}{\hat{r}_n} + (\hat{r}_n + \Delta \hat{r}_n) + \frac{1}{(\hat{r}_n + \Delta \hat{r}_n)} \right] \widehat{\mathbf{K}}^2 \mathbf{p}_{t_n} \\
&= \left[4 + \hat{r}_n + \frac{1}{\hat{r}_n} + \hat{r}_n (1 + \delta \hat{r}_n) + \frac{(1 + \delta \hat{r}_n)^{-1}}{\hat{r}_n} \right] \widehat{\mathbf{K}}^2 \mathbf{p}_{t_n} \\
&\cong \left[4 + \hat{r}_n + \frac{1}{\hat{r}_n} + \hat{r}_n (1 + \delta \hat{r}_n) + \frac{1 - \delta \hat{r}_n}{\hat{r}_n} \right] \widehat{\mathbf{K}}^2 \mathbf{p}_{t_n} \\
&= \left[4 + 2\hat{r}_n + \frac{2}{\hat{r}_n} + \hat{r}_n \delta \hat{r}_n - \frac{\delta \hat{r}_n}{\hat{r}_n} \right] \widehat{\mathbf{K}}^2 \mathbf{p}_{t_n} \\
&= \left[\frac{2(2\hat{r}_n + \hat{r}_n^2 + 1)}{\hat{r}_n} + \left(\hat{r}_n - \frac{1}{\hat{r}_n} \right) \delta \hat{r}_n \right] \widehat{\mathbf{K}}^2 \mathbf{p}_{t_n} \\
&= \left[\frac{2(\hat{r}_n + 1)^2}{\hat{r}_n} + \frac{\hat{r}_n^2 - 1}{\hat{r}_n} \delta \hat{r}_n \right] \widehat{\mathbf{K}}^2 \mathbf{p}_{t_n}, \tag{B.8a}
\end{aligned}$$

and

$$\begin{aligned}
g_n f_{n+1} - g_{n+1} f_n &= (\hat{r}_n^2 + \hat{r}_n) \left[\frac{1}{\hat{r}_{n+1}^2} + \frac{1}{\hat{r}_{n+1}} \right] \widehat{\mathbf{K}}^2 p_{t_n} - (\hat{r}_{n+1}^2 + \hat{r}_{n+1}) \left[\frac{1}{\hat{r}_n^2} + \frac{1}{\hat{r}_n} \right] \widehat{\mathbf{K}}^2 p_{t_n} \\
&= \left[\left\{ \frac{\hat{r}_n^2}{\hat{r}_{n+1}^2} + \frac{\hat{r}_n}{\hat{r}_{n+1}^2} + \frac{\hat{r}_n^2}{\hat{r}_{n+1}} + \frac{\hat{r}_n}{\hat{r}_{n+1}} \right\} - \left\{ \frac{\hat{r}_{n+1}^2}{\hat{r}_n^2} + \frac{\hat{r}_{n+1}}{\hat{r}_n^2} + \frac{\hat{r}_{n+1}^2}{\hat{r}_n} + \frac{\hat{r}_{n+1}}{\hat{r}_n} \right\} \right] \widehat{\mathbf{K}}^2 p_{t_n} \\
&= \left[\left\{ \frac{\hat{r}_n^2}{(\hat{r}_n + \Delta \hat{r}_n)^2} + \frac{\hat{r}_n}{(\hat{r}_n + \Delta \hat{r}_n)^2} + \frac{\hat{r}_n^2}{(\hat{r}_n + \Delta \hat{r}_n)} + \frac{\hat{r}_n}{(\hat{r}_n + \Delta \hat{r}_n)} \right\} \right. \\
&\quad \left. - \left\{ \frac{(\hat{r}_n + \Delta \hat{r}_n)^2}{\hat{r}_n^2} + \frac{(\hat{r}_n + \Delta \hat{r}_n)}{\hat{r}_n^2} + \frac{(\hat{r}_n + \Delta \hat{r}_n)^2}{\hat{r}_n} + \frac{(\hat{r}_n + \Delta \hat{r}_n)}{\hat{r}_n} \right\} \right] \widehat{\mathbf{K}}^2 p_{t_n} \\
&= \left[\left\{ (1 + \delta \hat{r}_n)^{-2} + \frac{1}{\hat{r}_n} (1 + \delta \hat{r}_n)^{-2} + \hat{r}_n (1 - \delta \hat{r}_n)^{-1} + (1 + \delta \hat{r}_n)^{-1} \right\} \right. \\
&\quad \left. - \left\{ (1 + \delta \hat{r}_n)^2 + \frac{1}{\hat{r}_n} (1 + \delta \hat{r}_n) + \hat{r}_n (1 + \delta \hat{r}_n)^2 + (1 + \delta \hat{r}_n) \right\} \right] \widehat{\mathbf{K}}^2 p_{t_n} \\
&\cong \left[\left\{ (1 - 2\delta \hat{r}_n) + \frac{1}{\hat{r}_n} (1 - 2\delta \hat{r}_n) + \hat{r}_n (1 + \delta \hat{r}_n) + (1 - \delta \hat{r}_n) \right\} \right. \\
&\quad \left. - \left\{ (1 + 2\delta \hat{r}_n) + \frac{1}{\hat{r}_n} (1 + \delta \hat{r}_n) + \hat{r}_n (1 + 2\delta \hat{r}_n) + (1 + \delta \hat{r}_n) \right\} \right] \widehat{\mathbf{K}}^2 p_{t_n} \\
&= \left[(-4\delta \hat{r}_n) + \frac{1}{\hat{r}_n} (-3\delta \hat{r}_n) + \hat{r}_n (-3\delta \hat{r}_n) + (-2\delta \hat{r}_n) \right] \widehat{\mathbf{K}}^2 p_{t_n} \\
&= \left[-3 \left(2 + \frac{1}{\hat{r}_n} + \hat{r}_n \right) \delta \hat{r}_n \right] \widehat{\mathbf{K}}^2 p_{t_n} \\
&= 3 \left[-\frac{(\hat{r}_n + 1)^2}{\hat{r}_n} \delta \hat{r}_n \right] \widehat{\mathbf{K}}^2 p_{t_n}. \tag{B.8b}
\end{aligned}$$

Combining Eqs. (B.8a) and (B.8b), the coefficient associated with the last term on the right side of Eq. (B.4) is

$$\begin{aligned}
3(g_n f_n + g_{n+1} f_{n+1}) + (g_n f_{n+1} - g_{n+1} f_n) &= 3 \left[\frac{2(\hat{r}_n + 1)^2}{\hat{r}_n} + \frac{\hat{r}_n^2 - 1}{\hat{r}_n} \delta \hat{r}_n \right] \widehat{\mathbf{K}}^2 p_{t_n} + 3 \left[-\frac{(\hat{r}_n + 1)^2}{\hat{r}_n} \delta \hat{r}_n \right] \widehat{\mathbf{K}}^2 p_{t_n} \\
&= 3 \left[\frac{2(\hat{r}_n + 1)^2}{\hat{r}_n} + \frac{(\hat{r}_n^2 - 1) - (\hat{r}_n + 1)^2}{\hat{r}_n} \delta \hat{r}_n \right] \widehat{\mathbf{K}}^2 p_{t_n}
\end{aligned}$$

$$= 3 \left[\frac{2(\hat{r}_n + 1)^2}{\hat{r}_n} - \frac{2(\hat{r}_n + 1)}{\hat{r}_n} \delta \hat{r}_n \right] \bar{K}^2 p_{t_n}. \quad (\text{B.9})$$

The expressions for the coefficients given by Eqs. (B.6), (B.7), and (B.9) are inserted into Eq. (B.4) to obtain

$$\begin{aligned} \hat{x}_{n+1} &= \hat{x}_n + \left[2\hat{r}_n (\hat{r}_n + 1) \bar{K} (p_{t_n} - P_{b_n}) + \left\{ \hat{r}_n (2\hat{r}_n + 1) \bar{K} p_{t_n} + \hat{r}_n (\hat{r}_n + 2) \bar{K} P_{b_n} \right\} \delta \hat{r}_n \right] \frac{\Delta t_n}{2} \\ &\quad + \left[\frac{4(\hat{r}_n + 1)^2}{\hat{r}_n} - \frac{4(\hat{r}_n + 1)(\hat{r}_n + 2)}{\hat{r}_n} \delta \hat{r}_n \right] \bar{K}^2 P_{b_n} \frac{\Delta t_n^2}{8} \\ &\quad - 3 \left[\frac{2(\hat{r}_n + 1)^2}{\hat{r}_n} - \frac{2(\hat{r}_n + 1)}{\hat{r}_n} \delta \hat{r}_n \right] \bar{K}^2 p_{t_n} \frac{\Delta t_n^2}{12} \\ &= \hat{x}_n + L_{0_n} + L_{1_n} \delta \hat{r}_n, \end{aligned} \quad (\text{B.10})$$

where

$$\begin{aligned} L_{0_n} &= \text{sum of the terms independent of } \delta \hat{r}_n \text{ in the expression for } \hat{x}_{n+1} \\ &= \left[2\hat{r}_n (\hat{r}_n + 1) \bar{K} (p_{t_n} - P_{b_n}) \right] \frac{\Delta t_n}{2} + \frac{4(\hat{r}_n + 1)^2}{\hat{r}_n} \bar{K}^2 P_{b_n} \frac{\Delta t_n^2}{8} - 3 \frac{2(\hat{r}_n + 1)^2}{\hat{r}_n} \bar{K}^2 p_{t_n} \frac{\Delta t_n^2}{12} \\ &= \hat{r}_n (\hat{r}_n + 1) \bar{K} (p_{t_n} - P_{b_n}) \Delta t_n + \frac{(\hat{r}_n + 1)^2}{\hat{r}_n} \bar{K}^2 P_{b_n} \frac{\Delta t_n^2}{2} - \frac{(\hat{r}_n + 1)^2}{\hat{r}_n} \bar{K}^2 p_{t_n} \frac{\Delta t_n^2}{2} \\ &= \hat{r}_n (\hat{r}_n + 1) \bar{K} (p_{t_n} - P_{b_n}) \Delta t_n - \frac{(\hat{r}_n + 1)^2}{\hat{r}_n} \frac{\Delta t_n^2}{2} \bar{K}^2 (p_{t_n} - P_{b_n}) \\ &= \left[\hat{r}_n (\hat{r}_n + 1) \bar{K} \Delta t_n - \frac{1}{2} \frac{(\hat{r}_n + 1)^2}{\hat{r}_n} \bar{K}^2 \Delta t_n^2 \right] (p_{t_n} - P_{b_n}), \end{aligned} \quad (\text{B.11a})$$

and $L_{1_n} =$ sum of the terms with $\delta \hat{r}_n$ as multiplier in the expression for \hat{x}_{n+1}

$$\begin{aligned}
&= \left[\hat{r}_n (2\hat{r}_n + 1) \widehat{K} p_{t_n} + \hat{r}_n (\hat{r}_n + 2) \widehat{K} p_{b_n} \right] \frac{\Delta t_n}{2} - \frac{4(\hat{r}_n + 1)(\hat{r}_n + 2)}{\hat{r}_n} \widehat{K}^2 p_{b_n} \frac{\Delta t_n^2}{8} \\
&\quad + 3 \frac{2(\hat{r}_n + 1)}{\hat{r}_n} \widehat{K}^2 p_{t_n} \frac{\Delta t_n^2}{12} \\
&= \hat{r}_n \left[(2\hat{r}_n + 1) \widehat{K} p_{t_n} + (\hat{r}_n + 2) \widehat{K} p_{b_n} \right] \frac{\Delta t_n}{2} - \frac{(\hat{r}_n + 1)(\hat{r}_n + 2)}{\hat{r}_n} \widehat{K}^2 p_{b_n} \frac{\Delta t_n^2}{2} \\
&\quad + \frac{\hat{r}_n + 1}{\hat{r}_n} \widehat{K}^2 p_{t_n} \frac{\Delta t_n^2}{2} \\
&= \hat{r}_n \left[(2\hat{r}_n + 1) p_{t_n} + (\hat{r}_n + 2) p_{b_n} \right] \widehat{K} \frac{\Delta t_n}{2} + \frac{\hat{r}_n + 1}{\hat{r}_n} \left[p_{t_n} - (\hat{r}_n + 2) p_{b_n} \right] \widehat{K}^2 \frac{\Delta t_n^2}{2}. \tag{B.11b}
\end{aligned}$$

Recall $\hat{x} = P_b \hat{r}^3$. Therefore, $\hat{x}_n = P_{b_n} \hat{r}_n^3$ and $\hat{x}_{n+1} = P_{b_{n+1}} \hat{r}_{n+1}^3$. Substituting for \hat{x}_n and \hat{x}_{n+1} in Eq. (B.10), we obtain

$$P_{b_{n+1}} \hat{r}_{n+1}^3 = P_{b_n} \hat{r}_n^3 + L_{0_n} + L_{1_n} \delta \hat{r}_n,$$

from which

$$\begin{aligned}
P_{b_{n+1}} &= P_{b_n} \frac{\hat{r}_n^3}{\hat{r}_{n+1}^3} + \frac{L_{0_n} + L_{1_n} \delta \hat{r}_n}{\hat{r}_{n+1}^3} \\
&= P_{b_n} \frac{\hat{r}_n^3}{\hat{r}_n^3 (1 + \delta \hat{r}_n)^3} + \frac{L_{0_n} + L_{1_n} \delta \hat{r}_n}{\hat{r}_n^3 (1 + \delta \hat{r}_n)^3} \\
&= P_{b_n} (1 + \delta \hat{r}_n)^{-3} + \frac{1}{\hat{r}_n^3} [L_{0_n} + L_{1_n} \delta \hat{r}_n] (1 + \delta \hat{r}_n)^{-3} \\
&\cong P_{b_n} (1 - 3\delta \hat{r}_n) + \frac{1}{\hat{r}_n^3} [L_{0_n} + L_{1_n} \delta \hat{r}_n] (1 - 3\delta \hat{r}_n).
\end{aligned}$$

Neglect of terms of order ≥ 2 yields

$$P_{b_{n+1}} = P_{b_n} (1 - 3\delta \hat{r}_n) + \frac{L_{0_n}}{\hat{r}_n^3} (1 - 3\delta \hat{r}_n) + \frac{L_{1_n} \delta \hat{r}_n}{\hat{r}_n^3}$$

$$\begin{aligned}
&= \left(P_{b_n} + \frac{L_{0_n}}{\hat{r}_n^3} \right) - \left[3P_{b_n} + 3\frac{L_{0_n}}{\hat{r}_n^3} - \frac{L_{1_n}}{\hat{r}_n^3} \right] \delta \hat{r}_n \\
&= \left(P_{b_n} + \frac{L_{0_n}}{\hat{r}_n^3} \right) - \left[3 \left(P_{b_n} + \frac{L_{0_n}}{\hat{r}_n^3} \right) - \frac{L_{1_n}}{\hat{r}_n^3} \right] \delta \hat{r}_n \\
&= A_n - (3A_n - B_n) \delta \hat{r}_n
\end{aligned} \tag{B.12}$$

where $A_n = P_{b_n} + \frac{L_{0_n}}{\hat{r}_n^3}$ (B.12a)

and $B_n = \frac{L_{1_n}}{\hat{r}_n^3}$. (B.12b)

Eqs. (B.12a) and (B.11a) are combined to obtain the following expressions for A_n :

$$\begin{aligned}
A_n &= P_{b_n} + \frac{L_{0_n}}{\hat{r}_n^3} \\
&= P_{b_n} + \frac{1}{\hat{r}_n^3} [\hat{r}_n (\hat{r}_n + 1) \Delta t_n] \bar{K} (p_{t_n} - P_{b_n}) - \frac{1}{2} \frac{1}{\hat{r}_n^3} \left(\frac{(\hat{r}_n + 1)^2}{\hat{r}_n} \Delta t_n^2 \right) \bar{K}^2 (p_{t_n} - P_{b_n}) \\
&= P_{b_n} + \left(\frac{\hat{r}_n + 1}{\hat{r}_n^2} \Delta t_n \bar{K} \right) (p_{t_n} - P_{b_n}) - \frac{1}{2} \left(\frac{(\hat{r}_n + 1)^2}{\hat{r}_n^4} \Delta t_n^2 \bar{K}^2 \right) (p_{t_n} - P_{b_n}) \\
&= P_{b_n} + \left(\frac{\hat{r}_n + 1}{\hat{r}_n^2} \Delta t_n \bar{K} \right) (p_{t_n} - P_{b_n}) - \frac{1}{2} \left(\frac{\hat{r}_n + 1}{\hat{r}_n^2} \Delta t_n \bar{K} \right)^2 (p_{t_n} - P_{b_n}) \\
&= P_{b_n} + a_n \left(1 - \frac{a_n}{2} \right) (p_{t_n} - P_{b_n}),
\end{aligned} \tag{B.13a}$$

where $a_n = \left(\frac{\hat{r}_n + 1}{\hat{r}_n^2} \Delta t_n \right) \bar{K}$.

Likewise, Eqs. (B.12b) and (B.11b) are combined to express B_n as follows:

$$B_n = \frac{L_{1_n}}{\hat{r}_n^3} = \frac{1}{\hat{r}_n^3} \left[\hat{r}_n \left\{ (2\hat{r}_n + 1)p_{t_n} + (\hat{r}_n + 2)P_{b_n} \right\} \bar{K} \frac{\Delta t_n}{2} + \frac{\hat{r}_n + 1}{\hat{r}_n} \left\{ p_{t_n} - (\hat{r}_n + 2)P_{b_n} \right\} \bar{K}^2 \frac{\Delta t_n^2}{2} \right]$$

$$\begin{aligned}
&= \frac{1}{2} \left[\left(\frac{2\hat{r}_n + 1}{\hat{r}_n^2} \Delta t_n \widehat{K} \right) p_{t_n} + \left(\frac{\hat{r}_n + 2}{\hat{r}_n^2} \Delta t_n \widehat{K} \right) P_{b_n} \right. \\
&\quad \left. + \left(\frac{\hat{r}_n + 1}{\hat{r}_n^2} \Delta t_n \widehat{K} \right) \left\{ \left(\frac{1}{\hat{r}_n^2} \Delta t_n \widehat{K} \right) p_{t_n} - \left(\frac{\hat{r}_n + 2}{\hat{r}_n^2} \Delta t_n \widehat{K} \right) P_{b_n} \right\} \right] \\
&= \frac{1}{2} \left[\left(\frac{2(\hat{r}_n + 1)}{\hat{r}_n^2} \Delta t_n \widehat{K} - \frac{1}{\hat{r}_n^2} \Delta t_n \widehat{K} \right) p_{t_n} + \left(\frac{\hat{r}_n + 1}{\hat{r}_n^2} \Delta t_n \widehat{K} + \frac{\Delta t_n \widehat{K}}{\hat{r}_n^2} \right) P_{b_n} \right. \\
&\quad \left. + \left(\frac{\hat{r}_n + 1}{\hat{r}_n^2} \Delta t_n \widehat{K} \right) \left\{ \frac{\Delta t_n \widehat{K}}{\hat{r}_n^2} p_{t_n} - \left(\frac{\hat{r}_n + 1}{\hat{r}_n^2} \Delta t_n \widehat{K} + \frac{\Delta t_n \widehat{K}}{\hat{r}_n^2} \right) P_{b_n} \right\} \right] \\
&= \frac{1}{2} \left[(2a_n - b_n) p_{t_n} + (a_n + b_n) P_{b_n} + a_n \{ b_n p_{t_n} - (a_n + b_n) P_{b_n} \} \right] \\
&= \frac{1}{2} \left[(2a_n - b_n + a_n b_n) p_{t_n} + (a_n + b_n)(1 - a_n) P_{b_n} \right], \tag{B.13b}
\end{aligned}$$

where $b_n = \frac{\Delta t_n \widehat{K}}{\hat{r}_n^2}$ and $a_n = \frac{\hat{r}_n + 1}{\hat{r}_n^2} \Delta t_n \widehat{K} = (\hat{r}_n + 1) b_n$.

The bubble diffusible gas pressure is given in terms of the scaled radius \hat{r}_{n+1} by Eq. (A.43):

$$P_{b_{n+1}} = P'_{amb_{n+1}} + \frac{2\widehat{\sigma}}{\hat{r}_{n+1}} + \widehat{M}\hat{r}_{n+1}^3, \tag{B.14}$$

where $P'_{amb} = (P_{amb} - P_\infty)$ is the ambient hydrostatic pressure corrected for the pressures of the infinitely-diffusible gases in the system (e.g., $P_\infty = P_{CO_2} + P_{H_2O}$). Substituting $\hat{r}_{n+1} = \hat{r}_n (1 + \delta\hat{r}_n)$ in Eq. (B.14), we obtain

$$\begin{aligned}
P_{b_{n+1}} &= P'_{amb_{n+1}} + \frac{2\widehat{\sigma}}{\hat{r}_n (1 + \delta\hat{r}_n)} + \widehat{M}\hat{r}_n^3 (1 + \delta\hat{r}_n)^3 \\
&= P'_{amb_{n+1}} + \frac{2\widehat{\sigma}}{\hat{r}_n} (1 + \delta\hat{r}_n)^{-1} + \widehat{M}\hat{r}_n^3 (1 + \delta\hat{r}_n)^3.
\end{aligned}$$

Substituting the first order approximations for $(1 + \delta\hat{r}_n)^{-1}$ and $(1 + \delta\hat{r}_n)^3$ about $\delta\hat{r}_n = 0$ yields

$$\begin{aligned}
P_{b_{n+1}} &\cong P'_{amb_{n+1}} + \frac{2\widehat{\sigma}}{\widehat{r}_n} (1 - \delta\widehat{r}_n) + \widehat{M}\widehat{r}_n^3 (1 + 3\delta\widehat{r}_n) \\
&= \left[P'_{amb_{n+1}} + \frac{2\widehat{\sigma}}{\widehat{r}_n} + \widehat{M}\widehat{r}_n^3 \right] - \left[\frac{2\widehat{\sigma}}{\widehat{r}_n} - 3\widehat{M}\widehat{r}_n^3 \right] \delta\widehat{r}_n .
\end{aligned} \tag{B.15}$$

The final equation for determining $\delta\widehat{r}_n$ is obtained by equating $P_{b_{n+1}}$ given by Eqs. (B.12) and (B.15);

$$A_n - (3A_n - B_n)\delta\widehat{r}_n = \left[P'_{amb_{n+1}} + \frac{2\widehat{\sigma}}{\widehat{r}_n} + \widehat{M}\widehat{r}_n^3 \right] - \left[\frac{2\widehat{\sigma}}{\widehat{r}_n} - 3\widehat{M}\widehat{r}_n^3 \right] \delta\widehat{r}_n ; \tag{B.16}$$

and rearranging terms to yield

$$\left[(3A_n - B_n) - \left(\frac{2\widehat{\sigma}}{\widehat{r}_n} - 3\widehat{M}\widehat{r}_n^3 \right) \right] \delta\widehat{r}_n - \left[A_n - \left(P'_{amb_{n+1}} + \frac{2\widehat{\sigma}}{\widehat{r}_n} + \widehat{M}\widehat{r}_n^3 \right) \right] = 0 . \tag{B.17}$$

The fractional change in bubble radius at the n^{th} integration step is then given by solving Eq. (B.17) for $\delta\widehat{r}_n$ to obtain:

$$\delta\widehat{r}_n = \frac{A_n - \left(P'_{amb_{n+1}} + \frac{2\widehat{\sigma}}{\widehat{r}_n} + \widehat{M}\widehat{r}_n^3 \right)}{(3A_n - B_n) - \left(\frac{2\widehat{\sigma}}{\widehat{r}_n} - 3\widehat{M}\widehat{r}_n^3 \right)} . \tag{B.18}$$

9.1.1.2 Tissue Gas Tension with Time-Dependent Changes in Tissue Blood Flow

With the tissue gas tension p_{t_n} constant in the interval $[t_n, t_{n+1}]$, consistent with the quasi-static approximation [see Eq. (B.5a)], p_{t_n} is updated to $p_{t_{n+1}}$ at the end of the interval based on calculations that account for gas transfer between blood, tissue, and bubbles during the interval. We use the integrating factor method to obtain a recursion formula for solving Eq. (A.13) for a single diffusible gas and a single bubble size group; i.e., for calculating $p_{t_{n+1}}$ at time t_{n+1} given p_{t_n} at time t_n with $k=1$ and $N_{bs}=1$. We first treat the blood flow coefficient $q(t)$ in Eq. (A.13) as a general function of time. We then modify the relation with a specific model for $q(t)$ under exercise conditions.

9.1.1.2.1 General Model of Time-Dependent Changes in Blood Flow

We multiply both sides of Eq. (A.13) by the integrating factor $\exp[I_q(t)]$, where $I_q(t)$ is the indefinite integral, $I_q(t) = \int q(t)dt$, and integrate between t_n and t_{n+1} :

$$p_t(t)\exp[I_q(t)]\Big|_{t_n}^{t_{n+1}} = \int_{t_n}^{t_{n+1}} q(t)p_a(t)\exp[I_q(t)]dt - \int_{t_n}^{t_{n+1}} \hat{G}S_{x_n} \exp[I_q(t)]dt, \quad (\text{B.19})$$

where $\hat{G} = \left(\frac{4\pi}{3}\right) \frac{n_b}{\alpha_t V_t \Lambda^3}$, and $S_{x_n} = \frac{\hat{x}_{n+1} - \hat{x}_n}{\Delta t_n}$ is the rate of gas loss into each of n_b

identically sized bubbles in the $[t_n, t_{n+1}]$ integration interval. Evaluating the left side and expanding the right side of Eq. (B.19) yields

$$\begin{aligned} & p_{t_{n+1}} \exp[I_q(t)]\Big|_{t=t_{n+1}} - p_{t_n} \exp[I_q(t)]\Big|_{t=t_n} \\ &= \int_{t_n}^{t_{n+1}} p_a(t)q(t)\exp[I_q(t)]dt - \int_{t_n}^{t_{n+1}} \hat{G}S_{x_n} \exp[I_q(t)]dt \\ &= \int_{t_n}^{t_{n+1}} p_a(t) \frac{d}{dt} \left\{ \exp[I_q(t)] \right\} dt - \int_{t_n}^{t_{n+1}} \hat{G}S_{x_n} \exp[I_q(t)]dt. \end{aligned}$$

Since $\frac{d}{dt} \left\{ \exp[I_q(t)] \right\} = q(t)\exp[I_q(t)]$

$$p_{t_{n+1}} = p_a(t)\exp[I_q(t)]\Big|_{t_n}^{t_{n+1}} - \int_{t_n}^{t_{n+1}} \exp[I_q(t)] \frac{d}{dt} [p_a(t)]dt - \int_{t_n}^{t_{n+1}} \hat{G}S_{x_n} \exp[I_q(t)]dt. \quad (\text{B.20})$$

The first two terms of Eq. (B.20) result from integrating by parts. In the interval $[t_n, t_{n+1}]$, $p_a(t) = p_{a_n} + v_n(t - t_n)$, and therefore, $\frac{d}{dt} [p_a(t)] = v_n$. Expanding the first term on the right side,

substituting v_n for $\frac{d}{dt} [p_a(t)]$ in the second term, and denoting $[I_q(t)]\Big|_{t=t_{n+1}}$ and $[I_q(t)]\Big|_{t=t_n}$ by $I_{q_{n+1}}$ and I_{q_n} , respectively, Eq. (B.20) becomes

$$\begin{aligned} & p_{t_{n+1}} \exp(I_{q_{n+1}}) - p_{t_n} \exp(I_{q_n}) \\ &= p_{a_{n+1}} \exp(I_{q_{n+1}}) - p_{a_n} \exp(I_{q_n}) - \int_{t_n}^{t_{n+1}} v_n \exp[I_q(t)]dt - \int_{t_n}^{t_{n+1}} \hat{G}S_{x_n} \exp[I_q(t)]dt \end{aligned}$$

$$= p_{a_{n+1}} \exp(I_{q_{n+1}}) - p_{a_n} \exp(I_{q_n}) - (v_n + \hat{G}S_{x_n}) \int_{t_n}^{t_{n+1}} \exp[I_q(t)] dt. \quad (\text{B.21})$$

Multiplying both sides of Eq. (B.21) by $\exp(-I_{q_{n+1}})$ and rearranging terms,

$$\begin{aligned} p_{t_{n+1}} &= p_{t_n} \exp(-I_{q_{n+1}}) \exp(I_{q_n}) + p_{a_{n+1}} - p_{a_n} \exp(-I_{q_{n+1}}) \exp(I_{q_n}) \\ &\quad - \exp(-I_{q_{n+1}}) (v_n + \hat{G}S_{x_n}) \int_{t_n}^{t_{n+1}} \exp[I_q(t)] dt \\ &= p_{t_n} \exp[-(I_{q_{n+1}} - I_{q_n})] + p_{a_{n+1}} - p_{a_n} \exp[-(I_{q_{n+1}} - I_{q_n})] \\ &\quad - (v_n + \hat{G}S_{x_n}) \int_{t_n}^{t_{n+1}} \exp[-(I_{q_{n+1}} - I_q(t))] dt. \end{aligned} \quad (\text{B.22})$$

Now, $p_{a_{n+1}} = p_{a_n} + v_n \Delta t_n$, and from the definition of I_q , $I_{q_{n+1}} - I_{q_n} = \int_{t_n}^{t_{n+1}} q(t) dt$ and

$I_{q_{n+1}} - I_q(t) = \int_t^{t_{n+1}} q(t) dt$. With these substitutions in Eq. (B.22), $p_{t_{n+1}}$ is expressed as:

$$p_{t_{n+1}} = (p_{t_n} - p_{a_n}) \exp\left[-\int_{t_n}^{t_{n+1}} q(t) dt\right] + p_{a_n} + v_n \Delta t_n - (v_n + \hat{G}S_{x_n}) \int_{t_n}^{t_{n+1}} \exp\left[-\int_{t_n}^{t_{n+1}} q(t) dt\right] dt. \quad (\text{B.23})$$

Eq. (B.23) is the general solution for determining tissue gas tension using any function $q(t)$ to represent changes in blood flow. The specification of $q(t)$ may be based on experimental data, if available, or on a model of blood flow changes during exercise. The integrals in Eq. (B.23) may require numerical evaluation if $q(t)$ is an empirical representation of experimental data or represented by a complex model that renders analytic treatment infeasible.

If $q(t)$ is constant, $\int_{t_n}^{t_{n+1}} q(t) dt = q \Delta t = \frac{\Delta t}{\tau}$, $\int_{t_n}^{t_{n+1}} \exp\left[-\int_{t_n}^{t_{n+1}} q(t) dt\right] dt = \tau \left[1 - \exp\left(-\frac{\Delta t}{\tau}\right)\right]$ and Eq. (B.23)

reduces to

$$p_{t_{n+1}} = p_{t_n} (1 - \varepsilon_n) + v_n \Delta t_n + \left[p_{a_n} - \tau (v_n + \hat{G}S_{x_n}) \right] \varepsilon_n, \quad (\text{B.24})$$

where $\varepsilon_n = 1 - \exp\left(-\frac{\Delta t_n}{\tau}\right)$.

9.1.1.2.2 Multi-Exponential Model of Time-Dependent Changes in Blood Flow

We assume a multi-exponential representation of changes in $\dot{Q}(t)$ to be general and to accommodate possible bi-phasic responses of blood flow to exercise. Such a representation, which allows evaluation of the integrals of $q(t)$ in Eq. (B.23) to be analytically tractable, is given by the following equation in the interval $[t_n, t_{n+1}]$:

$$\dot{Q}(t) = \dot{Q}_{ex_n} - (\dot{Q}_{ex_n} - \dot{Q}_n) \sum_{\ell=1}^{N_{exp}} f_{exp_{\ell,n}} \exp\left(-\frac{t-t_n}{\tau_{exp_{\ell,n}}}\right), \quad (B.25)$$

Where \dot{Q}_n = blood flow per unit volume of tissue at $t = t_n$,

\dot{Q}_{ex_n} = steady-state blood flow that would be reached if exercise is continued indefinitely at its prevailing level in the interval $[t_n, t_{n+1}]$,

N_{exp} = number of exponential components,

$f_{exp_{\ell,n}}$ = fraction of blood flow change associated with the ℓ^{th} exponential component in the interval $[t_n, t_{n+1}]$, and

$\tau_{exp_{\ell,n}}$ = time constant associated with ℓ^{th} exponential component in the interval $[t_n, t_{n+1}]$.

The fractions $f_{exp_{\ell,n}}$ should add up to 1, so that at $t = t_n$,

$$\dot{Q}(t) = \dot{Q}_{ex_n} - (\dot{Q}_{ex_n} - \dot{Q}_n) \sum_{\ell=1}^{N_{exp}} f_{exp_{\ell,n}} = \dot{Q}_n \cdot$$

As $t \rightarrow \infty$, $\dot{Q}(t) \rightarrow \dot{Q}_{ex_n}$. Also, $\dot{Q}(t) = \dot{Q}_n$ if $\dot{Q}_{ex_n} = \dot{Q}_n$ (resting conditions), and $\dot{Q}(t) = \dot{Q}_{ex_n}$ if $\tau_{exp_{\ell,n}} = 0$ for all exponential components (instantaneous change). With appropriate specification of $f_{exp_{\ell,n}}$ and $\tau_{exp_{\ell,n}}$, Eq. (B.25) can accommodate different rates of blood flow change as exercise begins (onset) and ends (recovery). It should be noted that the blood flow level \dot{Q}_{ex_n} remains unchanged until there is a change in exercise level.

We now evaluate the integrals in Eq. (B.23) using Eq. (B.25) to calculate $q(t)$, which is proportional to $\dot{Q}(t)$, and the change of variable, $(t - t_n) = \delta$, which leads to $\delta = 0$ at $t = t_n$, $\delta = t_{n+1} - t_n = \Delta t_n$ at $t = t_{n+1}$, and $dt = d\delta$.

$$\begin{aligned}
\int_{t_n}^{t_{n+1}} q(t) dt &= \int_{t_n}^{t_{n+1}} \left[q_{ex_n} - (q_{ex_n} - q_n) \sum_{\ell=1}^{N_{exp}} f_{exp_{\ell,n}} \exp\left(-\frac{t-t_n}{\tau_{exp_{\ell,n}}}\right) \right] dt \\
&= \int_0^{\Delta t_n} \left[q_{ex_n} - (q_{ex_n} - q_n) \sum_{\ell=1}^{N_{exp}} f_{exp_{\ell,n}} \exp\left(-\frac{\delta}{\tau_{exp_{\ell,n}}}\right) \right] d\delta \\
&= q_{ex_n} \Delta t_n - (q_{ex_n} - q_n) \int_0^{\Delta t_n} \sum_{\ell=1}^{N_{exp}} f_{exp_{\ell,n}} \exp\left(-\frac{\delta}{\tau_{exp_{\ell,n}}}\right) d\delta \\
&= q_{ex_n} \Delta t_n - (q_{ex_n} - q_n) \sum_{\ell=1}^{N_{exp}} \tau_{exp_{\ell,n}} f_{exp_{\ell,n}} \left[1 - \exp\left(-\frac{\Delta t_n}{\tau_{exp_{\ell,n}}}\right) \right]
\end{aligned} \tag{B.26}$$

Eq. (B.26) is considerably simplified by expanding the term in brackets to obtain

$$1 - \exp\left(-\frac{\Delta t_n}{\tau_{exp_{\ell,n}}}\right) = 1 - \left[1 - \left(\frac{\Delta t_n}{\tau_{exp_{\ell,n}}}\right) + \frac{1}{2} \left(\frac{\Delta t_n}{\tau_{exp_{\ell,n}}}\right)^2 \dots \right] = \frac{\Delta t_n}{\tau_{exp_{\ell,n}}} ,$$

where terms of order greater than 2 are neglected. Then Eq. (B.26) becomes

$$\begin{aligned}
\int_{t_n}^{t_{n+1}} q(t) dt &= q_{ex_n} \Delta t_n - (q_{ex_n} - q_n) \sum_{\ell=1}^{N_{exp}} \tau_{exp_{\ell,n}} f_{exp_{\ell,n}} \left[\frac{\Delta t_n}{\tau_{exp_{\ell,n}}} \right] \\
&= q_{ex_n} \Delta t_n - (q_{ex_n} - q_n) \Delta t_n \sum_{\ell=1}^{N_{exp}} f_{exp_{\ell,n}} \\
&= q_{ex_n} \Delta t_n - (q_{ex_n} - q_n) \Delta t_n , \quad \text{because } \sum_{\ell=1}^{N_{exp}} f_{exp_{\ell,n}} = 1 \\
&= q_n \Delta t_n
\end{aligned} \tag{B.27}$$

The error in the approximation $1 - \exp\left(-\frac{\Delta t_n}{\tau_{exp_{\ell,n}}}\right) \approx \frac{\Delta t_n}{\tau_{exp_{\ell,n}}}$ is less than 0.5% if $\frac{\Delta t_n}{\tau_{exp_{\ell,n}}} < 0.01$,

that is, if $\tau_{exp_{\ell,n}} > 100 \Delta t_n$. Assuming a nominal integration step size of 0.001 min,

$\tau_{exp_{\ell,n}} > 0.1$ min. This means that if the time constant is less than 0.1 min for any exponential component in Eq. (B.25), the integration step size must be reduced to keep the approximation error less than 0.5%.

Next, we evaluate $\int_{t_n}^{t_{n+1}} q(t) dt$, noting that the lower limit = $(t - t_n)$ for $q(t)$ as defined by Eq. (B.25) is valid in the interval $[t_n, t_{n+1}]$ with an initial value of q_n . Thus,

$$\begin{aligned}
\int_{t_n}^{t_{n+1}} q(t) dt &= \int_{t-t_n}^{t_{n+1}-t_n} \left[q_{ex_n} - (q_{ex_n} - q_n) \sum_{\ell=1}^{N_{exp}} f_{exp_{\ell,n}} \exp\left(-\frac{t-t_n}{\tau_{exp_{\ell,n}}}\right) \right] dt \\
&= \int_{\delta}^{\Delta t_n} \left[q_{ex_n} - (q_{ex_n} - q_n) \sum_{\ell=1}^{N_{exp}} f_{exp_{\ell,n}} \exp\left(-\frac{\delta}{\tau_{exp_{\ell,n}}}\right) \right] d\delta \\
&= q_{ex_n} (\Delta t_n - \delta) - (q_{ex_n} - q_n) \int_{\delta}^{\Delta t_n} \sum_{\ell=1}^{N_{exp}} f_{exp_{\ell,n}} \exp\left(-\frac{\delta}{\tau_{exp_{\ell,n}}}\right) d\delta \\
&= q_{ex_n} (\Delta t_n - \delta) - (q_{ex_n} - q_n) \sum_{\ell=1}^{N_{exp}} \tau_{exp_{\ell,n}} f_{exp_{\ell,n}} \left[\exp\left(-\frac{\delta}{\tau_{exp_{\ell,n}}}\right) - \exp\left(-\frac{\Delta t_n}{\tau_{exp_{\ell,n}}}\right) \right]
\end{aligned}$$

The integral associated with the last term on the right side of Eq. (B.23) is then

$$\begin{aligned}
&\int_{t_n}^{t_{n+1}} \exp\left[-\int_{t_n}^{t_{n+1}} q(t) dt\right] dt \\
&= \int_0^{\Delta t_n} \exp\left\{-q_{ex_n} (\Delta t_n - \delta) + (q_{ex_n} - q_n) \sum_{\ell=1}^{N_{exp}} \tau_{exp_{\ell,n}} f_{exp_{\ell,n}} \left[\exp\left(-\frac{\delta}{\tau_{exp_{\ell,n}}}\right) - \exp\left(-\frac{\Delta t_n}{\tau_{exp_{\ell,n}}}\right) \right]\right\} d\delta \quad (B.28)
\end{aligned}$$

The integral on the right side of Eq. (B.28) cannot be evaluated in closed form without approximation. Therefore, we expand the exponential terms, truncate the series by neglecting higher order terms, and then perform the integration, as described below:

$$\begin{aligned}
\exp\left(-\frac{\delta}{\tau_{exp_{\ell,n}}}\right) - \exp\left(-\frac{\Delta t_n}{\tau_{exp_{\ell,n}}}\right) &= \left[1 - \left(\frac{\delta}{\tau_{exp_{\ell,n}}}\right) + \frac{1}{2} \left(\frac{\delta}{\tau_{exp_{\ell,n}}}\right)^2 \dots \right] - \left[1 - \left(\frac{\Delta t_n}{\tau_{exp_{\ell,n}}}\right) + \frac{1}{2} \left(\frac{\Delta t_n}{\tau_{exp_{\ell,n}}}\right)^2 \dots \right] \\
&\approx \frac{\Delta t_n - \delta}{\tau_{exp_{\ell,n}}}, \quad \text{neglecting terms of order } > 2. \quad (B.29)
\end{aligned}$$

Eq. (B.28) is reduced using Eq. (B.29) as follows:

$$\int_{t_n}^{t_{n+1}} \exp \left[- \int_{t_n}^{t_{n+1}} q(t) dt \right] dt = \int_0^{\Delta t_n} \exp \left\{ -q_{ex_n} (\Delta t_n - \delta) + (q_{ex_n} - q_n) \sum_{\ell=1}^{N_{exp}} \tau_{exp_{\ell,n}} f_{exp_{\ell,n}} \frac{\Delta t_n - \delta}{\tau_{exp_{\ell,n}}} \right\} d\delta$$

$$= \int_0^{\Delta t_n} \exp \left\{ -q_{ex_n} (\Delta t_n - \delta) + (q_{ex_n} - q_n) (\Delta t_n - \delta) \sum_{\ell=1}^{N_{exp}} f_{exp_{\ell,n}} \right\} d\delta$$

Then, because $\sum_{\ell=1}^{N_{exp}} f_{exp_{\ell,n}} = 1$, we have

$$\int_{t_n}^{t_{n+1}} \exp \left[- \int_{t_n}^{t_{n+1}} q(t) dt \right] dt = \int_0^{\Delta t_n} \exp \left\{ -q_{ex_n} (\Delta t_n - \delta) + (q_{ex_n} - q_n) (\Delta t_n - \delta) \right\} d\delta$$

$$= \int_0^{\Delta t_n} \exp \left\{ -q_n (\Delta t_n - \delta) \right\} d\delta$$

$$= \left. \frac{\exp \left\{ -q_n (\Delta t_n - \delta) \right\}}{q_n} \right|_0^{\Delta t_n}$$

$$= \frac{1 - \exp(-q_n \Delta t_n)}{q_n} \tag{B.30}$$

Our final recursive relation for tissue gas tension is obtained by substituting the evaluated expressions for the integrals given by Eqs. (B.27) and (B.30) into Eq. (B.23) and rearranging terms:

$$p_{t_{n+1}} = (p_{t_n} - p_{a_n}) \exp(-q_n \Delta t_n) + p_{a_n} + v_n \Delta t_n - (v_n + \hat{G} S_{x_n}) \frac{1 - \exp(-q_n \Delta t_n)}{q_n}$$

$$= (p_{t_n} - p_{a_n}) [\exp(-q_n \Delta t_n) - 1] + p_{t_n} + v_n \Delta t_n - (v_n + \hat{G} S_{x_n}) \frac{1 - \exp(-q_n \Delta t_n)}{q_n}$$

$$= p_{t_n} + v_n \Delta t_n + (p_{a_n} - p_{t_n}) [1 - \exp(-q_n \Delta t_n)] - (v_n + \hat{G} S_{x_n}) \frac{1}{q_n} [1 - \exp(-q_n \Delta t_n)]$$

$$= p_{t_n} + v_n \Delta t_n + \left[p_{a_n} - p_{t_n} - \tau_n \left(v_n + \hat{G} \frac{\hat{x}_{n+1} - \hat{x}_n}{\Delta t_n} \right) \right] \varepsilon_n, \tag{B.31}$$

where $\tau_n = \frac{1}{q_n} = \frac{\alpha_t}{\alpha_b \dot{Q}_n}$, and $\varepsilon_n = 1 - \exp(-q_n \Delta t_n) = 1 - \exp\left(-\frac{\Delta t_n}{\tau_n}\right)$. Also, we have

substituted $S_{x_n} = \frac{\hat{x}_{n+1} - \hat{x}_n}{\Delta t_n}$ for the gas loss rate into bubbles.

The variables τ_n and ε_n in Eq. (B.31) depend on q_n , which is proportional to blood flow \dot{Q}_n at time t_n . The recursive relation for calculating \dot{Q}_n is obtained from Eq. (B.25):

$$\dot{Q}_{n+1} = \dot{Q}_{ex_n} - (\dot{Q}_{ex_n} - \dot{Q}_n) \sum_{\ell=1}^{N_{exp}} f_{exp\ell,n} \exp\left(-\frac{\Delta t}{\tau_{exp\ell,n}}\right).$$

The parameters in this relation include steady-state blood flows at different exercise intensities, and time constants and blood flow fractions associated with each exponential component. Note that $\dot{Q}_{n+1} = \dot{Q}_{ex_n}$ if the change in blood flow rate is instantaneous ($\tau_{exp\ell,n} = 0$ for all ℓ).

As an example, consider a tissue compartment with a resting half time of 100 min. The time constant is $100/\ln(2) = 144$ min, and compartmental blood flow per unit volume of tissue is $1/144$ or approximately 0.007 mL per min. The compartmental blood flow per unit volume of tissue during 50% maximum exercise would increase by a factor of about 2.5 to 0.0175 mL per min, corresponding to a time constant of 57 min. Exponential time constants associated with such a change in blood flow would range from a fraction of a minute to several minutes.

Eq. (B.31) is identical to Eq. (B.24) except for the dependency of τ – and hence ε – and G on time. The model we adopted for blood flow changes and the approximations we made for closed-form evaluation of the integral terms in the solution did not alter the basic structure of the recursive relation for calculating the tissue gas tension. This may not be true with more complex models of blood flow. The multi-exponential model is fairly realistic and the approximations (with second order terms neglected) are reasonable, requiring that blood flow time constants be greater than 0.1 min to limit the error to less than 0.5 % with an integration step size of 0.001 min. The demands on accuracy can always be met by reducing the step size, if the increased computational burden can be accommodated.

9.1.1.2.3 *Coupling of Compartmental O₂ Consumption and Blood flow*

We assume that exercise-induced changes in compartmental blood flow are driven by changes in compartmental O₂ consumption due to exercise, and that the latter changes are given by Eq. (A.25). The recursive relation for solving Eq. (A.25) is

$$\dot{V}_{O_{2n+1}} = \dot{V}_{O_{2n}} - \left(\dot{V}_{O_{2ex,n}} - \dot{V}_{O_{2n}} \right) \left\{ 1 - \exp \left(- \frac{\Delta t_n}{\tau \dot{V}_{O_{2n}}} \right) \right\}, \quad (\text{B.32})$$

where $\dot{V}_{O_{2n+1}}$ and $\dot{V}_{O_{2n}}$ are the O_2 consumption rates at times t_{n+1} and t_n , respectively,

$$\dot{V}_{O_{2ex,n}} = \Delta \dot{V}_{O_{2ex}} + \dot{V}_{O_{2rest}} = m_{V_{O_2}} I_{ex,n} + \dot{V}_{O_{2rest}} \quad (\text{B.33})$$

is the steady-state O_2 consumption at exercise intensity $I_{ex,n}$, and $\tau_{\dot{V}_{O_2}}$ is the time constant associated with the exponential change in \dot{V}_{O_2} in the interval $[t_n, t_{n+1}]$.

The steady-state blood flow during exercise is then estimated by assuming that compartmental blood flow increases linearly with compartmental O_2 consumption:

$$\dot{Q}_{ex,n} = m_Q \cdot (\dot{V}_{O_{2,n}} - \dot{V}_{O_{2,rest}}) + \dot{Q}_{rest} \quad (\text{B.34})$$

9.1.2 Multiple Bubbles of Different Sizes

The recursive relationships derived above are readily elaborated to accommodate the solution for the radii and gas pressures of multiple bubbles present in an arbitrary distribution of N_{bs} different sizes. Such elaboration entails repeating the calculations of \hat{r}_{n+1} and $P_{b_{n+1}}$ for the n_{b_m} bubbles of each size $m, m=1, 2, \dots, N_{bs}$, in the distribution.

The bubble gas pressures are obtained from Eq. (B.12)

$$P_{b_{m,n+1}} = A_{m,n} - (3A_{m,n} - B_{m,n}) \delta \hat{r}_{m,n}. \quad (\text{B.35})$$

where $A_{m,n}$ is obtained from Eq. (B.13a);

$$A_{m,n} = P_{b_{m,n}} + a_{m,n} \left(1 - \frac{a_{m,n}}{2} \right) (p_{t_n} - P_{b_{m,n}}), \quad (\text{B.36})$$

with $a_{m,n} = \left(\frac{\hat{r}_{m,n} + 1}{\hat{r}_{m,n}^2} \Delta t_n \right) \widehat{K}_m$; and $B_{m,n}$ is obtained from Eq. (13.b);

$$B_{m,n} = \frac{1}{2} \left[(2a_{m,n} - b_{m,n} + a_{m,n} b_{m,n}) p_{t_n} + (a_{m,n} + b_{m,n}) (1 - a_{m,n}) P_{b_{m,n}} \right], \quad (\text{B.37})$$

with $b_{m,n} = \frac{\Delta t_n}{\hat{r}_{m,n}^2} \widehat{K}_m$.

Finally, from Eq. (B.18)

$$\delta \hat{r}_{m,n} = \frac{A_{m,n} - \left(P'_{amb_{n+1}} + \frac{2\hat{\sigma}_m}{\hat{r}_{m,n}} + \hat{M}_m \hat{r}_{m,n}^3 \right)}{(3A_{m,n} - B_{m,n}) - \left(\frac{2\hat{\sigma}_m}{\hat{r}_{m,n}} - 3\hat{M}_m \hat{r}_{m,n}^3 \right)}. \quad (\text{B.38})$$

The tissue tension of the diffusible gas $p_{t_{n+1}}$ is calculated using Eq. (B.23) for any function $q_k(t)$ or Eq. (B.31) for $q_k(t)$ as a multiexponential, after modification to account for the net gas exchange between all bubbles and the tissue as such exchange differs for bubbles of different sizes. Accordingly, Eq. (B.23) is modified by summing the amounts of gas exchanged between bubbles and tissue for all bubbles of N_{bs} different sizes as follows:

$$p_{t_{n+1}} = (p_{t_n} - p_{a_n}) \exp \left[- \int_{t_n}^{t_{n+1}} q(t) dt \right] + p_{a_n} + v_n \Delta t_n - \left(v_n + \sum_{m=1}^{N_{bs}} \hat{G}_m S_{x_{m,n}} \right) \int_{t_n}^{t_{n+1}} \exp \left[- \int_t^{t_{n+1}} q(t) dt \right] dt \quad (\text{B.39})$$

where $\hat{x}_{m,n+1}$ and $\hat{x}_{m,n}$ are the gas contents at times t_{n+1} and t_n respectively in each of $n_{b_{m,n}}$ bubbles of radius r_m in the m^{th} bubble size group with

$$\hat{G}_m = \left(\frac{4\pi}{3} \right) \frac{n_{b_m}}{\alpha_t V_t \Lambda_m^3}, \text{ and}$$

$$S_{x_{m,n}} = \frac{\hat{x}_{m,n+1} - \hat{x}_{m,n}}{\Delta t_n}.$$

Similarly, Eq. (B.31) becomes

$$p_{t_{n+1}} = p_{t_n} + v_n \Delta t_n + \left[p_{a_n} - p_{t_n} - \tau_n \left(v_n + \frac{\sum_{m=1}^{N_{bs}} \hat{G}_m (\hat{x}_{m,n+1} - \hat{x}_{m,n})}{\Delta t_n} \right) \right] \varepsilon_n. \quad (\text{B.40})$$

With constant $q(t)$, τ_n becomes a constant equal to τ and Eq. (B.40) reduces to Eq. (B.24).

Determination of $\hat{r}_{m,n+1}$, $P_{b_{n+1}}$, and $p_{t_{n+1}}$ requires computation time in excess of that required for the $N_{bs} = 1$ case (multiple bubbles of the same size) roughly in proportion to the number of bubble sizes considered.

9.2 Multiple Diffusible Gases

With $N_g > 1$ diffusible gases in the tissue-bubble system, the recursive relations derived in the previous sections hold for each diffusible gas. Referring to Eq. (B.35), the pressure of the k^{th} diffusible gas in bubbles of m^{th} size is

$$P_{b_{k,m,n+1}} = A_{k,m,n} - (3A_{k,m,n} - B_{k,m,n})\delta\hat{r}_{m,n}. \quad (\text{B.41})$$

where

$$A_{k,m,n} = P_{b_{k,m,n}} + a_{k,m,n} \left(1 - \frac{a_{k,m,n}}{2} \right) (p_{t_{k,n}} - P_{b_{k,m,n}}), \quad (\text{B.42})$$

with $a_{k,m,n} = \left(\frac{\hat{r}_{m,n} + 1}{\hat{r}_{m,n}^2} \Delta t_n \right) \hat{K}_{k,m}$, and

$$B_{k,m,n} = \frac{1}{2} \left[(2a_{k,m,n} - b_{k,m,n} + a_{k,m,n} b_{k,m,n}) p_{t_{k,n}} + (a_{k,m,n} + b_{k,m,n})(1 - a_{k,m,n}) P_{b_{k,m,n}} \right], \quad (\text{B.43})$$

with $b_{k,m,n} = \frac{\Delta t_n}{\hat{r}_{m,n}^2} \hat{K}_{k,m}$.

Coefficients $A_{k,m,n}$ and $B_{k,m,n}$ at time t_n are different for each diffusible gas due to differences in the scaled permeabilities, \hat{K}_k , of the gases in the tissue.

The total diffusible gas pressure in a bubble must equal the hydrostatic pressure less the sum of the infinitely-diffusible gas partial pressures, P_∞ , plus the pressures due to surface tension and tissue elasticity as indicated by Eq. (B.14). Therefore, for bubbles of size m

$$\sum_{k=1}^{N_g} P_{b_{k,m,n+1}} = \sum_{k=1}^{N_g} A_{k,m,n} - \left[\sum_{k=1}^{N_g} (3A_{k,m,n} - B_{k,m,n}) \right] \delta\hat{r}_{m,n}$$

$$= P'_{amb,n+1} + \frac{2\bar{\sigma}}{\hat{r}_{m,n+1}} + \widehat{M}\hat{r}_{m,n+1}^3. \quad (\text{B.44})$$

Following the steps from Eq. (B.14) to Eq. (B.18), we obtain

$$\delta\bar{r}_{m,n} = \frac{\sum_{k=1}^{N_g} A_{k,m,n} - \left(P'_{amb,n+1} + \frac{2\bar{\sigma}}{\hat{r}_{m,n}} + \widehat{M}\hat{r}_{m,n}^3 \right)}{\sum_{k=1}^{N_g} (3A_{k,m,n} - B_{k,m,n}) - \left(\frac{2\bar{\sigma}}{\hat{r}_{m,n}} - 3\widehat{M}\hat{r}_{m,n}^3 \right)}. \quad (\text{B.45})$$

Note that Eq. (B.45) reduces to Eq. (B.18) if the number of diffusible gases $N_g = 1$.

The tissue tension of each diffusible gas is calculated using Eq. (B.39) for any function $q_k(t)$ or Eq. (B.40) for $q_k(t)$ as a multiexponential. For the k^{th} diffusible gas in the interval $[t_n, t_{n+1}]$, Eq. (B.39) becomes

$$p_{t_{k,n+1}} = (p_{t_{k,n}} - p_{a_{k,n}}) \exp \left[- \int_{t_n}^{t_{n+1}} q_k(t) dt \right] + p_{a_{k,n}} + v_{k,n} \Delta t_n - \left(v_{k,n} + \sum_{m=1}^{N_{bs}} \hat{G}_{k,m} S_{x_{k,mn}} \right) \int_{t_n}^{t_{n+1}} \exp \left[- \int_t^{t_{n+1}} q_k(t) dt \right] dt \quad (\text{B.46})$$

and Eq. (B.40) becomes

$$p_{t_{k,n+1}} = p_{t_{k,n}} (1 - \varepsilon_{k,n}) + v_{k,n} \Delta t_n + \left[p_{a_{k,n}} - \tau_{k,n} \left\{ v_{k,n} + \sum_{m=1}^{N_{bs}} \hat{G}_{k,m} S_{x_{k,mn}} \right\} \right] \varepsilon_{k,n}, \quad (\text{B.47})$$

where $\hat{G}_{k,m} = \left(\frac{4\pi}{3} \right) \frac{n_{b_m}}{\alpha_{t_k} V_t \Lambda_m^3}$,

$$\hat{x}_{k,m,n+1} = P_{b_{k,m,n+1}} \hat{r}_{m,n+1}^3,$$

$$S_{x_{k,mn}} = \frac{\hat{x}_{k,m,n+1} - \hat{x}_{k,m,n}}{\Delta t_n}, \text{ and}$$

$v_{k,n} = \frac{p_{a_{k,n+1}} - p_{a_{k,n}}}{\Delta t_n}$ is the rate of change in arterial tension of the k^{th} diffusible gas in the interval $[t_n, t_{n+1}]$. With constant $q_k(t)$, Eq. (B.47) applies with $\tau_{k,n}$ a constant equal to

τ_k . Omission of subscripts for gas-specific variables then renders Eq. (B.47) identical to Eq. (B.24).

9.2.1 Tissue O_2 Tension with O_2 as a Diffusible Gas

Eqs. (B.41) through (B.45) also apply when O_2 is considered to be among the N_g diffusible gases. However, Eqs. (B.46) and (B.47) require modification to account for the nonlinear relationship between O_2 content and O_2 partial pressure in arterial blood due to the Hb- O_2 dissociation curve.

Semi-analytic solutions similar to Eq. (B.46) and (B.47) can be derived for recursive calculation of P_{tO_2} in each integration interval. To simplify notation, we describe the derivation for cases involving multiple bubbles of the same size in a tissue and then elaborate the result for cases involving multiple bubbles of different size.

9.2.1.1 Multiple Bubbles of Same Size

We begin by substituting $\hat{x}_{O_2} = P_{bO_2} \hat{r}^3$ and $\hat{G}_{O_2} = \frac{4\pi}{3} \frac{n_b}{\alpha_{tO_2} V_t \Lambda^3}$ into Eq. (A.15) (with $N_{bs} =$

1) for O_2 mass balance in tissue to obtain:

$$\frac{d}{dt}(\alpha_{tO_2} P_{tO_2}) = \dot{Q}(t)[C_{aO_2} - C_{\bar{v}O_2}] - \alpha_{tO_2} \hat{G}_{O_2} \frac{d\hat{x}_{O_2}}{dt} - \dot{V}_{O_2}(t), \quad (B.48)$$

where $\dot{Q}(t)$ is blood flow per unit volume of tissue and the tissue O_2 consumption, $\dot{V}_{O_2}(t)$, is determined with the recursive formula in Eq. (B.32). We then approximate the blood O_2 content (plasma + Hb-bound) versus O_2 partial pressure curve by a linear segment for the time interval $[t_n, t_{n+1}]$ and express $C_{\bar{v}O_2}$, the venous O_2 content corresponding to partial pressure $p_{\bar{v}O_{2n}}$ at time t_n , as

$$C_{\bar{v}O_2} = C_{\bar{v}O_{2n}} + \alpha'_{O_{2n}} (p_{\bar{v}O_2} - p_{\bar{v}O_{2n}}), \quad (B.49)$$

where $\alpha'_{O_{2n}}$ is the slope of the whole blood solubility curve in the region of $p_{\bar{v}O_{2n}}$. Referring to the $a_1, a_2, b_1, b_2, p, \eta$, and p_{half} parameters defined with Eq. (A.21), this slope is given by

$$\begin{aligned}
\alpha'_{O_2n} &= \frac{dC_{O_2}}{dP_{O_2}} = \alpha_{b_{O_2}} + Hb_c \frac{dS_{O_2}}{dp_{O_2}} \\
&= \alpha_{b_{O_2}} + Hb_c \frac{dS_{O_2}}{dp} \frac{dp}{dp_{O_2}} \\
&= \alpha_{b_{O_2}} + Hb_c \left[\frac{(a_1 + 2a_2p)(1.0 + b_1p + b_2p^2) - (a_1p + a_2p^2)(b_1 + 2b_2p)}{(1.0 + b_1p + b_2p^2)^2} \right] \left[\frac{\eta p^{\eta-1}}{P_{half}} \right] \\
&= \alpha_{b_{O_2}} + Hb_c \left[\frac{(a_1 + a_1b_1p + a_1b_2p^2 + 2a_2p + 2a_2b_1p^2 + 2a_2b_2p^3) - (a_1b_1p + 2a_1b_2p^2 + 2a_2b_1p^2 + 2a_2b_2p^3)}{(1.0 + b_1p + b_2p^2)^2} \right] \left[\frac{\eta p^{\eta-1}}{P_{half}} \right] \\
&= \alpha_{b_{O_2}} + Hb_c \left[\frac{a_1 + 2a_2p - a_2(a_1 - b_1)p^2}{(1.0 + b_1p + b_2p^2)^2} \right] \left[\frac{\eta p^{\eta-1}}{P_{half}} \right], \tag{B.50}
\end{aligned}$$

with $p = \left(\frac{P_{\bar{v}_{O_2n}}}{P_{half}} \right)^\eta$.

Note that α'_{O_2n} has the units of solubility. Assuming that compartmental blood-tissue gas exchange is perfusion limited, end-capillary blood and tissue are at equilibrium; i.e., $P_{\bar{v}_{O_2}} = P_{t_{O_2}}$; and Eq. (B.49) becomes

$$\begin{aligned}
C_{\bar{v}_{O_2}} &= C_{\bar{v}_{O_2n}} - \alpha'_{O_2n} P_{\bar{v}_{O_2n}} + \alpha'_{O_2n} P_{t_{O_2}} \\
&= C'_{O_2n} + \alpha'_{O_2n} P_{t_{O_2}}, \tag{B.51}
\end{aligned}$$

where

$$C'_{O_2n} = C_{\bar{v}_{O_2n}} - \alpha'_{O_2n} P_{\bar{v}_{O_2n}}. \tag{B.52}$$

Substitution of Eq. (B.51) into Eq. (B.48) yields

$$\frac{d}{dt}(\alpha_{t_{O_2}} p_{t_{O_2}}) = \dot{Q}_n [C_{a_{O_2}} - C'_{O_{2n}} - \alpha'_{O_{2n}} p_{t_{O_2}}] - \alpha_{t_{O_2}} \hat{G}_{O_2} \frac{d\hat{x}_{O_2}}{dt} - \dot{V}_{O_{2n}}, \quad (\text{B.53})$$

which is valid for $t_n \leq t < t_{n+1}$ with blood flow of \dot{Q}_n and O_2 consumption of $\dot{V}_{O_{2n}}$. Dividing both sides of Eq. (B.53) by $\alpha_{t_{O_2}}$ yields

$$\begin{aligned} \frac{dp_{t_{O_2}}}{dt} &= \frac{\dot{Q}_n}{\alpha_{t_{O_2}}} [C_{a_{O_2}} - C'_{O_{2n}} - \alpha'_{O_{2n}} p_{t_{O_2}}] - \hat{G}_{O_2} \frac{d\hat{x}_{O_2}}{dt} - \frac{\dot{V}_{O_{2n}}}{\alpha_{t_{O_2}}} \\ &= \frac{\dot{Q}_n \alpha'_{O_{2n}}}{\alpha_{t_{O_2}}} \left[\frac{C_{a_{O_2}}}{\alpha'_{O_{2n}}} - \frac{C'_{O_{2n}}}{\alpha'_{O_{2n}}} - p_{t_{O_2}} \right] - \hat{G}_{O_2} \frac{d\hat{x}_{O_2}}{dt} - \frac{\dot{V}_{O_{2n}}}{\alpha_{t_{O_2}}} \\ &= \frac{\dot{Q}_n \alpha'_{O_{2n}}}{\alpha_{t_{O_2}}} \left(\frac{C_{a_{O_2}}}{\alpha'_{O_{2n}}} - p_{t_{O_2}} \right) - \frac{\dot{Q} C'_{O_{2n}}}{\alpha_{t_{O_2}}} - \hat{G}_{O_2} \frac{d\hat{x}_{O_2}}{dt} - \frac{\dot{V}_{O_{2n}}}{\alpha_{t_{O_2}}} \\ &= \frac{\dot{p}_{O_2} - p_{t_{O_2}}}{\tau_{O_{2n}}} - \hat{G}_{O_2} \frac{d\hat{x}_{O_2}}{dt} - \dot{\rho}_n, \end{aligned} \quad (\text{B.54})$$

where $\dot{p}_{O_2} = \frac{C_{a_{O_2}}}{\alpha'_{O_{2n}}}$, $\tau_{O_{2n}} = \frac{\alpha_{t_{O_2}}}{\alpha'_{O_{2n}} \dot{Q}_n}$ is a time constant that changes in each time interval depending on changes in blood flow and changes in the slope of the blood O_2 content versus O_2 partial pressure curve at the prevailing $p_{t_{O_2}}$, and $\dot{\rho}_n$ is a constant rate of change of pressure in each time interval, defined as $\dot{\rho}_n = \frac{\dot{V}_{O_{2n}} + \dot{Q}_n C'_{O_{2n}}}{\alpha_{t_{O_2}}}$,

which upon substitution for $C'_{O_{2n}}$ from Eq. (B.51) becomes

$$\dot{\rho}_n = \frac{\dot{V}_{O_{2n}} + \dot{Q}_n (C_{\bar{v}_{O_{2n}}} - \alpha'_{O_{2n}} p_{\bar{v}_{O_{2n}}})}{\alpha_{t_{O_2}}}. \quad (\text{B.55})$$

Note from Eq. (B.50) that $\alpha'_{O_{2n}} \geq \alpha_b$, which obviates excessively small values of $\alpha'_{O_{2n}}$ that could cause numerical errors. Rearranging terms, Eq. (B.54) for the interval $[t_n, t_{n+1}]$ becomes,

$$\frac{dp_{t_{O_2}}}{dt} + \frac{p_{t_{O_2}}}{\tau_{O_{2n}}} = \frac{\dot{p}_{O_2}}{\tau_{O_{2n}}} - \frac{d\hat{x}'_{O_2}}{dt}, \quad (\text{B.56})$$

where $\hat{x}'_{O_2} = \hat{G}_{O_2} \hat{x}_{O_2} + \dot{\rho}_n t$. (B.57)

Eq. (B.56) is identical in form to Eq. (A.22) with $k=1$ and $N_{bs} = 1$ for the tissue tension of an inert gas. Comparison of the two equations shows that variables \dot{p}_{O_2} , \dot{x}'_{O_2} , and $\tau_{O_{2n}}$ in Eq. (B.56) correspond respectively to variables p_a , \hat{x} , and τ in Eq. (A.22), and the constant G in Eq. (A.22) is 1 in Eq. (B.56). With these changes in variables and the value for G , the solution to Eq. (A.22) given by Eq. (B.31) is applicable to Eq. (B.53) as well. Thus, for identically sized bubbles in tissue, the recursive formula for tissue O_2 tension $p_{t_{O_2,n+1}}$ at time t_{n+1} , given the tissue O_2 tension $p_{t_{O_2,n}}$ at time t_n , is

$$p_{t_{O_2,n+1}} = p_{t_{O_2,n}} + v_{O_{2n}} \Delta t_n + \left[\dot{p}_{O_2} - p_{t_{O_2,n}} - \tau_{O_{2n}} \left\{ v_{O_{2n}} + \frac{\hat{x}'_{O_{2n+1}} - \hat{x}'_{O_{2n}}}{\Delta t_n} \right\} \right] \varepsilon_{O_{2n}}, \quad (B.58)$$

where $\varepsilon_{O_{2n}} = 1 - \exp\left(-\frac{\Delta t_n}{\tau_{O_{2n}}}\right)$. Using Eq. (B.57),

$$\frac{\dot{x}'_{O_{2n+1}} - \dot{x}'_{O_{2n}}}{\Delta t_n} = G_{O_2} \frac{x_{O_{2n+1}} - x_{O_{2n}}}{\Delta t_n} + \dot{p}_n \frac{(t_{n+1} - t_n)}{\Delta t_n} = \hat{G}_{O_2} \frac{\hat{x}_{O_{2n+1}} - \hat{x}_{O_{2n}}}{\Delta t_n} + \dot{p}_n,$$

which is substituted into Eq. (B.58) to yield:

$$p_{t_{O_2,n+1}} = p_{t_{O_2,n}} (1 - \varepsilon_{O_{2n}}) + v_{O_{2n}} \Delta t_n + \left[\dot{p}_{O_2} - \tau_{O_{2n}} \left\{ v_{O_{2n}} + \dot{p}_n + \hat{G}_{O_2} \frac{\hat{x}_{O_{2n+1}} - \hat{x}_{O_{2n}}}{\Delta t_n} \right\} \right] \varepsilon_{O_{2n}}. \quad (B.59)$$

The rate $v_{O_{2n}}$ for O_2 is defined by the difference in \dot{p}_{O_2} in the interval $[t_n, t_{n+1}]$;

$$v_{O_{2n}} = \frac{\dot{p}_{O_{2n+1}} - \dot{p}_{O_{2n}}}{\Delta t_n} = \frac{C_{a_{O_{2n+1}}} - C_{a_{O_{2n}}}}{\Delta t_n \alpha'_{O_{2n}}}, \quad (B.60)$$

where $C_{a_{O_{2n+1}}}$ and $C_{a_{O_{2n}}}$ are arterial O_2 contents corresponding to arterial O_2 partial pressures $p_{a_{O_{2n+1}}}$ and $p_{a_{O_{2n}}}$ at times t_{n+1} and t_n respectively.

9.2.1.2 Multiple Bubbles of Different Size

If the tissue contains multiple bubbles of different sizes, Eq. (B.46) or (B.47) is used to calculate the tissue tension of each of the inert gases. Referring to Eq. (B.59), the corresponding tissue O_2 tension is given by

$$\begin{aligned}
p_{t_{O_2_{n+1}}} &= p_{t_{O_2_n}} (1 - \varepsilon_{O_2_n}) + v_{O_2_n} \Delta t_n \\
&+ \left[p_{O_2_n} - \tau_{O_2_n} \left\{ v_{O_2_n} + \dot{p}_n + \frac{\sum_{m=1}^{N_{bs}} \hat{G}_{O_2_m} (\hat{x}_{O_2_{m,n+1}} - \hat{x}_{O_2_{m,n}})}{\Delta t_n} \right\} \varepsilon_{O_2_n} \right], \quad (B.61)
\end{aligned}$$

where $\hat{G}_{O_2_m} = \left(\frac{4\pi}{3} \right) \frac{n_{b_m}}{\alpha_{t_{O_2}} V_t \Lambda_m^3}$ for bubbles of m^{th} size. Note that the n_{b_m} are constant.

9.2.2 Variable Bubble Number: Single Time-Dependent Bubble Size Approximation

As noted in Appendix A, the accumulation of bubbles recruited with increasing supersaturation during decompression is accommodated in present models by assuming that each newly nucleated bubble instantaneously attains the size of prevailing already-nucleated bubbles, which allows r_{n+1} , $\mathbf{P}_{b_{n+1}}$, and $p_{t_{n+1}}$ to be tracked for only a single bubble size group ($N_{bs} = 1$) in which only n_b changes:

$N_b = \sum_m^{N_{bs}} n_{b_m}$. Maintenance of mass balance in this approach requires a change in

bubble gas content and a resultant adjustment in tissue gas tension corresponding to the difference between the nucleonic volume and the prevailing bubble volume whenever a nucleus is 'recruited' during decompression. These requirements are met by allowing the coefficient \hat{G}_k to vary with the number of bubbles and by modifying Eq. (B.47) as described below.

Let $\hat{G}_{k,n}$ denote the coefficient associated with the bubble content of gas k , $\hat{x}_{k,n}$, at the outset of the n^{th} integration step. The change in gas content, $\hat{x}_{k,n+1} - \hat{x}_{k,n}$, in the interval $[t_n, t_{n+1}]$ is preceded by a change in $\hat{G}_{k,n}$ at the beginning of the interval if any new bubbles are considered to be recruited at the beginning of the interval. We therefore consider the Δt_n interval to consist of two subintervals; an initial $\Delta t_{n,0}$ interval in which the bubble number increases from $\hat{G}_{k,n-1}$ to $\hat{G}_{k,n}$, and a subsequent $\Delta t_{n,1}$ interval in which the $\hat{G}_{k,n}$ bubbles evolve, as illustrated in Figure B.1. In the sub-interval $\Delta t_{n,0}$, newly recruited bubbles expand from gas content $\hat{x}_{k,n,0}$ to $\hat{x}_{k,n,1}$. The gas content $\hat{x}_{k,n,1}$ of $\Delta \hat{G}_{k,n}$ newly nucleated bubbles at time $(t_n + \Delta t_{n,0})$ is the same as that of $\hat{G}_{k,n-1}$ 'older' bubbles that grow from $\hat{x}_{k,n}$ at t_n to $\hat{x}_{k,n+1}$ at t_{n+1} . In the sub-interval $\Delta t_{n,1}$, the total gas content of

all bubbles changes from $\hat{x}_{k,n,1}$ to $\hat{x}_{k,n+1}$. The total number of bubbles is $\hat{G}_{k,n} = \hat{G}_{k,n-1} + \Delta\hat{G}_{k,n}$. Including the change in $\hat{G}_{k,n}$, Eq. (B.47) becomes

$$p_{t_{k,n+1}} = p_{t_{k,n}} (1 - \varepsilon_{k,n}) + v_{k,n} \Delta t_n + \left[p_{a_n} - \tau_k \left\{ v_{k,n} + \hat{G}_{k,n-1} \frac{\hat{x}_{k,n+1} - \hat{x}_{k,n}}{\Delta t_n} \right\} \right] \varepsilon_{k,n} - \left[\Delta\hat{G}_{k,n} \frac{\hat{x}_{k,n,1} - \hat{x}_{k,n,0}}{\Delta t_{n,0}} \tau_k \right] \varepsilon_{k,n,0} - \left[\Delta\hat{G}_{k,n} \frac{\hat{x}_{k,n+1} - \hat{x}_{k,n,1}}{\Delta t_{n,1}} \tau_k \right] \varepsilon_{k,n,1} \quad (\text{B.62})$$

where $\varepsilon_{k,n,0} = 1 - \exp\left(-\frac{\Delta t_{n,0}}{\tau_k}\right)$ and $\varepsilon_{k,n,1} = 1 - \exp\left(-\frac{\Delta t_{n,1}}{\tau_k}\right)$.

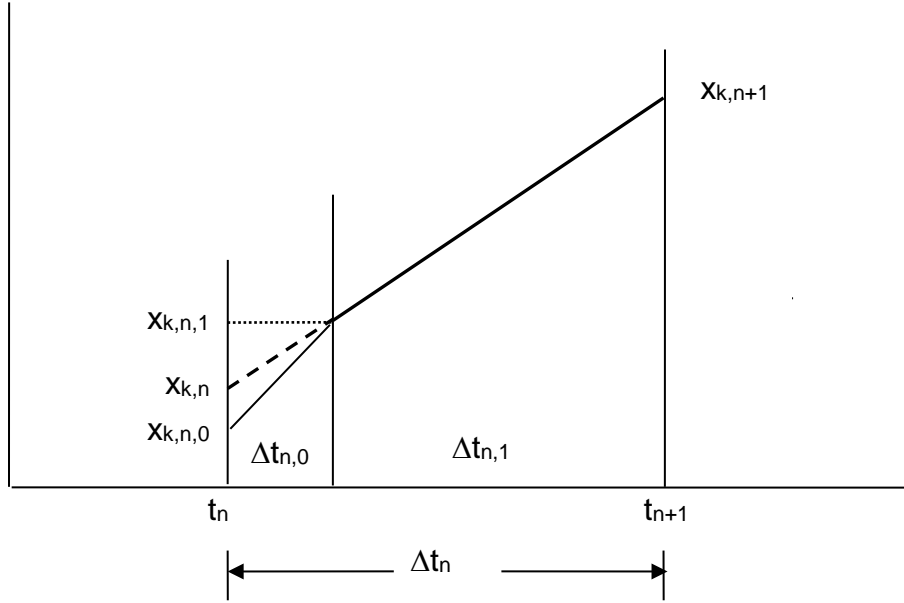


Fig. B.1: Sub-intervals of Δt_n accommodating growth of newly formed bubbles.

The contribution of the newly formed bubbles is evaluated assuming the change from $\hat{x}_{k,n,0}$ to $\hat{x}_{k,n,1}$ occurs instantaneously. We thus let $\Delta t_{n,0} \rightarrow 0$ and, consequently $\hat{x}_{k,n,1} \rightarrow \hat{x}_{k,n}$, to obtain

$$\begin{aligned} \lim_{\Delta t_{n,0} \rightarrow 0} \left[\Delta\hat{G}_{k,n} \frac{\hat{x}_{k,n,1} - \hat{x}_{k,n,0}}{\Delta t_{n,0}} \tau \right] \varepsilon_{k,n,0} &= \Delta\hat{G}_{k,n} (\hat{x}_{k,n} - \hat{x}_{k,n,0}) \lim_{\Delta t_{n,0} \rightarrow 0} \left[\frac{\tau_k}{\Delta t_{n,0}} \right] \varepsilon_{k,n,0} \\ &= \Delta\hat{G}_{k,n} (\hat{x}_{k,n} - \hat{x}_{k,n,0}) \lim_{\Delta t_{n,0} \rightarrow 0} \left[\frac{\tau_k}{\Delta t_{n,0}} \right] \left[1 - \exp\left(-\frac{\Delta t_{n,0}}{\tau_k}\right) \right] \end{aligned}$$

$$= \Delta \hat{G}_{k,n} (\hat{x}_{k,n} - \hat{x}_{k,n,0}) \quad \text{with the limit evaluating to 1.}$$

Also, as $\Delta t_{n,0} \rightarrow 0$, $\Delta t_{n,1} \rightarrow \Delta t_n$ and $\varepsilon_{k,n,1} \rightarrow \varepsilon_{k,n}$. Substituting these limits and using

$\hat{G}_{k,n} = \hat{G}_{k,n-1} + \Delta \hat{G}_{k,n}$, Eq. (B.62) becomes

$$\begin{aligned} p_{t_{k,n+1}} &= p_{t_{k,n}} (1 - \varepsilon_{k,n}) + v_{k,n} \Delta t_n + \left[p_{a_{k,n}} - \tau_k \left\{ v_{k,n} + \hat{G}_{k,n-1} \frac{\hat{x}_{k,n+1} - \hat{x}_{k,n}}{\Delta t_n} \right\} \right] \varepsilon_{k,n} \\ &\quad - \Delta \hat{G}_{k,n} (\hat{x}_{k,n} - \hat{x}_{k,n,0}) - \left[\Delta \hat{G}_{k,n} \frac{\hat{x}_{k,n+1} - \hat{x}_{k,n}}{\Delta t_{k,n}} \tau \right] \varepsilon_{k,n} \\ &= p_{t_{k,n}} (1 - \varepsilon_{k,n}) + v_{k,n} \Delta t_n + \left[p_{a_{k,n}} - \tau_k \left\{ v_{k,n} + \hat{G}_{k,n} \frac{\hat{x}_{k,n+1} - \hat{x}_{k,n}}{\Delta t_n} \right\} \right] \varepsilon_{k,n} \\ &\quad - \Delta \hat{G}_n (\hat{x}_{k,n} - \hat{x}_{k,n,0}) \end{aligned} \tag{B.63}$$

Following a similar development from Eq. (B.61), the tissue O₂ tension is given by

$$\begin{aligned} p_{t_{O_2,n+1}} &= p_{t_{O_2,n}} (1 - \varepsilon_{O_2,n}) + v_{O_2,n} \Delta t_n \\ &\quad + \left[p'_{O_2,n} - \tau_{O_2,n} \left\{ v_{O_2,n} + \dot{p}_n + \hat{G}_{O_2,n} \frac{(\hat{x}_{O_2,n+1} - \bar{x}_{O_2,n})}{\Delta t_n} \right\} \right] \varepsilon_{O_2,n} \\ &\quad - \Delta \hat{G}_{O_2,n} (\bar{x}_{O_2,n} - \hat{x}_{O_2,n,0}), \end{aligned} \tag{B.64}$$

where $\Delta \hat{G}_{O_2,n} = \left(\frac{4\pi}{3} \right) \frac{1}{\alpha_{t_{O_2}} V_t \Lambda^3} (n_{b_{t_n}} - n_{b_{t_{n-1}}})$.

In applying Eq. (B.63) and (B.64), the change $\Delta \hat{G}_{k,n}$ at time t_n is obtained from the number of nuclei recruited in the interval from the assumed nuclei size distribution; i.e., the number of nuclei versus their radii. The gas content $\hat{x}_{k,n,0}$ at t_n is that of the nuclei from which the $\Delta \hat{G}_{k,n}$ new bubbles were formed.

The number of nuclei recruited at the outset of any integration interval and the corresponding $\Delta \hat{G}_{k,n}$ must be determined in a fashion that ensures that nuclei already recruited from the distribution and lost to the vasculature as VGE are not double-counted in the nucleation process: The number of bubbles remaining in the compartment at any time may be fewer than the cumulative number of nuclei that have been recruited in the compartment at that time. Accordingly, the total number of nuclei

recruited must be tracked independently of the number of bubbles remaining in the compartment. The cumulative number of bubbles recruited for the n^{th} integration step is

$$N_{b_{\max,n}} = \text{MAX} \left[N_{b_{\max,n-1}}, N_b^0 \exp \left(- \frac{2\sigma}{P_{ss_n} \cdot \beta_{f_n}} \right) \right], \quad (\text{B.65})$$

where $N_{b_{\max,n-1}}$ is the cumulative number of nuclei that were recruited at the outset of the $(n-1)$ integration step. The number of bubbles recruited at the outset of the n^{th} integration step to join those already present in the compartment (of number $N_{b_{n-1}}$) is consequently

$$\Delta n_{b_n} = (N_{b_{\max,n}} - N_{b_{\max,n-1}}), \quad (\text{B.66})$$

so that the number of bubbles participating in the n^{th} integration step is

$$n_{b_n} = n_{b_{n-1}} + \Delta n_{b_n}. \quad (\text{B.67})$$

$$\text{Thus, } \Delta \hat{G}_{k,n} = \left(\frac{4\pi}{3} \right) \frac{\Delta n_{b_n}}{\alpha_{t_k} V_t \Lambda^3} \quad (\text{B.68})$$

$$\text{and } \hat{G}_{k,n} = \hat{G}_{k,n-1} \frac{N_{b_n}}{N_{b_{n-1}}}. \quad (\text{B.69})$$

Increases in the compartmental bubble number density and n_b as bubbles are nucleated from one integration step to the next with increasing supersaturation during decompression are accommodated in Eqs. (B.63) and (B.64) by the respective $\Delta \hat{G}_{k,n}$ factors and thereafter by the sustained change in n_{b_n} in the corresponding $\hat{G}_{k,n}$ factors.

9.3 Semi-Analytic Solution of the Fick Equation in the 3RUT-MB Model

The Fick equation for the 3RUT-MB model given by Equation (B.3) is reproduced following:

$$\frac{dx}{dt} + f(t)x = g(t). \quad (\text{B.3})$$

This is a linear differential equation in the dependent variable x with coefficients that vary with time. We apply the integrating factor method to obtain a numerical solution of this equation for $x(t)$ at time t_{n+1} given $x(t)$ at time t_n . Recursion of this solution through time provides the entire solution $x(t_i)$, $i = 0, 1, 2, \dots$

The integrating factor is $\exp[I_f(t)]$, where $I_f(t)$ is the indefinite integral $\int f(t)dt$. Both sides of Eq. (B.3) are multiplied by the integrating factor to obtain

$$\frac{d}{dt}[x(t) \exp\{I_f(t)\}] = g(t) \exp\{I_f(t)\}. \quad (\text{B.70})$$

Integration of Eq. (B.70) in the interval $t_n \leq t \leq t_{n+1}$ yields

$$\begin{aligned} x(t) \exp\{I_f(t)\} \Big|_{t_n}^{t_{n+1}} &= \int_{t_n}^{t_{n+1}} g(t) \exp\{I_f(t)\} dt \\ \text{i.e., } x(t_{n+1}) \exp\{I_f(t_{n+1})\} - x(t_n) \exp\{I_f(t_n)\} &= \int_{t_n}^{t_{n+1}} g(t) \exp\{I_f(t)\} dt. \end{aligned} \quad (\text{B.71})$$

Denote $x(t_n)$ and $x(t_{n+1})$ by x_n and x_{n+1} , respectively. Then from Eq. (B.71)

$$\begin{aligned} x_{n+1} &= x_n \exp\{-I_f(t_{n+1})\} \exp\{I_f(t_n)\} + \exp\{-I_f(t_{n+1})\} \int_{t_n}^{t_{n+1}} g(t) \exp\{I_f(t)\} dt \\ \text{i.e., } x_{n+1} &= x_n \exp[-\{I_f(t_{n+1}) - I_f(t_n)\}] + \int_{t_n}^{t_{n+1}} g(t) \exp[-\{I_f(t_{n+1}) - I_f(t)\}] dt. \end{aligned} \quad (\text{B.72})$$

Letting $t - t_n = \delta$ and $t_{n+1} - t_n = \Delta t_n$ in the interval $[t_n, t_{n+1}]$, Eq. (B.72) becomes

$$x_{n+1} = x_n \exp[-\{I_f(t_{n+1}) - I_f(t_n)\}] + \int_0^{\Delta t_n} g(\delta) \exp[-\{I_f(t_{n+1}) - I_f(\delta)\}] d\delta. \quad (\text{B.73})$$

We evaluate $I_f(t)$ using a straight-line approximation of $f(t)$ in the interval $t_n \leq t \leq t_{n+1}$ (Fig. B.3). Let $f_n = f(t_n)$ and $f_{n+1} = f(t_{n+1})$. The step size Δt_n may be adjusted based on the magnitude of the fractional increase in bubble radius calculated for the preceding integration step Δt_{n-1} .

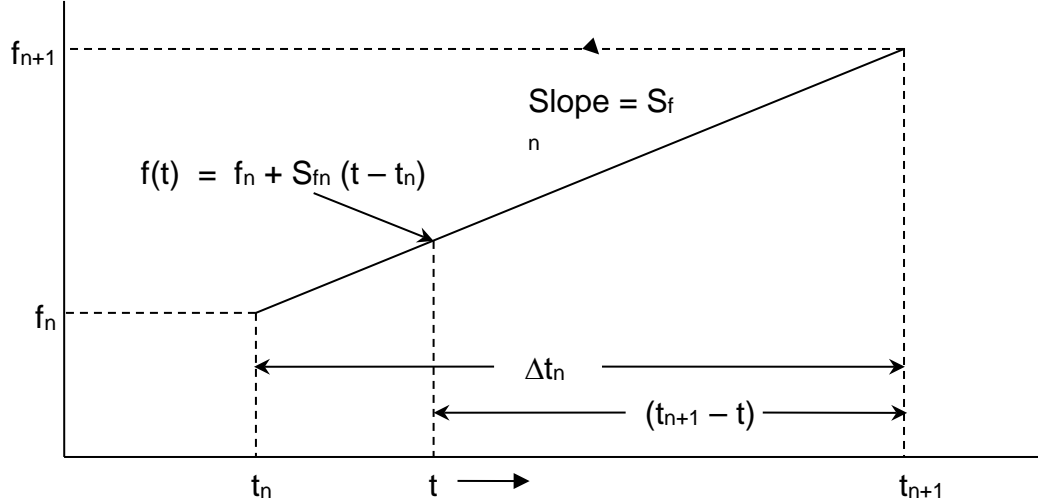


Fig. B.3: Straight-line approximation of $f(t)$ in the interval $t_n \leq t \leq t_{n+1}$.

Applying the trapezoidal rule of integration in the interval $[t_n, t_{n+1}]$,

$$I_f(t_{n+1}) - I_f(t_n) = \frac{f_n + f_{n+1}}{2} (t_{n+1} - t_n) = \frac{f_n + f_{n+1}}{2} \Delta t_n = \frac{\Delta t_n}{\theta_n} \quad (\text{B.74})$$

where $\theta_n = \frac{2}{f_n + f_{n+1}}$ is the “time constant” for the n^{th} integration step. For the interval $[t, t_{n+1}]$, we have

$$\begin{aligned} I_f(t_{n+1}) - I_f(t) &= \frac{f(t) + f_{n+1}}{2} (t_{n+1} - t) = \frac{f_n + S_{f_n}(t - t_n) + f_{n+1}}{2} (t_{n+1} - t) \\ &= \frac{f_n + f_{n+1} + S_{f_n}(t - t_n)}{2} [(t_{n+1} - t_n) - (t - t_n)] \end{aligned}$$

where $S_{f_n} = \frac{f_{n+1} - f_n}{\Delta t_n}$ is the slope of $f(t)$ in the interval $[t_n, t_{n+1}]$. In terms of δ , the above equation reads

$$I_f(t_{n+1}) - I_f(\delta) = \left[\frac{f_n + f_{n+1}}{2} + \frac{S_{f_n} \delta}{2} \right] (\Delta t_n - \delta) = \frac{\Delta t_n - \delta}{\theta_n} + \frac{S_{f_n} \delta}{2} (\Delta t_n - \delta) \quad (\text{B.75})$$

The function $g(t)$ is approximated in a similar fashion by a straight line in the interval $[t_n, t_{n+1}]$:

$$g(\delta) = g_n + S_{g_n} \delta, \quad 0 \leq \delta \leq \Delta t_n, \quad \delta = t - t_n, \quad (\text{B.76})$$

where $g_n = g(t_n)$ and $S_{g_n} = \frac{g_{n+1} - g_n}{\Delta t_n}$ is the slope of $g(t)$ in the interval $[t_n, t_{n+1}]$.

Substituting Eqs. (B.74), (B.75), and (B.76) into Eq. (B.73) yields

$$x_{n+1} = x_n \exp\left(-\frac{\Delta t_n}{\theta_n}\right) + I_{\phi_n}, \quad (\text{B.77})$$

where I_{ϕ_n} is the contribution to the solution due to $g(t)$ in Eq. (B.3). It is the particular integral given by

$$I_{\phi_n} = \int_0^{\Delta t_n} [g_n + S_{g_n} \delta] \exp\left[-\left\{\frac{\Delta t_n - \delta}{\theta_n} + \frac{S_{f_n} \delta}{2}(\Delta t_n - \delta)\right\}\right] d\delta. \quad (\text{B.78})$$

A closed-form expression for I_{ϕ_n} is not possible because of the δ^2 term contained in the exponent of the exponential factor. We could evaluate the integral using the trapezoidal rule of integration, but a more accurate evaluation is obtained by expanding the exponential factor in series form and truncating the series to a few terms. The truncated series will be valid only if the magnitude of the exponent is less than unity. Here the magnitude is

$$\begin{aligned} \left| \frac{\Delta t_n - \delta}{\theta_n} + \frac{S_{f_n} \delta}{2}(\Delta t_n - \delta) \right| &= (\Delta t_n - \delta) \left| \frac{1}{\theta_n} + \frac{S_{f_n} \delta}{2} \right| && \text{because } (\Delta t_n - \delta) \geq 0 \\ &= (\Delta t_n - \delta) \left| \frac{f_n + f_{n+1}}{2} + \frac{f_{n+1} - f_n}{2\Delta t_n} \delta \right| && \text{substituting for } \theta_n \text{ and } S_{f_n} \\ &\leq (\Delta t_n - \delta) \left| \frac{f_n + f_{n+1}}{2} + \frac{f_{n+1} - f_n}{2} \right| && \text{because } \delta \leq \Delta t_n \\ &\leq (\Delta t_n - \delta) |f_{n+1}|, \end{aligned}$$

which may not be less than unity, even with very small values of step size Δt_n . Therefore, we split the exponential factor into two factors and express I_{ϕ_n} as

$$I_{\phi_n} = \int_0^{\Delta t_n} [g_n + S_{g_n} \delta] \exp\left[-\frac{\Delta t_n - \delta}{\theta_n}\right] \exp\left[-\frac{S_{f_n} \delta}{2}(\Delta t_n - \delta)\right] d\delta. \quad (\text{B.79})$$

Now, the exponent of the second (right most) exponential factor in Eq. (B.79) has a magnitude

$$\begin{aligned} \left| \frac{S_{f_n} \delta}{2}(\Delta t_n - \delta) \right| &= (\Delta t_n - \delta) \left| \frac{f_{n+1} - f_n}{2\Delta t_n} \delta \right| && \text{substituting for } \theta_n \text{ and } S_{f_n} \\ &\leq \frac{\Delta t_n |f_{n+1} - f_n|}{2} && \text{because } \delta \leq \Delta t_n. \end{aligned}$$

Thus, the magnitude is no greater than the product of the step size Δt_n at the n^{th} integration step and the change in f_n therein, a magnitude that is consequently less than unity for sufficiently small values of the step size. Depending on the choice of step size, Eq. (B.79) may thus be evaluated to appropriate accuracy with a truncated series expansion of the second exponential factor.

We proceed by rewriting Eq. (B.79) with a series expansion of the second exponential factor truncated to include terms only through order 2:

$$\begin{aligned} I_{\phi_n} &= \int_0^{\Delta t_n} \exp\left[-\frac{\Delta t_n - \delta}{\theta_n}\right] [g_n + S_{g_n} \delta] \exp\left[-\frac{S_{f_n} \delta}{2}(\Delta t_n - \delta)\right] d\delta \\ &= \exp\left[-\frac{\Delta t_n}{\theta_n}\right] \int_0^{\Delta t_n} \exp\left[\frac{\delta}{\theta_n}\right] [g_n + S_{g_n} \delta] \left[1 - \frac{S_{f_n} \delta}{2}(\Delta t_n - \delta) + \frac{(S_{f_n} \delta)^2}{8}(\Delta t_n - \delta)^2\right] d\delta \\ &= \exp\left[-\frac{\Delta t_n}{\theta_n}\right] \int_0^{\Delta t_n} \exp\left[\frac{\delta}{\theta_n}\right] \left[\begin{aligned} &g_n + S_{g_n} \delta - \frac{g_n (S_{f_n} \delta)}{2}(\Delta t_n - \delta) - \frac{(S_{g_n} \delta)(S_{f_n} \delta)}{2}(\Delta t_n - \delta) \\ &+ \frac{g_n (S_{f_n} \delta)^2}{8}(\Delta t_n - \delta)^2 + \frac{(S_{g_n} \delta)(S_{f_n} \delta)^2}{8}(\Delta t_n - \delta)^2 \end{aligned} \right] d\delta \quad (\text{B.80}) \end{aligned}$$

The terms shown in brackets on the right side of Eq. (B.80) contain terms up to order 5 in δ . Since $\delta \leq t - t_n \leq t_{n+1} - t_n \leq \Delta t_n$, and the integration step size Δt_n may be chosen as small as desired, we neglect terms of order greater than 2 in δ , and simplify the integral expression for I_{ϕ_n} as follows:

$$I_{\phi_n} = \exp\left(-\frac{\Delta t_n}{\theta_n}\right) \int_0^{\Delta t_n} \exp\left(\frac{\delta}{\theta_n}\right) \left[g_n + \left(S_{g_n} - \frac{g_n S_{f_n} \Delta t_n}{2} \right) \delta + \left(\frac{g_n S_{f_n}}{2} - \frac{S_{g_n} S_{f_n} \Delta t_n}{2} + \frac{g_n S_{f_n}^2 \Delta t_n^2}{8} \right) \delta^2 \right] d\delta$$

$$= g_n I_{\phi 0_n} + \left(S_{g_n} - \frac{g_n S_{f_n} \Delta t_n}{2} \right) I_{\phi 1_n} + \left(\frac{g_n S_{f_n}}{2} - \frac{S_{g_n} S_{f_n} \Delta t_n}{2} + \frac{g_n S_{f_n}^2 \Delta t_n^2}{8} \right) I_{\phi 2_n} \quad (\text{B.81})$$

where

$$\begin{aligned} I_{\phi 0_n} &= \exp\left(-\frac{\Delta t_n}{\theta_n}\right) \int_0^{\Delta t_n} \exp\left(\frac{\delta}{\theta_n}\right) d\delta = \exp\left(-\frac{\Delta t_n}{\theta_n}\right) \left[\theta_n \exp\left(\frac{\delta}{\theta_n}\right) \right]_0^{\Delta t_n} = \theta_n \left[1 - \exp\left(-\frac{\Delta t_n}{\theta_n}\right) \right], \\ I_{\phi 1_n} &= \exp\left(-\frac{\Delta t_n}{\theta_n}\right) \int_0^{\Delta t_n} \delta \exp\left(\frac{\delta}{\theta_n}\right) d\delta = \exp\left(-\frac{\Delta t_n}{\theta_n}\right) \left[(\theta_n \delta - \theta_n^2) \exp\left(\frac{\delta}{\theta_n}\right) \right]_0^{\Delta t_n} \\ &= \exp\left(-\frac{\Delta t_n}{\theta_n}\right) \left[(\theta_n \Delta t_n - \theta_n^2) \exp\left(\frac{\Delta t_n}{\theta_n}\right) + \theta_n^2 \right] \\ &= (\theta_n \Delta t_n - \theta_n^2) + \theta_n^2 \exp\left(-\frac{\Delta t_n}{\theta_n}\right) \\ &= \theta_n^2 \left[\frac{\Delta t_n}{\theta_n} - \left\{ 1 - \exp\left(-\frac{\Delta t_n}{\theta_n}\right) \right\} \right], \end{aligned}$$

and

$$\begin{aligned} I_{\phi 2_n} &= \exp\left(-\frac{\Delta t_n}{\theta_n}\right) \int_0^{\Delta t_n} \delta^2 \exp\left(\frac{\delta}{\theta_n}\right) d\delta = \exp\left(-\frac{\Delta t_n}{\theta_n}\right) \left[(\theta_n \delta^2 - 2\theta_n^2 \delta + 2\theta_n^3) \exp\left(\frac{\delta}{\theta_n}\right) \right]_0^{\Delta t_n} \\ &= \exp\left(-\frac{\Delta t_n}{\theta_n}\right) \left[(\theta_n \Delta t_n^2 - 2\theta_n^2 \Delta t_n + 2\theta_n^3) \exp\left(\frac{\Delta t_n}{\theta_n}\right) - 2\theta_n^3 \right] \\ &= (\theta_n \Delta t_n^2 - 2\theta_n^2 \Delta t_n + 2\theta_n^3) - 2\theta_n^3 \exp\left(-\frac{\Delta t_n}{\theta_n}\right) \\ &= \theta_n^3 \left[\left(\frac{\Delta t_n}{\theta_n}\right)^2 - 2\left(\frac{\Delta t_n}{\theta_n}\right) + 2\left\{ 1 - \exp\left(-\frac{\Delta t_n}{\theta_n}\right) \right\} \right]. \end{aligned}$$

Substituting for $I_{\phi 0_n}$, $I_{\phi 1_n}$, and $I_{\phi 2_n}$ in Eq. (B.81), we obtain

$$\begin{aligned}
I_{\phi_n} = & g_n \theta_n \left\{ 1 - \exp\left(-\frac{\Delta t_n}{\theta_n}\right) \right\} + \left(S_{g_n} - \frac{g_n S_{f_n} \Delta t_n}{2} \right) \theta_n^2 \left[\frac{\Delta t_n}{\theta_n} - \left\{ 1 - \exp\left(-\frac{\Delta t_n}{\theta_n}\right) \right\} \right] \\
& + \left(\frac{g_n S_{f_n}}{2} - \frac{S_{g_n} S_{f_n} \Delta t_n}{2} + \frac{g_n S_{f_n}^2 \Delta t_n^2}{8} \right) \theta_n^3 \left[\left(\frac{\Delta t_n}{\theta_n} \right)^2 - 2 \left(\frac{\Delta t_n}{\theta_n} \right) + 2 \left\{ 1 - \exp\left(-\frac{\Delta t_n}{\theta_n}\right) \right\} \right]
\end{aligned} \tag{B.82}$$

Returning to Eq. (B.77), we can calculate x_{n+1} at the n^{th} integration step knowing x_n from the previous step and the solution for I_{ϕ_n} in Eq. (B.82). However, the solution for I_{ϕ_n} requires f_{n+1} and g_{n+1} (and thus the unknown r_{n+1}) to determine the slopes S_{f_n} and S_{g_n} . This poses no problem if the functions $f(t)$ and $g(t)$ are known functions of time. In our application, $f(t)$ and $g(t)$ are implicit functions of time related through bubble radius, as indicated by Eqs. (B.1) and (B.2). We solve for bubble radius and bubble pressure simultaneously by applying Eq. (B.77) as well as the constitutive equation for bubble pressure (Young-LaPlace relationship), as indicated by Eqs. (B.12) and (B.14).

The expression for I_{ϕ_n} also contains f_{n+1} in the exponential factors. Without further simplification, the expression becomes a nonlinear equation in r_{n+1} , or equivalently in the change in bubble radius δr_n , which requires an iterative solution at each integration step — a significant increase in computational overhead. In order to reduce the computations, the expression for I_{ϕ_n} in Eq. (B.82) is simplified by first expanding the exponential factors in series form and retaining only terms up to third order:

$$\begin{aligned}
\left\{ 1 - \exp\left(-\frac{\Delta t_n}{\theta_n}\right) \right\} &= 1 - \left[1 - \frac{\Delta t_n}{\theta_n} + \frac{1}{2} \left(\frac{\Delta t_n}{\theta_n} \right)^2 - \frac{1}{6} \left(\frac{\Delta t_n}{\theta_n} \right)^3 + \dots \right] \\
&\cong \frac{\Delta t_n}{\theta_n} - \frac{1}{2} \left(\frac{\Delta t_n}{\theta_n} \right)^2 + \frac{1}{6} \left(\frac{\Delta t_n}{\theta_n} \right)^3 .
\end{aligned} \tag{B.83}$$

With appropriate substitution of Eq. (B.83), Eq. (B.82) becomes

$$\begin{aligned}
I_{\phi_n} &= g_n \theta_n \left\{ \frac{\Delta t_n}{\theta_n} - \frac{1}{2} \left(\frac{\Delta t_n}{\theta_n} \right)^2 + \frac{1}{6} \left(\frac{\Delta t_n}{\theta_n} \right)^3 \right\} \\
&\quad + \left(S_{g_n} - \frac{g_n S_{f_n} \Delta t_n}{2} \right) \theta_n^2 \left[\frac{\Delta t_n}{\theta_n} - \left\{ \frac{\Delta t_n}{\theta_n} - \frac{1}{2} \left(\frac{\Delta t_n}{\theta_n} \right)^2 + \frac{1}{6} \left(\frac{\Delta t_n}{\theta_n} \right)^3 \right\} \right] \\
&\quad + \left(\frac{g_n S_{f_n}}{2} - \frac{S_{g_n} S_{f_n} \Delta t_n}{2} + \frac{g_n S_{f_n}^2 \Delta t_n^2}{8} \right) \theta_n^3 \left[\left(\frac{\Delta t_n}{\theta_n} \right)^2 - 2 \left(\frac{\Delta t_n}{\theta_n} \right) + 2 \left\{ \frac{\Delta t_n}{\theta_n} - \frac{1}{2} \left(\frac{\Delta t_n}{\theta_n} \right)^2 + \frac{1}{6} \left(\frac{\Delta t_n}{\theta_n} \right)^3 \right\} \right] \\
&= g_n \left(\Delta t_n - \frac{\Delta t_n^2}{2\theta_n} + \frac{\Delta t_n^3}{6\theta_n^2} \right) + \left(S_{g_n} - \frac{g_n S_{f_n} \Delta t_n}{2} \right) \left(\frac{\Delta t_n^2}{2} - \frac{\Delta t_n^3}{6\theta_n} \right) \\
&\quad + \left(\frac{g_n S_{f_n}}{2} - \frac{S_{g_n} S_{f_n} \Delta t_n}{2} + \frac{g_n S_{f_n}^2 \Delta t_n^2}{8} \right) \frac{\Delta t_n^3}{3} . \tag{B.84}
\end{aligned}$$

We now substitute $s_{g_n} = \frac{g_{n+1} - g_n}{\Delta t_n}$ and $s_{f_n} = \frac{f_{n+1} - f_n}{\Delta t_n}$ in Eq. (B.84), cancel out Δt_n in the numerator and the denominator of various terms, and retain only terms up to order 2 in Δt_n to obtain

$$\begin{aligned}
I_{\phi_n} &= g_n \left(\Delta t_n - \frac{\Delta t_n^2}{2\theta_n} + \frac{\Delta t_n^3}{6\theta_n^2} \right) + \left(S_{g_n} - \frac{g_n S_{f_n} \Delta t_n}{2} \right) \left(\frac{\Delta t_n^2}{2} - \frac{\Delta t_n^3}{6\theta_n} \right) \\
&\quad + \left(\frac{g_n S_{f_n}}{2} - \frac{S_{g_n} S_{f_n} \Delta t_n}{2} + \frac{g_n S_{f_n}^2 \Delta t_n^2}{8} \right) \frac{\Delta t_n^3}{3} \\
&= g_n \left(\Delta t_n - \frac{\Delta t_n^2}{2\theta_n} \right) + (g_{n+1} - g_n) \left(\frac{\Delta t_n}{2} - \frac{\Delta t_n^2}{6\theta_n} \right) - \frac{g_n (f_{n+1} - f_n)}{2} \left(\frac{\Delta t_n^2}{2} \right) \\
&\quad + \frac{g_n (f_{n+1} - f_n)}{2} \left(\frac{\Delta t_n^2}{3} \right) - \frac{(g_{n+1} - g_n)(f_{n+1} - f_n)}{2} \left(\frac{\Delta t_n^2}{3} \right) \\
&= [2g_n + (g_{n+1} - g_n)] \frac{\Delta t_n}{2} - \left[\frac{g_n}{2} + \frac{g_{n+1} - g_n}{6} \right] \left(\frac{\Delta t_n^2}{\theta_n} \right) - \left[\frac{g_n}{2} - \frac{g_n}{3} + \frac{g_{n+1} - g_n}{3} \right] \frac{(f_{n+1} - f_n)}{2} \Delta t_n^2 \\
&= (g_n + g_{n+1}) \frac{\Delta t_n}{2} - \frac{2g_n + g_{n+1}}{6} \frac{f_n + f_{n+1}}{2} \Delta t_n^2 - \frac{2g_{n+1} - g_n}{6} \frac{(f_{n+1} - f_n)}{2} \Delta t_n^2
\end{aligned}$$

Substituting $\theta_n = \frac{2}{f_n + f_{n+1}}$,

$$\begin{aligned}
I_{\phi_n} &= (g_n + g_{n+1}) \frac{\Delta t_n}{2} - \frac{2g_n + g_{n+1}}{6} \frac{f_n + f_{n+1}}{2} \Delta t_n^2 - \frac{2g_{n+1} - g_n}{6} \frac{(f_{n+1} - f_n)}{2} \Delta t_n^2 \\
&= (g_n + g_{n+1}) \frac{\Delta t_n}{2} - [(2g_n + g_{n+1})(f_n + f_{n+1}) + (2g_{n+1} - g_n)(f_{n+1} - f_n)] \frac{\Delta t_n^2}{12} \\
&= (g_n + g_{n+1}) \frac{\Delta t_n}{2} - [3(g_n f_n + g_{n+1} f_{n+1}) + (g_n f_{n+1} - g_{n+1} f_n)] \frac{\Delta t_n^2}{12} \tag{B.85}
\end{aligned}$$

Eq. (B.85) is a second-order approximation to I_{ϕ_n} . Note that this does not compromise accuracy as we already limited I_{ϕ_n} to terms containing powers of Δt_n less than 3 to obtain Eq. (B.81). It is not necessary to include higher power terms in Δt_n as accuracy may be improved to any desired level by sufficiently decreasing the step size.

Returning to the solution Eq. (B.77), we expand the exponential factor retaining only terms up to order 2 in Δt_n so that

$$x_{n+1} = x_n \exp\left(-\frac{\Delta t_n}{\theta_n}\right) + I_{\phi_n} = x_n \left[1 - \frac{\Delta t_n}{\theta_n} + \frac{1}{2} \left(\frac{\Delta t_n}{\theta_n}\right)^2\right] + I_{\phi_n}. \tag{B.86}$$

Substituting for I_{ϕ_n} from Eq. (B.85) and $\theta_n = \frac{2}{f_n + f_{n+1}}$ into Eq. (B.86) yields

$$\begin{aligned}
x_{n+1} &= x_n - x_n (f_n + f_{n+1}) \frac{\Delta t_n}{2} + x_n (f_n + f_{n+1})^2 \frac{\Delta t_n^2}{8} \\
&\quad + (g_n + g_{n+1}) \frac{\Delta t_n}{2} - [3(g_n f_n + g_{n+1} f_{n+1}) + (g_n f_{n+1} - g_{n+1} f_n)] \frac{\Delta t_n^2}{12} \tag{B.87}
\end{aligned}$$

Equation (B.87) simplifies to our final expression for x_{n+1} :

$$\begin{aligned}
x_{n+1} &= x_n + [(g_n + g_{n+1}) - (f_n + f_{n+1})x_n] \frac{\Delta t_n}{2} + [(f_n + f_{n+1})^2 x_n] \frac{\Delta t_n^2}{8} \\
&\quad - [3(g_n f_n + g_{n+1} f_{n+1}) + (g_n f_{n+1} - g_{n+1} f_n)] \frac{\Delta t_n^2}{12} \tag{B.88}
\end{aligned}$$

10. Appendix C. Summary of Recursive Equations for Solution of 3RUT-MBe1 Model

Subscripts:

Compartments: $i = 1, 2, \dots, n_c$ (suppressed)

Bubble size group: $m = 1, 2, \dots, N_{bs}$ (suppressed)

Diffusible gases: $k = 1, 2, \dots, N_g$

Time intervals: $n = 1, 2, \dots$

Number of bubble size groups: $N_{bs} = 1$

Scaled model parameters:

$$\begin{aligned} \hat{r} &= \Lambda r & \hat{K}_k &= 3\Lambda^2 K_k & \hat{\sigma} &= \Lambda \sigma & \hat{M} &= \left(\frac{4\pi}{3}\right) \frac{M}{\Lambda^3} \\ \hat{r}_{\min}^o &= \Lambda r_{\min}^o & \hat{r}_{\min_n} &= \Lambda r_{\min_n} & \hat{\sigma}_c &= \Lambda \sigma_c \\ \hat{\beta}^o &= \Lambda \beta^o & \hat{\beta}_{f_n} &= \Lambda \beta_{f_n} \\ \hat{V}_t &= \Lambda^3 V_t \end{aligned}$$

$$P_\infty = P_{H_2O} + P_{tCO_2} \quad (C.1)$$

$$t_{n+1} = t_n + \Delta t_n \quad (C.2)^a$$

Bubble Number

$$\beta_{ex_n} = 1 + m_{\beta_{ex}} I_{ex_n} \quad (C.3)$$

$$P_{crush_n} = \text{MAX} \left[P_{crush_{n-1}}, (P_{amb_n} - P_\infty) - \sum_{k=1}^{N_g} P_{t_{k,n}} \right] \quad (C.4)^b$$

^a The integration step size Δt_n is arbitrary and may be altered at any integration step, based on the magnitude of changes in bubble radii, δr_n , to reduce computation time, but it should be small enough to yield results with desired accuracy.

^b The initial $P_{crush_0} \equiv P_{crush}^o$ is determined from saturation conditions at profile start (see footnotes c and e in this Appendix).

$$\text{If } P_{\text{crush}_n} \leq P_{\text{crush}_{n-1}}, P_{\text{crush}_n} = P_{\text{crush}}^0 + (P_{\text{crush}_{n-1}} - P_{\text{crush}}^0) \cdot \exp(-\Delta t_n / \tau_{Pc}) \quad (\text{C.5})$$

$$\hat{\beta}_{f_n} = \beta_{\text{ex}_n} \left[\frac{2\hat{\sigma}_c \hat{\beta}^0}{2(\hat{\sigma}_c - \hat{\sigma}) + P_{\text{crush}_n} \hat{r}_{\text{min}}^0} \right]; \quad \hat{r}_{\text{min}}^0 = \hat{\beta}^0 \left[\ln(N_b^0) - \ln(N_b^{\text{min}}) \right] \quad (\text{C.6})$$

$$P_{\text{ss}_n} = \left[\sum_{k=1}^{N_g} p_{t_{k,n}} + P_{\infty} \right] - P_{\text{amb}_n} \quad (\text{C.7})$$

$$N_{b_{\text{max},n}} = \text{MAX} \left[N_{b_{\text{max},n-1}}, N_b^0 \exp \left(-\frac{2\hat{\sigma}}{P_{\text{ss}_n} \cdot \hat{\beta}_{f_n}} \right) \right] \quad (\text{C.8})$$

$$\Delta n_{b_n} = (N_{b_{\text{max},n}} - N_{b_{\text{max},n-1}})$$

$$n_{b_n} = n_{b_{n-1}} + \Delta n_{b_n} \quad (\text{C.9})$$

$$\hat{r}_{\text{min}_n} = \hat{\beta}_{f_n} \left[\ln(N_b^0) - \ln(N_b^{\text{min}}) \right] \quad (\text{C.10})$$

$$\hat{x}_{k,n}^0 = P_{b_{k,n}} \hat{r}_{\text{min}_n}^3 \quad (\text{C.11})$$

Bubble Radius and Pressure

$$b_{k,n} = \bar{K}_k \frac{\Delta t_n}{\hat{r}_n^2} \quad (\text{C.12})$$

$$a_{k,n} = (1 + \hat{r}_n) b_{k,n} \quad (\text{C.13})$$

$$A_{k,n} = P_{b_{k,n}} + a_{k,n} \left(1 - \frac{a_{k,n}}{2} \right) (p_{t_{k,n}} - P_{b_{k,n}}) \quad (\text{C.14})$$

$$B_{k,n} = \frac{1}{2} \left[(2a_{k,n} - b_{k,n} + a_{k,n} b_{k,n}) p_{t_{k,n}} + (a_{k,n} + b_{k,n}) (1 - a_{k,n}) P_{b_n} \right] \quad (\text{C.15})$$

$$\delta \hat{r}_n = \frac{\sum_{k=1}^{N_g} A_{k,n} - \left(P'_{\text{amb}_{n+1}} + \frac{2\hat{\sigma}}{\hat{r}_n} + \bar{M} \hat{r}_n^3 \right)}{\sum_{k=1}^{N_g} (3A_{k,n} - B_{k,n}) - \left(\frac{2\hat{\sigma}}{\hat{r}_n} - 3\bar{M} \hat{r}_n^3 \right)}; \quad P'_{\text{amb}} = P_{\text{amb}} - P_{\infty} \quad (\text{C.16})$$

$$\hat{r}_{n+1} = \hat{r}_n (1 + \delta \hat{r}_n) \quad (\text{C.17})$$

$$P_{b_{k,n+1}} = A_{k,n} - (3A_{k,n} - B_{k,n}) \delta \hat{r}_n \quad (\text{C.18})$$

Tissue Gas Tensions

$$\dot{V}_{O_2,n} = m_{V_{O_2}} \cdot I_{ex_n} + \dot{V}_{O_2,rest} \quad (\text{C.19})$$

$$\dot{Q}_{ex_n} = m_Q \cdot (\dot{V}_{O_2,n} - \dot{V}_{O_2,rest}) + \dot{Q}_{rest} \quad (\text{C.21})$$

Inert Gases

$$\tau_{k_n} = \frac{\alpha_{t_k}}{\alpha_{b_k} \dot{Q}_n} \quad (\text{C.23})$$

$$\varepsilon_{k,n} = 1 - \exp\left(-\frac{\Delta t_n}{\tau_{k_n}}\right) \quad (\text{C.24})$$

$$\hat{G}_{k_n} = \left(\frac{4\pi}{3}\right) \frac{n_{b_n}}{\alpha_{t_k} \hat{V}_t} = \hat{G}_{k_{n-1}} \left(\frac{n_{b_n}}{n_{b_{n-1}}}\right) \quad (\text{C.25})$$

$$\Delta \hat{G}_{k_n} = \left(\frac{4\pi}{3}\right) \frac{\Delta n_{b_n}}{\alpha_{t_k} \hat{V}_t} \quad (\text{C.26})$$

$$\hat{x}_{k,n+1} = P_{b_{k,n+1}} \hat{r}_{n+1}^3 \quad (\text{C.27})$$

$$p_{a_{k,n+1}} = p_{a_k} @t_{n+1} = F_{I_{k,n+1}} \left[\left(P_{amb_{n+1}} - P_{A_{H_2O}} \right) - P_{A_{CO_2}} \left(1 - \frac{1}{RQ} \right) \right] \quad (\text{C.28})$$

$$v_{k,n} = \frac{p_{a_{k,n+1}} - p_{a_{k,n}}}{\Delta t_n} \quad (\text{C.29})$$

$$p_{t_{k,n+1}} = p_{t_{k,n}} (1 - \varepsilon_{k,n}) + v_{k,n} \Delta t_n + \left[p_{a_{k,n}} - \tau_k \left\{ v_{k,n} + \hat{G}_{k_n} \frac{\hat{x}_{k,n+1} - \hat{x}_{k,n}}{\Delta t_n} \right\} \right] \varepsilon_{k,n} - \Delta \hat{G}_{k_n} (\hat{x}_{k,n} - \hat{x}_{k,n}^o) \quad (\text{C.30})^c$$

Oxygen

$$\alpha'_{O_{2n}} = \alpha_{b_{O_2}} + H_{bc} \left[\frac{a_1 + 2a_2 p - a_2 (a_1 - b_1) p^2}{(1.0 + b_1 p + b_2 p^2)^2} \right] \left[\frac{\eta p^{\eta-1}}{P_{half}} \right]; \quad p = \left(\frac{p_{\bar{v}_{O_{2n}}}}{P_{half}} \right)^\eta \quad (\text{C.31})$$

$$\tau_{O_{2n}} = \frac{\alpha_{t_{O_2}}}{\dot{Q}_n \alpha'_{O_{2n}}} \quad (\text{C.32})$$

$$\varepsilon_{O_{2n}} = 1 - \exp\left(-\frac{\Delta t_n}{\tau_{O_{2n}}}\right) \quad (\text{C.33})$$

$$\hat{G}_{O_{2n}} = \left(\frac{4\pi}{3} \right) \frac{n_{b_n}}{\alpha_{t_{O_2}} \hat{V}_t} = \hat{G}_{O_{2n-1}} \left(\frac{n_{b_n}}{n_{b_{n-1}}} \right) \quad (\text{C.34})$$

$$\Delta \hat{G}_{O_{2n}} = \left(\frac{4\pi}{3} \right) \frac{\Delta n_{b_n}}{\alpha_{t_{O_2}} \hat{V}_t} \quad (\text{C.35})$$

$$\hat{x}_{O_{2n+1}} = P_{b_{O_{2n+1}}} \hat{f}_{n+1}^3 \quad (\text{C.36})$$

$$p_{a_{O_{2n+1}}} = p_{a_{O_2}} @ t_{n+1} = P_{amb_{n+1}} - P_{H_2O} - P_{ACO_2} - \sum p_{a_{k,n+1}} \quad (\text{C.37})$$

^c The initial tissue tension of the k^{th} inert gas under saturation steady-state conditions, $p_{t_{k,0}}$, is the arterial tension, $p_{a_{k,0}}$, for the gas given by Eq. (C.28) for the saturation pressure and breathing gas mix.

$$C_{a_{O_2,n}} = \alpha_{b_{O_2}} p_{a_{O_2,n}} + Hb_c S_{O_2} (@ P_{O_2} = p_{a_{O_2,n}}) \quad (C.38)^d$$

$$C_{a_{O_2,n+1}} = \alpha_{b_{O_2}} p_{a_{O_2,n+1}} + Hb_c S_{O_2} (@ P_{O_2} = p_{a_{O_2,n+1}}) \quad (C.39)^c$$

$$\dot{p}_{O_2,n} = \frac{C_{a_{O_2,n}}}{\alpha'_{O_2,n}} ; \quad \dot{p}_{O_2,n+1} = \frac{C_{a_{O_2,n+1}}}{\alpha'_{O_2,n}} \quad (C.40)$$

$$v_{O_2,n} = \frac{\dot{p}_{O_2,n+1} - \dot{p}_{O_2,n}}{\Delta t_n} \quad (C.41)$$

$$C_{\bar{v}_{O_2,n}} = \alpha_{b_{O_2}} p_{\bar{v}_{O_2,n}} + Hb_c S_{O_2} (@ P_{O_2} = p_{\bar{v}_{O_2,n}}) \quad (C.42)$$

$$\dot{p}_n = \frac{\dot{V}_{O_2,n} + \dot{Q}_n (C_{\bar{v}_{O_2,n}} - \alpha'_{O_2,n} p_{\bar{v}_{O_2,n}})}{\alpha_{t_{O_2}}} \quad (C.43)$$

^d The percent hemoglobin saturation, S_{O_2} , at prevailing oxygen tension p_{O_2} is computed with Lobdell's equation:⁶⁹

$$S_{O_2} = \frac{a_1 p + a_2 p^2}{1.0 + b_1 p + b_2 p^2} ; \quad p = \left(\frac{p_{O_2}}{p_{half}} \right)^\eta ,$$

where

$$a_1 = 0.34332,$$

$$a_2 = 0.64073,$$

$$b_1 = 0.34128,$$

$$b_2 = a_2 = 0.64073,$$

$$\eta = 1.58678, \text{ and}$$

$$p_{half} = \text{half-saturation } p_{O_2} \text{ of hemoglobin}$$

(with p_{O_2} in units of mm-Hg, $p_{half} = 25.0$ mm-Hg.)

$$\begin{aligned}
p_{t_{O_2n+1}} &= p_{t_{O_2n}} (1 - \varepsilon_{O_2n}) + v_{O_2n} \Delta t_n \\
&+ \left[\dot{p}_{O_2n} - \tau_{O_2n} \left\{ v_{O_2n} + \dot{p}_n + \hat{G}_{O_2n} \frac{(\hat{x}_{O_2n+1} - \hat{x}_{O_2n})}{\Delta t_n} \right\} \right] \varepsilon_{O_2n} \\
&- \Delta \hat{G}_{O_2n} (\hat{x}_{O_2n} - \hat{x}_{O_2n,0})
\end{aligned} \tag{C.44}^e$$

VGE formation

$$LR = (V_b - V_{r0}) \dot{N}_{VGE} \Delta t_n, \tag{C.45}$$

$$n_{b_{n+1}} = \text{MAX} [0, N_{b_n} (1 - LR)], \tag{C.46}$$

^e The initial tissue O₂ tension under saturation steady-state conditions, $p_{t_{O_20}}$, is the partial pressure, $p_{\bar{v}_{O_20}}$, corresponding to $C_{\bar{v}_{O_20}} = C_{a_{O_20}} - \frac{\dot{V}_{O_20}}{Q_0}$, where $C_{a_{O_20}}$ is given by Eq. (C.38) at $p_{a_{O_2}}$ given by Eq. (C.37) for the saturation pressure and breathing gas mix. $p_{\bar{v}_{O_20}}$ is determined by numerically inverting the blood O₂ content versus partial pressure curve, Eq. (C.42), at $C_{\bar{v}_{O_20}}$.

11. Appendix D. Hazard Function Formulation and Optimization

The hazard function in present work was elaborated from that in the BVM(3) probabilistic gas and bubble dynamics model developed earlier for air and N₂-O₂ diving.^{26,27} In the latter model, the instantaneous risk of DCS at time t in exposure i , $h_i(t)$, is the sum of a weighted time-dependent dose, $\Delta_{i,j}(t)$, in each of $j = 1, 2, \dots, n_c$ hypothetical tissue compartments. That is,

$$h_i(t) = \sum_{j=1}^{n_c} w_j \Delta_{i,j}(t), \quad (\text{D.1})$$

where w_j is the weight – constant over all i and independent of time and all parameters in $\Delta_{i,j}(t)$ – associated with the j^{th} compartment, and

$$\Delta_{i,j}(t) = [V_{i,j}(t) - V_j(0)] . \quad (\text{D.2})$$

$V_{i,j}(t)$ in Eq. (D.2) is the bubble volume in the j^{th} compartment at time t in the i^{th} exposure, and $V_j(0)$ is the initial nucleonic bubble volume in the compartment. The initial nucleonic bubble volume in each compartment is constant and the same for all exposures. Because the hazard, $h_i(t)$, is a failure rate that must integrate over time to a dimensionless quantity, w_j in Eq. (D.1) has dimensions of 1/(volume \times time).

While an implementation of the Van Liew and Hlastala two-region unstirred tissue model^{28,31,70} was used to model bubble evolution in the BVM(3) probabilistic model, the more theoretically robust 3RUT-MB model was used for this purpose in present work. Eq. (D.2) was elaborated using Eq. (A.12) to obtain the hazard function used in present work:

$$h(t) = \sum_j^{n_c} w_j (V_{b,j} - V_{r0_j}) \cdot (N_{b,j})^{\beta_{N,j}}, \quad (\text{D.3a})$$

where $m=1$ has been assumed, the time-dependence of the compartmental bubble number is explicitly indicated, and a compartment-specific power term, $\beta_{N,j}$, for the prevailing bubble number has been arbitrarily added to potentiate the contribution of the bubble number to the hazard as the bubble number increases.

It is shown in Appendix A that the compartmental bubble volumes in the 3RUT-MB model scale with an arbitrary compartmental Λ_j^3 factor having dimension 1/volume. The scaled counterparts of the volumes in Eq. (D.3a), $\hat{V}_{i,j}(t) = \Lambda_j^3 V_{i,j}(t)$ and

$\hat{V}_j(0) = \Lambda_j^3 V_j(0)$, can then be calculated with the piecewise-analytic solution derived in Appendix B with arbitrarily specified values of Λ_j .

The best fit of a given expression for $h(t)$ to a collection of DCS incidence and time of onset data is obtained by adjusting the parameters of $h(t)$ to maximize the likelihood of $h(t)$ about the data. The likelihood is the joint probability of the observed outcomes for all exposures in the data. For N independent exposures, the likelihood is given by

$$L = \prod_{i=1}^N P(O_i)^{1-\delta_i} P(E_i)^{\delta_i}, \quad (D.4)$$

where δ_i is the outcome variable for the i^{th} exposure: $\delta_i = 1$ for failure (event occurred) and $\delta_i = 0$ for no failure until end of observation (right-censored observation). Marginal outcomes, for which $0 < \delta_i < 1$, are also allowed. Referring to Eqs. (1) and (2) in the body of this report, Eq. (D.4) is elaborated to yield

$$L = \prod_{i=1}^N \left[\left\{ \exp\left(-\int_0^{t_i} h_i(t) dt\right) \right\}^{(1-\delta_i)} \cdot \left\{ \exp\left(-\int_0^{t_{1i}} h_i(t) dt\right) \right\}^{\delta_i} \cdot \left\{ 1 - \exp\left(-\int_{t_{1i}}^{t_{2i}} h_i(t) dt\right) \right\}^{\delta_i} \right], \quad (D.5)$$

where t_{1i} is the last time in exposure i at which failure had not yet occurred, t_{2i} is the first time in exposure i at which failure was known to have occurred, and t_i is the right-censored time for exposure i . The likelihood is given in terms of the parameters in the model used to compute $\Delta_{i,j}(t)$, represented by vector ρ , and the weights w_j of the tissue compartments, represented by vector \mathbf{W} :

$$L \equiv L(\rho, \mathbf{W}). \quad (D.6a)$$

The vectors ρ and \mathbf{W} comprise the β vector in Eqs. (11) and (12) in the body of this report. It is now recognized that because the compartmental weights are constant and independent of the other model parameters, a set of optimum w_j , $j = 1, 2, \dots, n_c$, exists for a given data set for any set ρ of other compartmental parameter values.⁷¹ This optimal set \mathbf{W} can be determined independently for the trial set ρ in each iteration of the optimization procedure. In present work however, the likelihood was conventionally maximized with the Marquart iterative nonlinear parameter optimization algorithm⁴⁶ without making any distinction between the ρ and \mathbf{W} vectors.

12. Appendix E. Summary Description of A1309 Model Training Data

| Data Set | Profile Description Summary | # Exposures | # DCS Observed |
|------------------------|---|-------------|----------------|
| USAF | | | |
| (4.37 psia, Unknown A) | 60 min PB; 4.37 psia EVA sim/240 min;180 min GL PstB | 43 | 23 |
| (4.37 psia, Unknown B) | 15 min PB; 4.37 psia EVA sim/240 min;138 min GL PstB | 12 | 7 |
| (5.45 psia, Unknown) | 60 min PB; 5.45 psia (25K ft) EVA sim/240 min | 21 | 1 |
| (6 psia, Unknown) | 60 min PB; 6 psia (22.5K ft) EVA sim/240 min | 24 | 1 |
| (9.5 psia, Unknown) | 60 min PB; 9.5 psia (11.5K ft) EVA sim/240 min | 42 | 0 |
| 100% Suit-A | 0PB; 15.0K ft (8.3 psia) EVA sim/6hr, males | 10 | 0 |
| 100% Suit-B | 0PB; 16.5K ft (7.8 psia) EVA sim/6hr, males | 10 | 0 |
| 100% Suit-C | 0PB; 18.1K ft (7.3 psia) EVA sim/6hr, males | 11 | 0 |
| 100% Suit-D | 0PB; 18.1K ft (7.3 psia) EVA sim/6hr, females | 9 | 0 |
| 100% Suit-E | 0PB; 19.8K ft (6.8 psia) EVA sim/6hr, males | 11 | 0 |
| 100% Suit-F | 0PB; 19.8K ft (6.8 psia) EVA sim/6hr, females | 10 | 1 |
| 7.8 psia-A | 0PB; 7.8 psia, 50% O ₂ , EVA sim/360 min, males | 94 | 1 |
| 7.8 psia-B | 0PB; 7.8 psia, 50% O ₂ , EVA sim/360 min, females | 92 | 4 |
| 8.3 psia-A | 0PB; 8.3 psia, 50% O ₂ , EVA sim/360 min, males | 20 | 1 |
| 8.3 psia-B | 0PB; 8.3 psia, 50% O ₂ , EVA sim/360 min, females | 11 | 0 |
| 9.5 psia Validation-A | 0PB; 9.5 psia, 40% O ₂ , EVA sim/360 min, females | 20 | 0 |
| 9.5 psia Validation-B | 0PB; 9.5 psia, 40% O ₂ , EVA sim/360 min, males | 12 | 0 |
| BSI-A | Bends Screening Index study: 60 min PB; 30.0K ft (4.37 psia), rest/480 min | 17 | 10 |
| BSI-B | Bends Screening Index study: 60 min PB; 30.0K ft (4.37 psia), knee bends-overhead presses/480 min | 36 | 32 |
| BSI-C | Bends Screening Index study: 60 min PB; 27.6K ft (4.87 psia), knee bends-overhead presses/480 min | 83 | 66 |
| BSI-D | Bends Screening Index study: 60 min PB; 25.0K ft (5.45 psia), knee bends-overhead presses/480 min | 28 | 22 |
| BSI-E | Bends Screening Index study: 60 min PB; 22.5K ft (6.1 psia), knee bends-overhead presses/480 min | 46 | 24 |
| Bubb Threshold-A | 0PB; 16.0K ft (8.0 psia), 50% O ₂ , EVA sim/360 min | 25 | 0 |
| Bubb Threshold-B | 0PB; 14.4K ft (8.5 psia), 50% O ₂ , EVA sim/360 min | 10 | 0 |
| Bubb Threshold-C | 0PB; 12.3K ft (9.0 psia), 50% O ₂ , EVA sim/360 min | 23 | 3 |
| Bubb Threshold-D | 0PB; 11.5K ft (9.5 psia), 50% O ₂ , EVA sim/360 min | 6 | 0 |
| Bubb Threshold-E | 0PB;10.28K ft (10.0 psia), 50% O ₂ , EVA sim/360 min | 9 | 0 |
| Bubb Threshold-F | 0PB; 9.0K ft (10.5 psia), 50% O ₂ , EVA sim/360 min | 2 | 0 |

| Data Set | Profile Description Summary | # Exposures | # DCS Observed |
|-----------|--|-------------|----------------|
| CO2-A | CO ₂ in PB gas: 60 min PB, 100% O ₂ ; 25K ft EVA sim/180 min | 38 | 4 |
| CO2-B | CO ₂ in PB gas: 60 min PB, 97% O ₂ , 3% CO ₂ ; 25K ft EVA sim/180 min | 37 | 3 |
| CO2-C | CO ₂ in PB gas: 60 min PB, 100% O ₂ ; 25K ft EVA sim/360 min | 25 | 24 |
| CO2-D | CO ₂ in PB gas: 60 min PB, 97% O ₂ , 3% CO ₂ ; 25K ft EVA sim/360 min | 25 | 19 |
| DNT-A | Inflight denitrogenation-staged ascent: 60 min PB;29.5K ft, 100 kcal rope pull exercise/240 min | 39 | 24 |
| DNT-B | Inflight denitrogenation-staged ascent:75 min PB;29.5K ft, 100 kcal rope pull exercise/240 min | 18 | 7 |
| DNT-C | Inflight denitrogenation-staged ascent: 135 min PB;29.5K ft, 100 kcal rope pull exercise/240 min | 33 | 15 |
| DNT-D | Inflight denitrogenation-staged ascent: 15 min PB;8.0K ft/60 min;29.5K ft, 100 kcal rope pull exercise/240 min | 17 | 11 |
| DNT-E | Inflight denitrogenation-staged ascent: 15 min PB;8.0K ft/120 min;29.5K ft, 100 kcal rope pull exercise/240 min | 15 | 6 |
| DNT-F | Inflight denitrogenation-staged ascent: 15 min PB;12.0K ft/60 min;29.5K ft, 100 kcal rope pull exercise/240 min | 16 | 10 |
| DNT-G | Inflight denitrogenation-staged ascent: 15 min PB;12.0K ft/120 min;29.5K ft, 100 kcal rope pull exercise/240 min | 16 | 7 |
| DNT-H | Inflight denitrogenation-staged ascent: 15 min PB;16.0K ft/60 min;29.5K ft, 100 kcal rope pull exercise/240 min | 31 | 12 |
| DNT-I | Inflight denitrogenation-staged ascent: 15 min PB;16.0K ft/120 min;29.5K ft, 100 kcal rope pull exercise/240 min | 33 | 13 |
| DNT-J | Inflight denitrogenation-staged ascent: 15 min PB;18.0K ft/ 60 min;29.5K ft, 100 kcal rope pull exercise/240 min | 34 | 21 |
| DNT-K | Inflight denitrogenation-staged ascent: 15 min PB;18.0K ft/120 min;29.5K ft, 100 kcal rope pull exercise/240 min | 31 | 14 |
| EffctEx-A | 60 min PB; 29.5K ft rest/240 min | 46 | 15 |
| EffctEx-B | 60 min PB; 29.5K ft isometric stacked weight, arm exercise/240 min | 25 | 10 |
| EffctEx-C | 60 min PB; 29.5K ft isotonic stacked weight, arm exercise/240 min | 22 | 9 |
| EffctEx-D | 60 min PB; 29.5K ft isometric stacked weight, leg exercise/240 min | 26 | 7 |
| EffctEx-E | 60 min PB; 29.5K ft isotonic stacked weight, leg exercise/240 min | 25 | 8 |
| EffctEx-F | 60 min PB; 27.5K ft rest/240 min | 13 | 5 |
| EffctEx-G | 60 min PB; 27.5K ft isometric stacked weight, arm exercise/240 min | 7 | 3 |
| EffctEx-H | 60 min PB; 27.5K ft isotonic stacked weight, arm exercise/240 min | 8 | 7 |
| EffctEx-I | 60 min PB; 27.5K ft isometric stacked weight, leg exercise/240 min | 8 | 3 |
| EffctEx-J | 60 min PB; 27.5K ft isotonic stacked weight, leg exercise/240 min | 8 | 4 |
| EffctEx-K | 60 min PB; 25.0K ft rest/240 min | 4 | 2 |
| EffctEx-L | 60 min PB; 25.0K ft isometric stacked weight, arm exercise/240 min | 2 | 1 |
| EffctEx-M | 60 min PB; 25.0K ft isotonic stacked weight, arm exercise/240 min | 2 | 1 |
| EffctEx-N | 60 min PB; 25.0K ft isometric stacked weight, leg exercise/240 min | 2 | 0 |
| EffctEx-O | 60 min PB; 25.0K ft isotonic stacked weight, leg exercise/240 min | 2 | 1 |
| EffctEx-P | 60 min PB; 22.5K ft rest/240 min | 1 | 1 |
| EffctEx-U | 60 min PB; 20.0K ft rest/240 min | 1 | 0 |

| Data Set | Profile Description Summary | # Exposures | # DCS Observed |
|-------------------|--|-------------|----------------|
| EffctEx-V | 60 min PB; 20.0K ft isometric stacked weight, arm exercise/240 min | 1 | 1 |
| EffctEx-W | 60 min PB; 20.0K ft isotonic stacked weight, arm exercise/240 min | 1 | 1 |
| EffctEx-X | 60 min PB; 20.0K ft isometric stacked weight, leg exercise/240 min | 1 | 1 |
| EffctEx-Y | 60 min PB; 20.0K ft isotonic stacked weight, leg exercise/240 min | 1 | 0 |
| 35K-A | 75 min PB;35K ft rest/180 min, males | 37 | 21 |
| 35K-B | 75 min PB;35K ft, 30% VO ₂ peak exercise/180 min, males | 30 | 28 |
| 35K-C | 75 min PB;35K ft rest/180 min, females | 36 | 19 |
| 35K-D | 75 min PB;35K ft, 30% VO ₂ peak exercise/180 min, females | 31 | 31 |
| 40K-A | 90 min PB; 40K ft (2.72 psia) resting/90 min | 40 | 18 |
| ZPB-A | Bends Threshold study: 0PB; 22.5 K ft, rest/360 min, males | 20 | 12 |
| ZPB-B | Bends Threshold study: 0PB; 22.5 K ft, EVA sim/360 min, males | 21 | 7 |
| ZPB-C | Bends Threshold study: 0PB; 21.2 K ft, EVA sim/360 min, males | 20 | 1 |
| ZPB-D | Bends Threshold study: 0PB; 23.8 K ft, EVA sim/360 min, males | 10 | 5 |
| PE1-A | 60 min PB (10 min 75% VO ₂ peak exercise, 50 min rest); 30K ft EVA sim/240 min | 26 | 11 |
| PE1-B | 60 PB (rest), EVA sim/240 min | 28 | 21 |
| PE2-A | 240 min PB (rest); EVA sim/240 min | 32 | 15 |
| PE2-B | 90 min PB (rest); EVA sim/240 min | 32 | 21 |
| MV-A | ADRAC Validation A) 90 min PB; 35K ft EVA sim/180 min | 31 | 29 |
| MV-B | ADRAC Validation B) 30 min PB; 25K ft, 30% VO ₂ peak exercise-rest cycles/240 min | 31 | 19 |
| MV-C | ADRAC Validation C) 15 min PB; 22.5K ft, 30% VO ₂ peak exercise-rest cycles/240 min | 30 | 9 |
| MV-D | ADRAC Validation D) 0PB; 18.0K ft, 30% VO ₂ peak exercise-rest cycles/360 min | 30 | 4 |
| MV-E | ADRAC Validation E) 75 min PB; 30K ft rest/240 min | 31 | 18 |
| NASA | | | |
| Test 1a; Rprt 204 | 210 min PB; 4.3 psia LB exercise/3 hr | 11 | 4 |

| Data Set | Profile Description Summary | # Exposures | # DCS Observed |
|------------------------|---|-------------|----------------|
| Test 1b; Rprt 206 | 0PB; 10.2 psia*/12hr; 10.2 psia O2/40 min; 4.3 psia LB exercise/3 hr | 13 | 3 |
| Test 1c; Rprt 208 | 0PB; 10.2 psia*/12hr; 10.2 psia O2/90 min; 4.3 psia LB exercise/3 hr | 12 | 4 |
| Test 1d; Rprt 418 | 0PB; 10.2 psia*/18hr; 10.2 psia O2/40 min; 4.3 psia LB exercise/3 hr | 3 | 2 |
| Test 2a; Rprt 209 | 210 min PB; 9.2 psia/10 min; 4.3 psia EVA sim/230 min | 23 | 7 |
| Test 2b; Rprt 211 | 0PB; 10.2 psia*/12hr; 10.2 psia O2/40 min; 9.2 psia/10 min; 4.3 psia EVA sim/240 min | 22 | 6 |
| Test 3a; Rprt 212 | 240 min PB; 9.2 psia/10 min; 4.3 psia EVA sim/350 min | 28 | 6 |
| Test 3b; Rprt 215 | 45 min PB; 10.2 psia*/12hr; 10.2 psia O2/40 min; 4.3 psia EVA sim/350 min | 35 | 8 |
| Test 3c; Rprt 213 | A:[240 min PB; 9.2 psia/10 min; 4.3 psia EVA sim/350 min]; 13hr SI; repeat A | 14 | 3 |
| Test 3d; Rprt 217 | 45 min PB; 10.2 psia*/12hr; A:[10.2 psia O2/40 min; 9.2 psia/10 min; 4.3 psia EVA sim/350 min]; 10.2 psia*/980 min; repeat A | 12 | 2 |
| Test 4a; Rprt 219 | 45 min PB; 10.2 psia*/12hr; 10.2 psia O2/40 min; 9.2 psia/10 min; 4.3 psia EVA sim/170 min | 12 | 1 |
| Test 4b; Rprt 220 | 45 min PB; 10.2 psia*/12hr; A:[10.2 psia O2/40 min; 9.2 psia/10 min; 4.3 psia EVA sim/170 min]; 10.2 psia*/80 min; repeat A | 12 | 0 |
| Test 4c; Rprt 221 | 45 min PB; 10.2 psia*/12hr; A:[10.2 psia O2/40 min; 9.2 psia/10 min; 4.3 psia EVA sim/170 min]; 10.2 psia*/80 min; repeat A; 10.2 psia*/14hr; repeat A | 12 | 0 |
| Test 4d; Rprt 222 | 45 min PB; 10.2 psia*/12hr; A:[10.2 psia O2/40 min; 9.2 psia/10 min; 4.3 psia EVA sim/170 min]; 10.2 psia*/80 min; repeat A; 10.2 psia*/14hr; repeat A; 10.2 psia*/80 min; repeat A | 12 | 0 |
| Test 4e; Rprt 223 | 45 min PB; 10.2 psia*/12hr; A:[10.2 psia O2/40 min; 9.2 psia/10 min; 4.3 psia EVA sim/170 min]; 10.2 psia*/80 min; repeat A; 10.2 psia*/14hr; repeat A; 10.2 psia*/80 min; repeat A; 10.2 psia*/14hr; repeat A | 12 | 0 |
| Test 4f; Rprt 224 | 45 min PB; 10.2 psia*/12hr; A:[10.2 psia O2/40 min; 9.2 psia/10 min; 4.3 psia EVA sim/170 min]; 10.2 psia*/80 min; repeat A; 10.2 psia*/14hr; repeat A; 10.2 psia*/80 min; repeat A; 10.2 psia*/14hr; repeat A; 10.2 psia*/80 min; repeat A | 12 | 0 |
| Test 5a; Rprt 237, 238 | 6hr PB; 4.3 psia EVA sim/360 min | 38 | 4 |
| Test 5b; Rprt 239 | 8hr PB; 4.3 psia EVA sim/360 min | 11 | 0 |
| Test 6; Rprt 241, 243 | 2hr PB; 10.2 psia, 28% O2/24hr; 6.0 psia, 60% O2, EVA sim/6hr | 29 | 1 |
| Test 7a; Rprt 257 | 0PB; 6.5 psia (21K ft) mod EVA sim (~400 kcal/hr)/180 min | 11 | 4 |
| Test 7b; Rprt 258 | 0PB; 6.5 psia (21K ft) mod EVA sim (~200 kcal/hr)/180 min | 11 | 2 |
| Test 8a; Rprt 378, 379 | 0PB; 6.5 psia (21K ft) EVA sim/180 min | 40 | 7 |
| Test 8b; Rprt 378, 379 | 3d x 30 min heavy treadmill exercise/day; 0PB; 6.5 psia (21K ft) EVA sim/180 min | 41 | 10 |
| Test 9a; Rprt 407, 409 | ARGO, Phase I; 0PB; 6.5 psia EVA sim/180 min | 24 | 1 |
| Test 9b; Rprt 408, 410 | ARGO, Phase I: 3d 6deg HDT; 0PB; 6.5 psia EVA sim, nonambulatory/180 min | 23 | 2 |
| Test 9c; Rprt 419, 420 | ARGO, Phase II: 4hr PB; 4.3 psia EVA sim/180 min | 11 | 3 |
| Test 9d; Rprt 421 | ARGO, Phase II: 2hr adynamia, 4hr PB (adynamia); 4.3 psia EVA sim, adynamia/180 min | 7 | 0 |
| Test 9e; Rprt 421 | ARGO, Phase II: 2hr adynamia, 4hr PB (UB exercise, 3.5hr @ 188 kcal/hr); 4.3 psia EVA sim, adynamia/180 min | 7 | 0 |
| Test 10; Rprt 413, 414 | flying after diving: 20fsw (dry), light exercise/400 min; SI, air/14hr; 10.1 psia (10.0K ft), rest/3hr | 19 | 1 |

| Data Set | Profile Description Summary | # Exposures | # DCS Observed |
|-------------------------|---|-------------|----------------|
| Test 11a; Rprt 453, 454 | ARGO Phase III: 3hr PB; 4.3 psia EVA sim, nonambulatory/240 min | 28 | 3 |
| Test 11b; Rprt 450, 451 | 0PB; 6.5 psia: (2 min walk, 4 min rest) cycles wVGE dtctn/120 min | 4 | 0 |
| PRP I | NASA Prebreathe Reduction Protocol [‡] , Phase I | 49 | 9 |
| PRP II | NASA Prebreathe Reduction Protocol [‡] , Phase II | 50 | 0 |
| PRP III | NASA Prebreathe Reduction Protocol [‡] , Phase III | 10 | 2 |
| PRP IV | NASA Prebreathe Reduction Protocol [‡] , Phase IV | 69 | 8.3 |
| | Totals | 2594 | 858.3 |

* 26.5% O₂

‡ NASA Prebreathe Reduction Program (PRP): Man-trials conducted at Duke University, Memorial Hermann-Texas Medical Center, and Defense and Civil Institute of Environmental Medicine.

Note: Four man-exposures; man-flight numbers 88073, 91097, 93022, and 93033; of the 1194 exposures extracted from the original USAFAL Hypobaric Decompression Sickness Database are not counted in this table but were included in the model training data. Each of these exposures had a unique profile that could not be associated with any study in the database and each culminated with occurrence of DCS.

13. Appendix F. Pearson χ^2 Statistics for Optimized 3RUT-MBe1 Model on its A1309 Training Data

| Data Set | # Exposures (N) | # DCS Incidents | | A1309-3RUT MBe1 (Pearson Residual) ² | | | cumulative χ^2 | P |
|---------------------|--------------------|-----------------|----------------|--|--------------------|------|---------------------|---|
| | | Observed (f) | Predicted n | π | $(f-n)^2/n(1-\pi)$ | | | |
| Test 9e | 7 | 0 | 0.000 | 0.00 | 0.000 | 0.00 | --- | |
| Bubb Threshold-F | 2 | 0 | 0.000 | 0.00 | 0.000 | 0.00 | --- | |
| 8.3 psia-A | 20 | 1 | 0.984 | 0.05 | 0.000 | 0.00 | --- | |
| Bubb Threshold-E | 9 | 0 | 0.003 | 0.00 | 0.003 | 0.00 | --- | |
| Test 1b | 13 | 3 | 3.090 | 0.24 | 0.003 | 0.01 | --- | |
| Test 1a | 11 | 4 | 3.882 | 0.35 | 0.006 | 0.01 | --- | |
| MV-D | 30 | 4 | 4.143 | 0.14 | 0.006 | 0.02 | --- | |
| Bubb Threshold-D | 6 | 0 | 0.014 | 0.00 | 0.014 | 0.03 | --- | |
| Test 3d | 12 | 2 | 2.205 | 0.18 | 0.023 | 0.06 | --- | |
| Test 4a | 12 | 1 | 1.172 | 0.10 | 0.028 | 0.08 | --- | |
| (9.5 psia, Unknown) | 42 | 0 | 0.034 | 0.00 | 0.034 | 0.12 | --- | |
| Test 2a | 23 | 7 | 6.597 | 0.29 | 0.035 | 0.15 | --- | |
| 9.5 psia Val-B | 12 | 0 | 0.038 | 0.00 | 0.038 | 0.19 | --- | |
| DNT-E | 15 | 6 | 5.587 | 0.37 | 0.049 | 0.24 | --- | |
| Test 8a | 40 | 7 | 7.604 | 0.19 | 0.059 | 0.30 | --- | |
| 9.5 psia Val-A | 20 | 0 | 0.064 | 0.00 | 0.064 | 0.36 | --- | |
| Test 9c | 11 | 3 | 2.635 | 0.24 | 0.067 | 0.43 | --- | |
| Test 7b | 11 | 2 | 2.378 | 0.22 | 0.077 | 0.51 | --- | |
| PRP IV | 69 | 8.3 | 9.089 | 0.13 | 0.079 | 0.58 | 0.900 | |
| ZPB-D | 10 | 5 | 5.456 | 0.55 | 0.084 | 0.67 | 0.955 | |
| DNT-C | 33 | 15 | 14.052 | 0.43 | 0.111 | 0.78 | 0.978 | |
| EffctEx-Y | 1 | 0 | 0.118 | 0.12 | 0.134 | 0.91 | 0.989 | |
| EffctEx-U | 1 | 0 | 0.118 | 0.12 | 0.134 | 1.05 | 0.994 | |
| BSI-A ? | 17 | 10 | 10.731 | 0.63 | 0.135 | 1.18 | 0.997 | |
| PRP III | 10 | 2 | 2.507 | 0.25 | 0.137 | 1.32 | 0.998 | |
| Test 7a | 11 | 4 | 3.388 | 0.31 | 0.160 | 1.48 | 0.999 | |
| EffctEx-L | 2 | 1 | 0.711 | 0.36 | 0.183 | 1.66 | 0.999 | |
| EffctEx-M | 2 | 1 | 0.711 | 0.36 | 0.183 | 1.84 | 1.000 | |
| EffctEx-O | 2 | 1 | 0.711 | 0.36 | 0.183 | 2.03 | 1.000 | |
| DNT-A | 39 | 24 | 22.667 | 0.58 | 0.187 | 2.21 | 1.000 | |
| MV-E | 31 | 18 | 16.671 | 0.54 | 0.229 | 2.44 | 1.000 | |
| EffctEx-G | 7 | 3 | 3.640 | 0.52 | 0.235 | 2.68 | 1.000 | |
| 100% Suit-A | 10 | 0 | 0.268 | 0.03 | 0.275 | 2.95 | 1.000 | |
| PE2-B | 32 | 21 | 19.512 | 0.61 | 0.291 | 3.24 | 1.000 | |
| Bubb Threshold-B | 10 | 0 | 0.326 | 0.03 | 0.337 | 3.58 | 1.000 | |
| EffctEx-K | 4 | 2 | 1.422 | 0.36 | 0.364 | 3.95 | 1.000 | |

| Data Set | # Exposures | # DCS Incidents | | (Pearson Residual) ² | | | cumulative χ^2 | P |
|-----------------------------------|-------------|-----------------|------------------------|---------------------------------|-------|--------------------|---------------------|---|
| | | Observed | Predicted | n | π | $(f-n)^2/n(1-\pi)$ | | |
| | (N) | (f) | A1309-3RUT MBe1 | | | | | |
| DNT-I | 33 | 13 | 11.345 | 0.34 | 0.368 | 4.31 | 1.000 | |
| DNT-H | 31 | 12 | 13.698 | 0.44 | 0.377 | 4.69 | 1.000 | |
| Test 11b | 4 | 0 | 0.361 | 0.09 | 0.396 | 5.09 | 1.000 | |
| EffctEx-J | 8 | 4 | 4.918 | 0.61 | 0.445 | 5.53 | 1.000 | |
| Test 8b | 41 | 10 | 8.189 | 0.20 | 0.501 | 6.03 | 1.000 | |
| 8.3 psia-B | 11 | 0 | 0.541 | 0.05 | 0.569 | 6.60 | 1.000 | |
| ZPB-B | 21 | 7 | 8.733 | 0.42 | 0.589 | 7.19 | 1.000 | |
| Test 3a | 28 | 6 | 7.832 | 0.28 | 0.595 | 7.79 | 1.000 | |
| EffctEx-I | 8 | 3 | 4.160 | 0.52 | 0.674 | 8.46 | 1.000 | |
| 100% Suit-B | 10 | 0 | 0.694 | 0.07 | 0.746 | 9.21 | 1.000 | |
| MV-B | 31 | 19 | 16.599 | 0.54 | 0.747 | 9.95 | 1.000 | |
| PE1-B | 28 | 21 | 18.824 | 0.67 | 0.768 | 10.72 | 1.000 | |
| Test 5b | 11 | 0 | 0.817 | 0.07 | 0.883 | 11.60 | 1.000 | |
| Test 5a | 38 | 4 | 6.225 | 0.16 | 0.951 | 12.55 | 1.000 | |
| DNT-D | 17 | 11 | 8.841 | 0.52 | 1.099 | 13.65 | 1.000 | |
| EffctEx-N | 2 | 0 | 0.711 | 0.36 | 1.103 | 14.76 | 0.999 | |
| 35K-B | 30 | 28 | 25.949 | 0.86 | 1.200 | 15.96 | 0.999 | |
| MV-C | 30 | 9 | 11.987 | 0.40 | 1.239 | 17.20 | 0.999 | |
| 35K-A | 37 | 21 | 24.255 | 0.66 | 1.268 | 18.46 | 0.998 | |
| 100% Suit-F, females | 10 | 1 | 2.660 | 0.27 | 1.411 | 19.87 | 0.997 | |
| DNT-F | 16 | 10 | 7.611 | 0.48 | 1.430 | 21.30 | 0.995 | |
| Test 3c | 14 | 3 | 5.162 | 0.37 | 1.434 | 22.74 | 0.993 | |
| DNT-G | 16 | 7 | 4.782 | 0.30 | 1.468 | 24.21 | 0.991 | |
| ZPB-A | 20 | 12 | 9.249 | 0.46 | 1.522 | 25.73 | 0.987 | |
| (4.37 psia PB15-PstB138, Unknown) | 12 | 7 | 8.946 | 0.75 | 1.664 | 27.39 | 0.982 | |
| Test 9b | 23 | 2 | 4.484 | 0.19 | 1.710 | 29.10 | 0.975 | |
| Test 3b | 35 | 8 | 5.187 | 0.15 | 1.791 | 30.89 | 0.966 | |
| Test 1c | 12 | 4 | 2.181 | 0.18 | 1.854 | 32.75 | 0.955 | |
| 100% Suit-D, females | 9 | 0 | 1.550 | 0.17 | 1.873 | 34.62 | 0.940 | |
| DNT-B | 18 | 7 | 9.923 | 0.55 | 1.919 | 36.54 | 0.922 | |
| 100% Suit-C | 11 | 0 | 1.660 | 0.15 | 1.955 | 38.49 | 0.901 | |
| PE1-A | 26 | 11 | 7.738 | 0.30 | 1.958 | 40.45 | 0.877 | |
| Test 4b | 12 | 0 | 1.685 | 0.14 | 1.960 | 42.41 | 0.851 | |
| Test 4c | 12 | 0 | 1.813 | 0.15 | 2.136 | 44.55 | 0.817 | |
| Test 4d | 12 | 0 | 1.859 | 0.15 | 2.200 | 46.75 | 0.778 | |
| Test 9d | 7 | 0 | 1.677 | 0.24 | 2.205 | 48.95 | 0.736 | |
| Test 4e | 12 | 0 | 1.937 | 0.16 | 2.309 | 51.26 | 0.689 | |
| Bubb Threshold-A | 25 | 0 | 2.145 | 0.09 | 2.347 | 53.61 | 0.639 | |
| Test 4f | 12 | 0 | 1.975 | 0.16 | 2.364 | 55.97 | 0.588 | |
| 35K-C | 36 | 19 | 23.599 | 0.66 | 2.602 | 58.58 | 0.528 | |
| Test 2b | 22 | 6 | 3.110 | 0.14 | 3.127 | 61.70 | 0.451 | |
| PRP II | 50 | 0 | 2.959 | 0.06 | 3.145 | 64.85 | 0.378 | |
| EffctEx-P | 1 | 1 | 0.230 | 0.23 | 3.344 | 68.19 | 0.305 | |

| Data Set | # Exposures | # DCS Incidents | | | | | | |
|-----------------------------------|-------------|-----------------|------------------------|-------|----------------------------------|---------------------|-------|--|
| | | Observed | Predicted | | | | | |
| | (N) | (f) | n | π | (f-n) ² /n(1- π) | cumulative χ^2 | P | |
| | | | A1309-3RUT MBe1 | | | | | |
| | | | | | (Pearson Residual) ² | | | |
| EffctEx-C | 22 | 9 | 13.329 | 0.61 | 3.567 | 71.76 | 0.236 | |
| Test 9a | 24 | 1 | 4.679 | 0.19 | 3.594 | 75.35 | 0.178 | |
| (4.37 psia PB60-PstB180, Unknown) | 43 | 23 | 28.968 | 0.67 | 3.768 | 79.12 | 0.129 | |
| 7.8 psia-B | 92 | 4 | 9.933 | 0.11 | 3.973 | 83.09 | 0.089 | |
| 100% Suit-E | 11 | 0 | 2.926 | 0.27 | 3.987 | 87.08 | 0.059 | |
| EffctEx-F | 13 | 5 | 8.458 | 0.65 | 4.048 | 91.13 | 0.038 | |
| EffctEx-H | 8 | 7 | 4.157 | 0.52 | 4.049 | 95.18 | 0.024 | |
| EffctEx-B | 25 | 10 | 15.071 | 0.60 | 4.296 | 99.47 | 0.015 | |
| Test 1d | 3 | 2 | 0.580 | 0.19 | 4.306 | 103.78 | 0.008 | |
| PE2-A | 32 | 15 | 9.418 | 0.29 | 4.688 | 108.47 | 0.004 | |
| 35K-D | 31 | 31 | 26.814 | 0.86 | 4.839 | 113.30 | 0.002 | |
| PRP I | 49 | 9 | 4.448 | 0.09 | 5.124 | 118.43 | 0.001 | |
| DNT-J | 34 | 21 | 14.473 | 0.43 | 5.125 | 123.55 | 0.000 | |
| DNT-K | 31 | 14 | 8.050 | 0.26 | 5.940 | 129.49 | 0.000 | |
| (6 psia, Unknown) | 24 | 1 | 6.287 | 0.26 | 6.023 | 135.52 | 0.000 | |
| MV-A | 31 | 29 | 22.970 | 0.74 | 6.111 | 141.63 | 0.000 | |
| CO2-D | 25 | 19 | 12.301 | 0.49 | 7.182 | 148.81 | 0.000 | |
| BSI-E | 46 | 24 | 15.287 | 0.33 | 7.438 | 156.25 | 0.000 | |
| EffctEx-V | 1 | 1 | 0.118 | 0.12 | 7.449 | 163.70 | 0.000 | |
| EffctEx-W | 1 | 1 | 0.118 | 0.12 | 7.449 | 171.15 | 0.000 | |
| EffctEx-X | 1 | 1 | 0.118 | 0.12 | 7.449 | 178.59 | 0.000 | |
| 40K-A | 40 | 18 | 26.500 | 0.66 | 8.077 | 186.67 | 0.000 | |
| EffctEx-E | 25 | 8 | 15.071 | 0.60 | 8.353 | 195.03 | 0.000 | |
| BSI-B | 36 | 32 | 23.655 | 0.66 | 8.585 | 203.61 | 0.000 | |
| ZPB-C | 20 | 1 | 7.399 | 0.37 | 8.784 | 212.39 | 0.000 | |
| 7.8 psia-A | 94 | 1 | 10.154 | 0.11 | 9.252 | 221.65 | 0.000 | |
| EffctEx-A | 46 | 15 | 25.627 | 0.56 | 9.949 | 231.59 | 0.000 | |
| Test 11a | 28 | 3 | 11.234 | 0.40 | 10.080 | 241.67 | 0.000 | |
| CO2-A | 38 | 4 | 13.394 | 0.35 | 10.175 | 251.85 | 0.000 | |
| BSI-D | 28 | 22 | 12.885 | 0.46 | 11.944 | 263.79 | 0.000 | |
| (5.45 psia, Unknown) | 21 | 1 | 8.834 | 0.42 | 11.992 | 275.79 | 0.000 | |
| CO2-B | 37 | 3 | 13.225 | 0.36 | 12.302 | 288.09 | 0.000 | |
| BSI-C ? | 83 | 66 | 48.068 | 0.58 | 15.895 | 303.98 | 0.000 | |
| Test 10 | 19 | 1 | 0.047 | 0.00 | 19.577 | 323.56 | 0.000 | |
| EffctEx-D | 26 | 7 | 17.856 | 0.69 | 21.073 | 344.63 | 0.000 | |
| CO2-C | 25 | 24 | 12.226 | 0.49 | 22.190 | 366.82 | 0.000 | |
| Bubb Threshold-C (?) | 23 | 3 | 0.244 | 0.01 | 31.459 | 398.28 | 0.000 | |
| Test 6 | 29 | 1 | 0.028 | 0.00 | 34.358 | 432.64 | 0.000 | |
| Totals: | 2594 | 858.3 | 896.453 | | | | | |